Development and Validation of Microfluidic Lab-on-chip Analyzers for the *In Situ* Quantification of Dissolved Iron and Manganese Species in Seawater

DISSERTATION

ZUR ERLANGUNG DES DOKTORGRADES

DER MATHEMATISCH - NATURWISSENSCHAFTLICHEN FAKULTÄT

DER CHRISTIAN-ALBRECHTS-UNIVERSITÄT ZU KIEL

VORGELEGT VON

FELIX GEIßLER

Kiel, August 2019

1. Gutachter: Prof. Eric P. Achterberg

2. Gutachter: Dr. Ralf Prien

Datum der Disputation: 15.11.2019

Summary

There has been an increasing demand over the last decades for autonomous *in situ* measurement systems for the quantification of physical and chemical parameters in the marine environment. The demand is largely linked to the need to address the present undersampling of the world's oceans. The need for reliable and well resolved time series, both on a temporal and spatial scale, cannot be satisfied with conventional approaches involving collection of discrete samples during ship campaigns followed by their analysis in a land-based laboratory. The high demand for autonomous *in situ* measurements is also linked to the associated extensive logistical efforts and the risk of compromising the integrity of the samples during manual sample collection, and thus limiting the investigation of highly dynamic biogeochemical processes.

Of particular interest is the acquisition of time series for dissolved trace metals such as iron (Fe) and manganese (Mn) in marine waters. Those trace metals are essential micronutrients for marine organisms. Iron and Mn regulate cell functions such as photosynthesis and their bioavailability affects therefore the growth and composition of phytoplankton communities, representing the world's largest sink for atmospheric carbon dioxide. Thus, well resolved data of Fe and Mn distributions and fluxes will help to better understand micronutrient cycling, associated biological responses and marine ecosystem dynamics as a response to episodic events. Well resolved micronutrient time series can further improve parameterization of biogeochemical models, allowing us to project feedbacks to climate changes. However, the determination of Fe and Mn in a complex matrix such as seawater is challenging as these elements can be present at very low concentrations in open ocean regions (down to 10^{-12} mol·L^{-1}) and exhibit complex speciation chemistry.

This PhD project investigates whether the well-established spectrophotometric approaches for Fe and Mn using Ferrozine (FZ) and 1-(2-pyridylazo)-2-naphthol (PAN) as complexing agents, respectively, can be utilized for reliable and accurate *in situ* quantification of dissolved Fe (DFe) and Mn (DMn) species in an autonomous wet chemical analyzer based on lab-on-chip (LoC) technology. Those systems are based around a microfluidic chip and integrate all steps of analysis (sampling, sample treatment, chemical reaction, detection, data processing) into a single instrument. Their small physical size, portability as well as low power and reagent consumption is key for envisaged autonomous long-term deployments.

The following main findings were obtained:

- Laboratory based characterization of the performance of the LoC analyzer systems showed linear detection regimes ranging from the respective detection limits, 1.9 nM for DFe and 27.1 nM for DMn, to several μM of the respective trace metal. This range enables determinations in marine environments where elevated DFe and DMn concentrations are present, such as regions near trace metal sources, e.g. coastal and estuarine systems, hydrothermal vents or regions characterized by extensive dust deposition. However, for deployments in open ocean regions, detection limits down to 0.1 nM are required. Thus, further research has to be undertaken in order to quantify distributions *in situ* in oceanic regions characterized by trace metal depletion.

- It was found that the design of the LoC analyzer for the detection of DFe needed to be re-worked in order to allow on-line acidification of the water sample prior to the addition of the FZ reagent. This was necessary as a 16 % to 75 % underestimation of *in situ* determined DFe concentrations compared to those obtained from analysis via inductively coupled plasma mass spectrometry (ICP-MS) of discretely collected samples during a test campaign conducted in the Kiel fjord (Germany) was observed using the first design version. Laboratory based acidification experiments with a natural water sample showed full recovery of spectrophotometrically determined DFe concentrations when the sample was acidified to pH ~ 1 prior to the addition of FZ reagent in order to liberate all Fe from its natural organic complexes and make it therefore accessible to FZ. However, Fe contamination originated from acid induced Fe leaching from the analyzers materials were observed during a second test deployment.

- The composition of the PAN reagent for DMn determination was successfully adapted for the use in a microfluidic manifold for long-term deployments. The stability of the PAN reagent could be enhanced by adaptation of the used surfactant volume. A siderophore type Fe masking agent, which was supposed to suppress any Fe interference with the PAN method, showed limited life time and also removed Mn from the PAN accessible pool resulting in an underestimation of Mn concentrations.

- A test deployment in the Kiel fjord was successfully conducted with a DMn LoC analyzer. The processed *in situ* DMn concentrations were in good agreement with those of discrete samples analysed via ICP-MS. An accuracy of > 99 % was obtained for certain periods.

Overall, the here presented work demonstrates that the spectrophotometric determination of DMn species on a system based around a microfluidic chip is a powerful tool for the acquisition of reliable and temporally well resolved *in situ* DMn time series in coastal waters. The *in situ* quantification of DFe species needs further improvements, but in its current state it represents a useful technique for recording relative changes of DFe concentrations in seawater.

This PhD project contributes to the vastly needed development of autonomous *in situ* observing platforms for trace metals in marine waters. It can help to better understand fundamental biogeochemical processes linked to the distribution of dissolved trace metals. Furthermore, data from further deployments can be used to calculate trace metal fluxes, fill gaps in databases and provide a baseline for predictions of consequences of climate driven change.

Zusammenfassung

In den letzten Jahrzehnten ist die Nachfrage nach autonomen *In-situ*-Messsystemen zur Quantifizierung physikalischer und chemischer Parameter in marinen Gewässern drastisch gestiegen. Die hohe Nachfrage ist weitestgehend damit verbunden, der derzeitigen Unterprobung der Weltozeane entgegenzuwirken. Der Bedarf an zuverlässigen und zeitlich sowie räumlich gut aufgelösten Zeitserien kann mit den konventionellen Methoden der manuellen Probennahme während Schiffsausfahrten und deren Analyse in landgestützten Laboratorien nicht erfüllt werden. Des Weiteren birgt die konventionelle Probennahme und –analyse ein erhebliches Risiko bezüglich der Intergrität der Proben und ist mit übermäßigem logistischem Aufwand verbunden. Daher ist eine genaue Untersuchung von hochdynamischen biogeochemischen Prozessen stark eingeschränkt.

Von besonderem Interesse ist die *In-situ*-Erfassung von Zeitserien für Spurenmetalle wie Eisen (Fe) und Mangan (Mn) im Meerwasser. Diese Spurenmetalle stellen essentielle Mikronährstoffe für Meeresoganismen dar. So regulieren Fe und Mn wichtige Zellfunktionen wie die Photosynthese und beeinflussen daher durch ihre Bioverfügbarkeit das Wachstum und die Zusammensetzung ganzer Phytoplanktongemeinschaften, eine der weltweit größten Kohlendioxidsenken. Somit können gut aufgelöste Daten der Verteilung und Flüsse von gelöstem Fe (DFe) und Mn (DMn) dazu beitragen, Kreisläufe von Mikronährstoffen und die damit verbundenen biologischen Feedbacks sowie die Dynamik des marinen Ökosystems als Reaktion auf episodische Ereignisse besser zu verstehen. Verlässliche Zeitreihen von Mikronährstoffen guter Auflösung können die Parametrisierung biogeochemischer Modelle weiter verbessern, sodass Rückkopplungen auf den Klimawandel projiziert werden können. Jedoch ist die Bestimmung von Fe und Mn in einer so komplexen Matrix wie Meerwasser mit erheblichen Schwierigkeiten verbunden. Die Spurenmetalle liegen in sehr geringen Konzentrationen in Regionen des offenen Ozeans (bis zu 10^{-12} mol·L^{-1}) sowie in einer Vielzahl von unterschiedlichen Spezien vor.

Die vorliegende Dissertation untersucht, inwiefern die etablierten spektrophotometrischen Verfahren zur die Bestimmung von Fe und Mn mit den Komplexbildnern Ferrozin (FZ) und 1-(2-Pyridylazo)-2-naphthol (PAN) eingesetzt werden können, um zuverlässige und präzise *In-situ*-Messungen von im Meerwasser befindlichem DFe und DMn mittels eines autonomen nass-chemischen Analysators auf Basis der ‚Lab-on-chip' (LoC)-Technologie

zu erhalten. Solche Systeme stellen mikrofluidische Plattformen dar, die alle Schritte einer nasschemischen Analyse, von der Probennahme, über die Probenbehandlung, chemischer Reaktion, Detektion und der Datenverarbeitung in nur einem einzigen Gerät ermöglichen. Hierbei stellt deren geringe physische Größe, Portabilität, sowie ihr geringer Strom- und Reagenzienverbrauch ein Schlüsselelement für geplante autonome *In-situ*-Langzeitmessungen dar.

Im Folgenden die wichtigsten Ergebnisse dieser Studie:

- Die im Labor durchgeführte Charakterisierung der LoC-Analysatoren zeigte ein lineares Verhalten über einen weiten Konzentrationsbereich, von der unteren Nachweisgrenze (1.9 nM für DFe und 27.1 nM für DMn) bis zu mehreren μM des jeweiligen Spurenmetalls. Dieser Detektionsbereich ermöglicht Bestimmungen in ozeanischen Regionen, die erhöhte Spurenmetallkonzentrationen aufweisen. Hierzu zählen z.B. Regionen, die durch einen erhöhten Eintrag von Wüstenstaub charakterisiert sind oder Regionen in der Nähe von Spurenmetallquellen wie Küsten-, Fjord- und Flussmündungssystemen oder hydrothermalen Quellen in der Tiefsee. Für den Einsatz im offenen Ozean sind jedoch Nachweisgrenzen von bis zu 0.1 nM erforderlich. Daher müssen weitere Forschungsarbeiten durchgeführt werden, um Verteilungen von Spurenmetallen in ozeanischen Regionen, die durch Spurenmetallverarmung gekennzeichnet sind, *in situ* quantifizieren zu können.

- Es wurde festgestellt, dass das ursprüngliche Design des LoC-Analysators für die DFe-Bestimmung überarbeitet werden musste, um eine On-line-Ansäuerung der Wasserprobe zu ermöglichen. Dies war notwendig, da während einer Testkampagne in der Kieler Förde (Deutschland) mit der ersten Analysatorgeneration eine Unterbestimmung der *in situ* bestimmten DFe-Konzentrationen zwischen 16 % und 75 % verglichen zu diskreten Proben, analysiert mittels ICP-MS, beobachtet wurde. Laborbasierte Ansäuerungsexperimente mit einer natürlichen Wasserprobe zeigten, dass eine vollständige Wiederfindung der spektrophotometrisch bestimmtem DFe-Konzentration erzielt werden kann, wenn die Wasserprobe vor der Zugabe des FZ-Reagenzes auf pH ~ 1 angesäuert wird. Dies ermöglicht eine Freisetzung der gesamten in natürlichen organischen Komplexen gebundenen Fe-Ionen, die somit für FZ zugänglich sind. Allerdings wurde während einer Testkampagne mit der

zweiten Analysatorgeneration festgestellt, dass die Anwendung von Säure zum Herauslösen von Fe aus den verwendeten Materialen führte, was eine Kontaminierung der Wasserprobe zur Folge hatte.

- Die Zusammensetzung des PAN-Reagenzes zur DMn-Bestimmung wurde erfolgreich für den Einsatz in einem mikrofluidischen System für Langzeitmessungen angepasst. Die Stabilität des PAN-Reagenzes konnte durch Anpassung der verwendeten Tensid-Konzentration verbessert werden. Ein Fe-Maskierungsmittel aus der Gruppe der Siderophoren, welches jegliche Fe induzierte Störung mit der PAN-Methode unterdrücken sollte, zeigte eine begrenzte Lebensdauer und wies ebenfalls eine Affinität zu Mn-Ionen auf. Dies führte zur Entfernung von Mn-Ionen aus dem für PAN zugänglichen Pool und somit zu einer Unterbestimmung der DMn-Konzentration.

- Eine Testkampagne mit einem DMn LoC-Analysator wurde erfolgreich in der Kieler Förde durchgeführt. Die *in situ* bestimmten DMn-Konzentrationen waren in guter Übereinstimmung mit denen der mittels ICP-MS analysierten diskreten Proben. Genauigkeiten von mitunter > 99 % wurden erzielt.

Insgesamt zeigt die hier vorgestellte Arbeit, dass die spektrophotometrische DMn-Bestimmung auf einem mikrofluidischen Chip basierenden System ein leistungsfähiges Mittel für den Erwerb zuverlässiger und gut aufgelöster *In-situ*-DMn-Zeitreihen in Küstengewässern ist. Die *In-situ*-DFe-Quantifizierung bedarf weiterer Verbesserungen, stellt aber in ihrem derzeitigen Zustand eine nützliche Technik zur Erfassung relativer Änderungen der DFe-Konzentrationen im Meerwasser dar.

Die vorliegende Arbeit trägt zur dringend notwendigen Entwicklung autonomer *In-situ*-Beobachtungsplattformen für Spurenmetalle in Meeresgewässern bei. Der Einsatz solcher Systeme hilft, grundlegende biogeochemische Prozesse im Zusammenhang mit der Verteilung gelöster Spurenmetalle besser zu verstehen. Darüber hinaus können Daten zukünftig durchzuführender Messkampagnen verwendete werden, um Spurenmetallflüsse zu berechnen, Lücken in Datenbanken zu schließen und bieten somit die Grundlage zur Vorhersage über Folgen des Klimawandels.

Acknowledgements

Firstly, I would like to express my special gratitude to my supervisor Prof. Eric Achterberg for giving me the opportunity to work on this project. This PhD would not have been achievable without his constant support, guidance, inspiring discussions and helpful advices when things were not as 'fantastic' as hoped.

I would like to thank my co-supervisors Prof. Douglas Wallace, Prof. Matthew Mowlem and Prof. Douglas Connelly for their valuable contribution. I really benefitted from the exchange of ideas and their insightful comments helped me to improve my research.

I am deeply grateful to Dr. Alexander Beaton and Urska Martincic for sharing their experience in microfluidics, for their constant technical support and maintenance of the analyzer systems, and for making my stays in Southampton as enjoyable as they were.

I would like to thank all members of the AG Achterberg at GEOMAR for their helpfulness and for creating such a collaborative and pleasant working atmosphere. My special thanks goes to Dr. Mark Hopwood for his constant support and insightful comments. His profound knowledge on trace metals was essential for the analysis of trace metal samples and for planning and setting up experiments. I would like to thank Dr. Mario Esposito for his patience and wise advices when the analyzers were not working as intended. Also his tireless commitment during deployments was really much appreciated. I thank my office colleague Evangelia Louropoulou for creating a warm as well as productive working atmosphere and for the very much appreciated conversations about things beyond research. I am very grateful to Jana, Müni and Maria for their support in taking discrete samples in any weather and at any time.

I would like to express my appreciation to the HOSST graduate school for financial support and for organizing inspiring seminars and summer schools which gave me the unique opportunity to collaborate with scientists from all over the world on topics far away from our individual comfort zones. A big thank you goes also to all fellow HOSSTies and TOSSTies for making our seminars and summer schools as pleasant as they were.

Finally, I would like to express my deepest gratitude to my family and friends for their patience and support during the last 3.5 years.

Table of Contents

Abbreviations

[X]	Molar concentration of X
AA	Ascorbic acid
BPA	4,7-Diphenyl-1,10-phenanthroline
cmc	Critical micelle concentration
DFe	Dissolved iron
DFO-B	Desferrioxamin B
DIC	Dissolved inorganic carbon
DMn	Dissolved manganese
DOC	Dissolved organic carbon
DOM	Dissolved organic matter
DPD	N,N-Dimethyl-p-phenylenediamine
DZn	Dissolved zinc
ε	Molar extinction coefficient in $L \cdot mol^{-1} \cdot cm^{-1}$
$Fe(FZ)_3$	Ferrozine-Fe(II) complex
FZ	Ferrozine
GFAAS	Graphite furnace atomic absorption spectrometry
HDPE	High density polyethylene
HNLC	High Nitrate Low Chlorophyll
ICP-MS	Inductively coupled plasma mass spectrometry
ID	Inner diameter
λ	Wavelength
LDPE	Low density polyethylene
LED	Light emitting diode
LoC	Lab-on-chip
LOD	Limit of detection
$Mn(PAN)_2$	Mn(II)-PAN complex
PAN	1-(2-Pyridylazo)-2-naphthol
PD	Photodiode
PEEK	Polyether ether ketone
PES	Polyether sulfone
PMMA	Poly(methyl methacrylate)

PTFE	Polytetrafluoroethylene
PVC	Polyvinyl chloride
PVP	Polyvinylpyrrolidone
RGT	Reagent solution
S	Salinity
SDS	Sodium dodecyl sulfate
STD	Standard solution
T4CPP	Meso-tetrakis[4-(carboxymethyleneoxy)phenyl]porphyrin
TA	Total alkalinity
TdFe	Total dissolvable Fe
TPTZ	2,4,6-Tris(2-pyridyl)-s-triazine
TRL	Technology readiness level

1 Introduction

The following chapter aims to introduce the reader to the biogeochemistry of the trace metals iron and manganese and their quantitative determination in natural waters. For this purpose the following questions will be addressed throughout the chapter:

- Why is it important to determine the concentration of iron and manganese in natural waters from a biogeochemical perspective?
- What are the challenges for measuring iron and manganese in natural aquatic environments?
- Which methods are most suitable for the quantitative detection of iron and manganese in natural waters?
- How can we measure iron and manganese *in situ* in natural waters?
- What is key for miniaturizing chemical *in situ* analyzers and how can we validate their performance?

For this purpose the biogeochemical cycles of iron and manganese, including their speciation characteristics, will be briefly introduced. However, the main focus of this chapter lies on the determination of iron and manganese and the key steps of developing and validating miniaturized microfluidic analyzers for measuring iron and manganese concentrations *in situ* in natural waters.

1.1 Biogeochemistry of iron and manganese

The transition metals iron (Fe) and manganese (Mn) are relatively high abundant in the earth's crust with ~ 4.32 % (4^{th} rank) and ~ 0.07 % (12^{th} rank) [Wedepohl, 1995], respectively. In contrast, Fe and Mn concentrations in open ocean waters are relatively low ranging from 10^{-12} moles per liter ($pmol \cdot L^{-1}$) to 10^{-9} moles per liter ($nmol \cdot L^{-1}$) [Boyd and Ellwood, 2010; van Hulten et al., 2016], therefore also referred as trace metals. However, despite their scarcity in natural waters Fe and Mn are important micronutrients and form

key elemental resources for a variety of microbial processes in the marine environment depending on their speciation.

1.1.1 Iron cycling

The cycling of trace metals in marine basins is characterized by the interplay of a vast number of physical, chemical and biological processes, e.g. lithogenic inputs, dissolution, precipitation, scavenging, biological uptake, remineralization and sedimentation processes. An overview of these processes for Fe in the Atlantic Ocean as an example, is illustrated in **Figure 1.1** taken from Tagliabue et al. (2017).

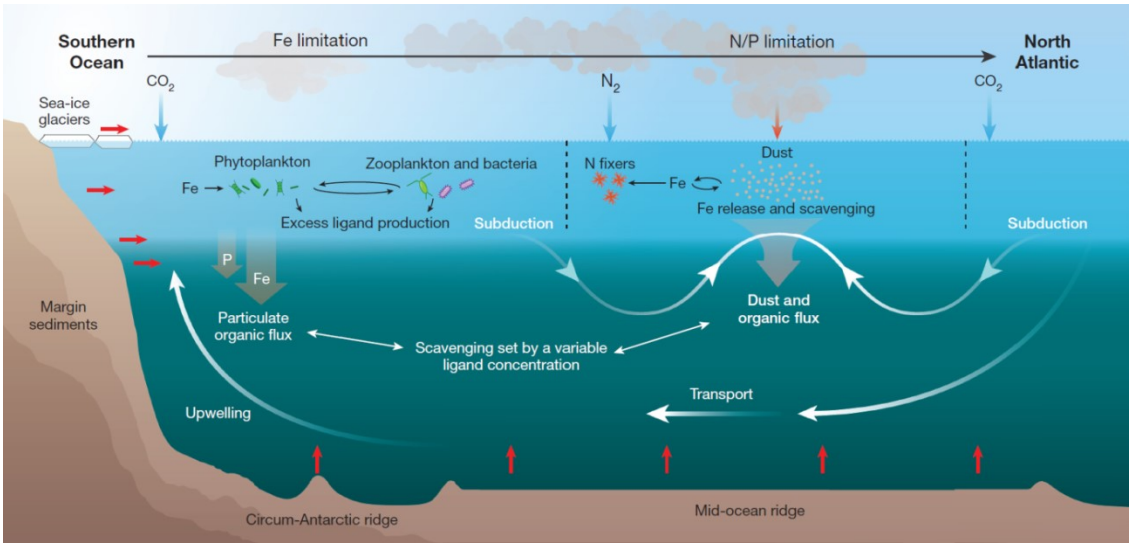

Figure 1.1: Major processes of the Fe cycle using the example of the Atlantic Ocean. Iron inputs to the basin are depicted with red arrows, biological processes where Fe is participating with black arrows, whereas fluxes and transport of Fe is illustrated in white color. [Tagliabue et al., 2017]

1.1.1.1 Sources and distribution of iron

Iron is introduced to marine waters from melting sea-ice glaciers, continental margins, hydrothermal vents, atmospheric deposition (e.g. dust, precipitation) and riverine inputs (**Figure 1.1**), with the strengths of the specific supply and their relative importance for primary production differing between ocean regions. Estimated fluxes of the 'dissolved' (< 0.45 µm, see section 1.1.1.3) Fe fraction (DFe) from the different sources into the global ocean are compiled in **Table 1**.

Table 1: Estimations of DFe fluxes from different sources into the world's oceans.

Sources	DFe flux [Gmol·yr^{-1}]	Reference
Hydrothermal activity	18 – 180 (30 – 90)	[Ussher et al., 2004], ([de Baar and de Jong, 2001])
Atmosphere (wet deposition)	10 – 26	[de Baar and de Jong, 2001; Jickells and Spokes, 2001]
River	2.6	[de Baar and de Jong, 2001]
Sediment	0.9 – 4.5	[Raiswell and Canfield, 2012]
Subglacial runoff	0.2	[Raiswell and Canfield, 2012]
Icebergs	0.002 – 0.003	[Raiswell and Canfield, 2012]

Hydrothermal activity represents with a global flux of 18 – 180 Gmol·yr^{-1} the major DFe supplier to the world's oceans, especially for deep waters [Ussher et al., 2004]. However, it has been thought that the majority of the hydrothermally released DFe was not transported away from the hydrothermal vicinity as high sedimental Fe concentrations can be found in those areas as a result of DFe removal by precipitation, with little far field impact [Ussher et al., 2004]. This conceptual view of the impact of hydrothermalism on the global Fe cycle has been revolutionized in recent years indicating that stabilization of hydrothermal dissolved iron may facilitate its long-range oceanic transport [Resing et al., 2015; Tagliabue and Resing, 2016]

Dissolved Fe is brought to surface waters mainly via atmospheric deposition of dust, most prominent in the North Atlantic and North Pacific Ocean beneath equatorial dust plumes. A dust input of 400 – 1000 Tg·yr^{-1} containing, on average, 3.5 % Fe was assessed on a global scale [Jickells and Spokes, 2001]. However, estimates of the solubility of this Fe vary widely as a variety of natural and methodological issues affect dust dissolution efficiency. It can be further estimated that 70 % of this atmospheric flux arises by dry deposition and 30 % by wet deposition, with subsequent dissolution in seawater after dry deposition being

low – but significant on a global scale. The solubility of Fe in seawater after wet deposition is higher, assessed at 14 %, resulting in an aeolian DFe input of 10 – 26 Gmol·yr^{-1} to the global ocean [de Baar and de Jong, 2001; Jickells and Spokes, 2001].

The riverine input to the oceans, with a global water discharge of ~ 37·10^{12} m^3·yr^{-1}[Meybeck and Ragu, 1997], is extremely variable and unevenly distributed with most water entering into the central Atlantic Ocean from the Amazon, Orinoco, Congo and Mississippi river systems [de Baar and de Jong, 2001] and the Arctic also receiving disproportionately high riverine inputs – 11 % of global riverine input into a basin accounting for 1 % of ocean volume [McClelland et al., 2012]. Stallard and Edmond (1983) estimated an average global riverine DFe concentration of 0.7 μM resulting in a mean DFe flux of ~26 Gmol·yr^{-1} into the coastal zones of the world's oceans, mainly as small colloidal particles. However, during estuarine mixing of fresh river waters with seawater about 90 % of the colloidal particles originating from river water are flocculated together with organic matter, as a result of a strong gradient in ionic strength, and are therefore removed from the dissolved phase. The remaining 10 % of DFe can be transported towards high salinity open ocean waters which equals a riverine derived net DFe flux of 2.6 Gmol·yr^{-1} [de Baar and de Jong, 2001]. Yet the 10 % estimation is a crude approximation and not a carefully weighted mean. Removal rates seem to vary both spatially, between river systems, and temporally within individual systems with rates reported from ~ 60 % to > 95 % [Boyle et al., 1977; Sholkovitz, 1978; Sholkovitz et al., 1978].

Benthic recycling of DFe species is supposed to be an important DFe source only in anoxic areas where low water column O_2 concentrations allow for high efflux into bottom waters [Dale et al., 2015]. Although measurable fluxes may also arise in the absence of these phenomena from gradual release of Fe in a chemically stabilized organically complexed form [Ussher et al., 2004]. Raiswell and Canfield (2012) estimated that 0.9 – 4.5 Gmol·yr^{-1} of DFe are delivered from sediments into the water column.

The DFe input from glaciers consists of several distinct supply mechanisms including localized dust plumes of glacial flour (e.g. Alaska Iceland, Patagonia) [Crusius et al., 2011], surface and subsurface glacial discharge [Raiswell et al., 2018] and icebergs [Raiswell et al., 2008]. Dissolved Fe fluxes of 0.02 Gmol·yr^{-1} and 0.16 Gmol·yr^{-1} from Greenland and up to 0.005 Gmol·yr^{-1} and 0.009 Gmol·yr^{-1} from Antarctica were assessed for oxic and anoxic meltwater, respectively, giving a total DFe flux of ~ 0.2 Gmol·yr^{-1} from subglacial meltwater runoff [Raiswell and Canfield, 2012]. The Fe supply from melting icebergs is

derived from terrestrial sources such as glacial debris and incorporated atmospheric dust, producing a DFe input of only 0.002 – 0.003 Gmol·yr^{-1} [Raiswell and Canfield, 2012]. However, much larger delivery of Fe of 16 – 24 Gmol·yr^{-1} was reported for ascorbic acid-extractable Fe from iceberg sediments to the global ocean. The relationship between labile sedimentary inputs, such as the potentially large supply from icebergs, and Fe supply and utilization by marine biota is unclear. Labile sedimentary sources can enter solution, but the rates of this process are often limited by the low nanomolar concentrations of ligands in seawater. A large sedimentary source can therefore be a relatively insufficient supply, even if labile, when mixing does not permit adequate exposure to Fe ligands to solubilize more than a small fraction of the labile Fe present. This 'ligand limitation' of solubilization may severely limit the transfer of some Fe sources, including rivers [Buck et al., 2007], glaciers [Lippiatt et al., 2010] and hydrothermal vents [Resing et al., 2015], into the dissolved phase and thus be the 'bottleneck' that constrains the effect of these sources upon transport towards open ocean regions and primary production.

In general, DFe concentrations exhibit a high variability in seawater with a range over four to five orders of magnitude [de Baar and de Jong, 2001]. Iron typically shows a nutrient-like vertical distribution in open ocean waters with the lowest concentrations found in the surface waters ranging from 0.03 to 0.5 nM and increasing concentrations with depth to 0.3 – 1.4 nM. In shallower coastal waters and enclosed seas DFe concentrations between 1 and 10 nM can be found. Estuaries and tidal channels contain 10 – 400 nM DFe. Elevated DFe concentrations in the range of 300 – 3000 nM can be found in suboxic and anoxic waters of semi-enclosed marine basins, such as the Black Sea and the Baltic. Pore waters of marine sediments and hot reducing hydrothermal vent fluids can contain DFe up to the μM and mM range, respectively [de Baar and de Jong, 2001].

1.1.1.2 Biogeochemical role of iron

The Fe cycle is closely linked to the biogeochemical cycles of phosphorus, nitrogen and carbon (**Figure 1.1**), with interactions controlling and defining the chemistry and biology of the world's oceans [Raiswell and Canfield, 2012]. Iron for example is involved in the removal and supply of phosphorus due to the high adsorption capacity of iron(oxyhydr)oxide phases to phosphate, regulating therefore the phosphate availability [Ruttenberg and Sulak, 2011]. Furthermore, Fe plays an essential role in the ocean's nitrogen cycle. Nitrogen fixation (transformation of unreactive and metabolically unusable

atmospheric nitrogen gas into bioavailable ammonia) is mainly accomplished by cyanobacteria via nitrogenase enzyme complexes [Jacq et al., 2014; Morel and Price, 2007]. Iron is an essential part of those complexes with a requirement of 38 Fe atoms per enzyme unit making it one of the most Fe-rich enzymes in nature [Whittaker et al., 2011]. Therefore, low Fe concentrations are considered to limit critical steps in the nitrogen cycle [Morel and Price, 2007]. Approximately one-third of the surface waters in the open ocean, mainly the Southern Ocean, the subarctic Pacific and the equatorial Pacific, are characterized by repletion of the macronutrients nitrate and phosphate by upwelling processes, and depletion of phytoplankton biomass/chlorophyll [Boyd et al., 2007]. Due to the prevalent high concentration of macronutrients in these areas, also known as 'High Nitrate Low Chlorophyll' (HNLC), the restriction in phytoplankton growth is acknowledged to be the result of limited Fe availability [Martin et al., 1991], as Fe is involved in important cellular processes like photosynthesis and respiration [Sunda, 2001]. Artificial Fe fertilization experiments were successfully undertaken in HNLC regions in order to prove the assumption that increased Fe concentration could stimulate phytoplankton growth [Boyd et al., 2007; de Baar et al., 2005]. As primary producer, phytoplankton is a major sink for atmospheric carbon dioxide by fixing carbon photosynthetically in the euphotic zone and subsequently transferring a fraction of the fixed carbon to deep waters and sediments by sinking [Basu and Mackey, 2018], thus linking Fe to the global carbon cycle [Breitbarth et al., 2010]. The potential of artificial Fe fertilizations as mitigation measure for the increasing atmospheric carbon dioxide concentrations is discussed and deemed controversial because of a limited effectiveness and potential ecosystem effects [Dean, 2009; Lampitt et al., 2008]. Artificial iron addition experiments conducted in the Gulf of Alaska and Southern Ocean indicated that between 480 mol [Boyd et al., 2004] and 3300 mol of carbon [Buesseler et al., 2004], respectively, can be exported into deeper waters (100 - 250 m) per mol of added Fe. However, the carbon sequestration efficiency for natural Fe fertilization (e.g. dust, volcanic ash, hydrothermal vents etc. [Breitbarth et al., 2010]) conducted in the Southern Ocean was estimated to be much higher ranging from 8640 molC/molFe [Pollard et al., 2009] to 154,000 molC/molFe [Chever et al., 2010]. This discrepancy might be a result of a ~ 75 % loss of Fe when artificially added to marine waters due to insufficient stabilization and less bioavailable Fe compared to Fe originated from natural Fe supply. Furthermore, other limiting factors become important when adding Fe artificially, such as light and zooplankton grazing [Breitbarth et al., 2010].

1.1.1.3 Bioavailability and speciation of iron

The bioavailability of Fe, defined as the fraction which can be used by organisms for biological uptake, controls productivity, species composition and trophic structure of planktonic communities in large regions of the oceans [Sunda, 2001] and is mainly determined by the speciation and solubility characteristics of Fe. A physico-chemical classification of different Fe species can be made by size and oxidation states, which are closely linked to Fe solubility.

Size classes

The size classification of Fe in aquatic environments originated historically due to the application of filtering methods through membranes with a defined pore size. The definition of different Fe species in terms of their size is illustrated in **Figure 1.2**.

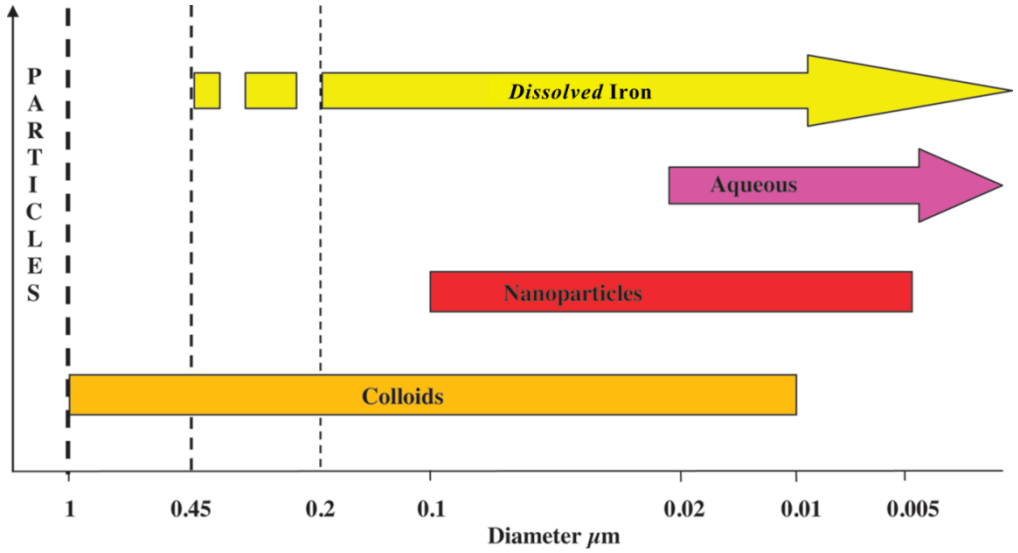

Figure 1.2: Different Fe size fractions apparent in aquatic environments (adapted from Raiswell and Canfield (2012)).

Usually, Fe is determined in natural waters as the dissolved fraction (in the following named as DFe). It is operationally defined as the portion remaining in a seawater sample after filtration through a 0.45 µm membrane filter. In more recent studies, DFe is defined by applying filtering procedures through 0.2 µm membranes. The DFe fraction encompasses a variety of different chemical and physical Fe forms, including colloids, nanoparticles and aqueous species with latter being operationally defined by filtering seawater through membranes with 0.02 µm pore size. Colloidal (10 nm to 1 µm) and nanoparticulate (5 nm to 100 nm) fractions mainly consist of Fe(oxyhydr)oxide aggregates,

possibly coprecipitated with organic matter [Raiswell and Canfield, 2012]. The aqueous fraction mainly comprises inorganic Fe(II) species in anoxic seawater, such as free Fe(II) ions (76 %) or $FeCO_3$ (23 %), and Fe(III) species under oxic conditions, mainly present as $Fe(OH)_2^+$, $Fe(OH)_3$ and $Fe(OH)_4^-$ [Millero et al., 1995]. It has to be noted that the above mentioned size limits of the different fractions are not strictly defined throughout the scientific environment and can vary between different studies and laboratories.

Redox speciation

Iron is a highly redox-sensitive element and its ions are present in two different oxidation states, Fe(II) and Fe(III). In the oxygenated seawater DFe pool, Fe(III) is the thermodynamically more stable species due to the formation of Fe(III) hydrolysis complexes. The oxidation kinetics of Fe(II) to Fe(III) can be described by the following rate law [Millero et al., 1987; Santana-Casiano et al., 2006]:

$$-\frac{d[\mathrm{Fe(II)}]}{dt} = k[\mathrm{Fe(II)}][\mathrm{O_2}][\mathrm{OH^-}]^2 \qquad (1.1)$$

With k being a temperature and ionic strength dependent rate constant. The reaction rate of the oxidation increases with higher Fe(II) concentrations [Fe(II)], higher oxygen concentrations [O_2] as well as higher hydroxide concentrations [OH^-], which comes along with an increased pH value. Thus the proportion of DFe expected to be present in the Fe(II) or Fe(III) forms will be influenced by the prevalent redox conditions determined by the aforementioned parameters, with an Fe(II) half-life in seawater ranging from 30 s to several hours [Moffett, 2001]. Under oxic conditions the proportion of [Fe(II)]/[Fe(III)] is estimated to be on the order of 10^{-10}, whereas an order of 10^7 would be expected under reducing conditions in anoxic seawater systems [Waite, 2001]. A transformation from Fe(III) to Fe(II) species occurs in seawater, mainly via photoreduction processes. Photoreduction of Fe(III) hydrolysis complexes to Fe(II) arises from 'ligand to metal charge transfer' reactions as most of the Fe(III) species are complexed by photoreactive organic ligands absorbing light in the solar spectral range and thus being an important transformation process in surface waters [Moffett, 2001].

Solubility and organic complexation of iron in seawater

Due to its high affinity for hydrolysis, Fe(III) is mainly prevalent in aquatic media as Fe hydroxide complexes. At lower pH values (pH < 5) free Fe(III) ions will be present (Fe^{3+} in **Figure 1.3**). The theoretical solubility of Fe(III) indicates DFe concentrations of the order of 0.1 nM [Waite, 2001] in seawater at a pH of ~ 8 at 20 °C, with the solubility curve showing its minimum at this pH value.

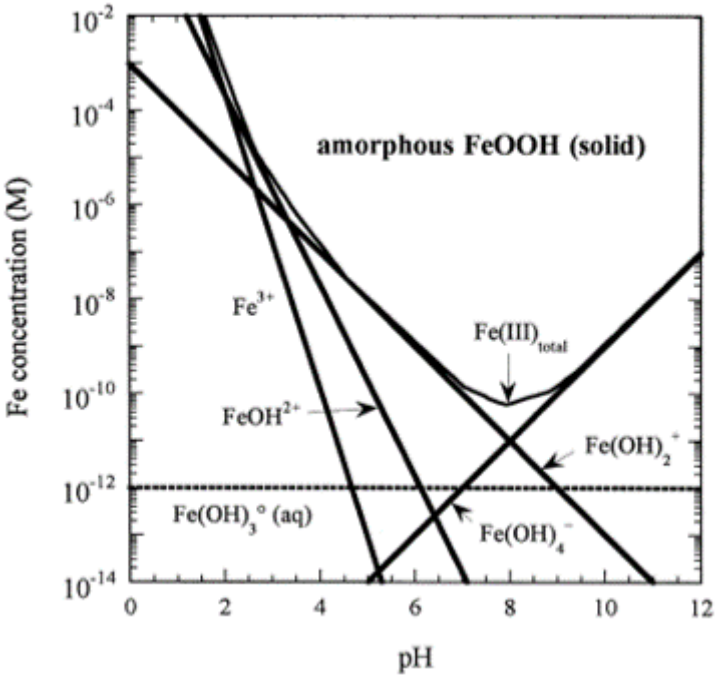

Figure 1.3: Solubility of different Fe(III) species as a function of pH [Stumm and Morgan, 1995].

However, DFe concentrations exceeding this solubility restriction were found in the world's oceans. It was suggested and also shown that organic complexation with stabilizing ligands plays a major role in Fe(III) speciation, buffering Fe(III) in the dissolved phase and preventing precipitation. Kuma and co-workers, for example, observed a decrease in DFe concentrations when irradiating the seawater sample with UV light, compared to untreated samples. The lower Fe(III) solubility was explained by decomposition of the organic ligands by UV light followed by the generation of particulate Fe(III) species [Kuma et al., 1996]. Furthermore, it was shown that 99.97 % of the dissolved Fe(III) phase in the surface waters of the central North Pacific was chelated by natural organic ligands [Rue and Bruland, 1995]. A spectrum of organic ligands is present in natural waters, enhancing the solubility of Fe. In a range of studies L_1 and L_2 ligands have been determined as two contrasting classes along the spectrum. Ligands of the type L_1 have a strong binding affinity as well as specificity to metals and are prevalent in relatively low concentrations and

predominant in open ocean as well as offshore coastal waters. Their stability constants were determined to be similar to siderophore-type ligands [Rue and Bruland, 1995]. A siderophore-aided dissolution has been suggested to enhance Fe concentrations beyond the Fe(III) solubility restriction. It was also found that organisms produce this type of ligands in order to promote the ability of Fe for uptake [Boiteau et al., 2016]. The L_2 type ligands exhibit a lower affinity to Fe, and are thought to include polysaccharides and humic substances [Öztürk et al., 2002; Raiswell and Canfield, 2012] and might be important in coastal and nearshore waters [Öztürk et al., 2002]. However, the interactions between Fe and humic species are complicated, especially in estuarine environments, due to gradients in chemical and physical properties such as salinity, activity coefficients of dissolved species as well as formation constants of Fe-ligand complexes. Additionally, ~ 90 % of DFe is removed along an estuary from solution due to the aggregation of Fe and humic substances to large colloids once DFe enters saline waters (e.g. by riverine input) [Boyle et al., 1977]. Nevertheless, the DFe concentration in coastal and estuarine waters may be orders of magnitude higher compared to DFe concentrations in open ocean waters [Breitbarth et al., 2009].

1.1.2 Manganese cycling

Manganese is, after Fe and titanium, the most abundant transition element in the earth's crust [Taylor, 1964], with the oxidation states Mn(II), Mn(III) and Mn(IV) representing the most stable Mn states in nature [Raiswell and Canfield, 2012]. The physico-chemical processes as well as the input fluxes of Mn in the water column are summarized in **Figure 1.4**.

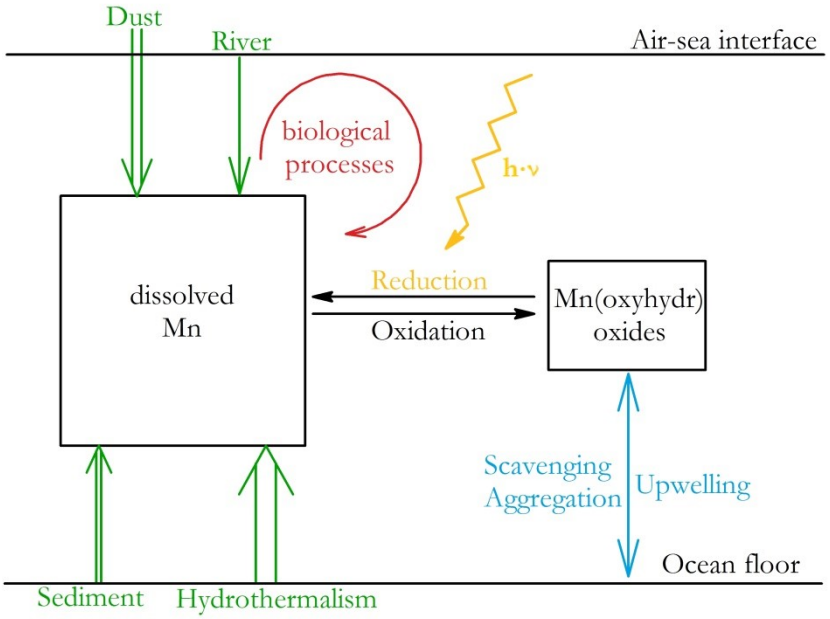

Figure 1.4: Scheme of the biogeochemical cycle of Mn in the ocean. Input fluxes are depicted in green color, chemical processes in black, photochemical processes occurring in the surface ocean in yellow, biological processes in red and removing/resupply processes in blue.

1.1.2.1 Sources and distribution of manganese

The distribution of Mn in the oceans is determined by its external inputs, such as atmospheric and riverine input, as well as sediment resuspension and hydrothermal supply (**Figure 1.4** and **Figure 1.5**). On a global scale, most of the Mn present in the world's ocean is originating from hydrothermal activity, with a modelled total input of 106,259 Mmol·yr^{-1} (relative amount: 64.3 %) [van Hulten et al., 2016]. Compared to Fe, it is assumed that hydrothermal sources deliver a high soluble Mn fraction to the oceans. Hydrothermal activity is the main Mn source in the Pacific, Indian, Southern and Arctic Ocean (**Figure 1.5(d)**), whereas most of the Mn in the Atlantic Ocean is originating from atmospheric input by dry deposition (dust) with 29,355 Mmol·yr^{-1} (**Figure 1.5(a)**).

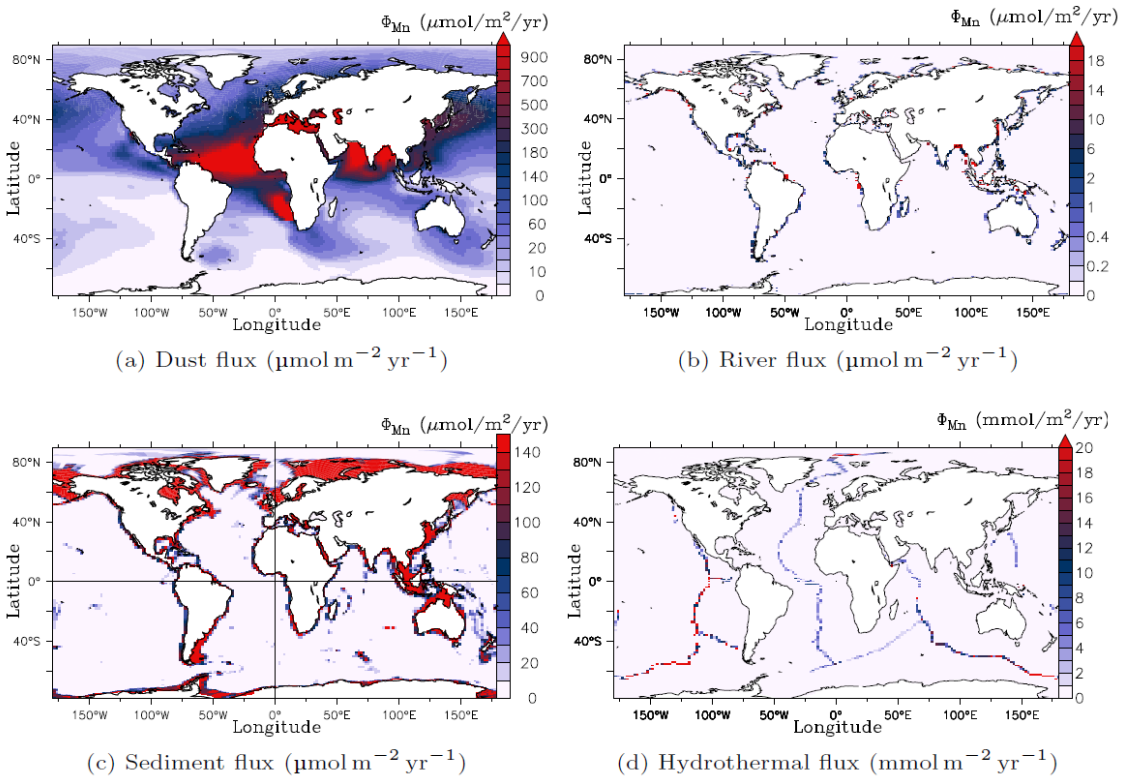

Figure 1.5: Mn input fluxes (dust, river, sediment, hydrothermal) to the world's oceans in μmol(mmol)/m²/yr [van Hulten et al., 2016].

On a global scale 31.5 % (52,117 Mmol·yr^{-1}) of the total Mn interior is brought via dust deposition to the world's oceans, with the largest contribution to the upper ocean. It is assumed that between 13 % and 92 % of the Mn contained in aerosols can be transferred into the dissolved phase depending on the origin and nature of the air mass [Baker et al., 2006]. Sediments deliver 4.1 % (6,727 Mmol·yr^{-1}) of the total Mn pool towards the water column. The Mn flux from sediments in certain regions, especially in shelf and slope regions of the polar oceans, can be of the same order as the dust deposition flux (**Figure 1.5(c)**) and is predominantly controlled by reductive processes keeping Mn(II) in solution [Vieira et al., 2018]. The Mn input flux from rivers is with 0.1 % of the total Mn input low on a global scale, but important on a local scale in estuary regions (**Figure 1.5(b)**).

A typical vertical distribution of dissolved Mn (DMn) in open ocean waters of e.g. the eastern Atlantic Ocean features elevated surface concentrations between 1.1 nM and 3.2 nM, rapidly decreasing with depth over the top few hundred meters to 0.15 nM observed in deeper waters [Statham et al., 1998]. The high surface concentration of Mn is a result of atmospheric inputs as well as photoreductive processes [van Hulten et al., 2016] (**Figure 1.4**). Removal of Mn from the dissolved phase via oxidative processes and scavenging leads to a decrease of DMn concentrations with increasing depth. In coastal

waters and fjordic systems like around the British Isles with salinities < 33 spatially highly variable DMn concentrations in the order of tens to hundreds of nM were found due to the supply of Mn through reducing sediments and continental runoff [Kremling and Hydes, 1988; Statham et al., 2005]. Also in regions with distinct hydrothermal activity elevated DMn concentrations in the hundreds of nM regime can be found [Chin et al., 1994].

1.1.2.2 Biogeochemical role of manganese

Manganese is an essential micronutrient in the world's oceans and critical for biological processes, such as photosynthesis and thus phytoplankton growth especially in Fe deficient seawater [Peers and Price, 2004]. Manganese is an essential part of the photosystem II, an enzyme located in the thylakoid membranes of all types of plants, algae and cyanobacteria, where the light-dependent reactions of photosynthesis take place. This multisubunit protein complex facilitates the formation of oxygen in the photosynthetic water-splitting process via the oxygen-evolving complex, a cluster of four Mn ions and one calcium ion [Barber, 2012]. It was found that the reproduction rate of marine phytoplankton and thus photosynthesis is limited when [Mn] < 100 pM [Brand et al., 1983], concentrations which can be found for example in the surface of the Southern Ocean [Middag et al., 2011]. Therefore, it is potentially a co-limiting factor for the regulation of primary production in HNLC regions and is involved in important enzymatic processes as an active metal center in metal-enzyme-complexes [Middag et al., 2011; Twining and Baines, 2013; Wolfe-Simon et al., 2006]. Additionally, it is assumed that the Mn cycle and the nitrogen cycle are closely linked as Mn facilitates the formation of dinitrogen via the oxidation of nitrate by Mn(II) in for example the suboxic waters in the Black Sea [Murray et al., 1995] and the reduction of ammonia by MnO_2 in Mn-rich continental margin sediments [Luther et al., 1997]. Furthermore, the oxidized form of Mn can play an important role in the scavenging of rare earth elements and other elements due to inorganic adsorption processes while sinking [Tachikawa et al., 1997].

1.1.2.3 Manganese speciation in natural waters

In natural waters, Mn is mainly present as soluble Mn(II) as well as insoluble Mn(III) and Mn(IV) (oxyhydr)oxides. Therefore, the DMn phase in natural waters mainly consists of bioavailable Mn(II) species, whereas Mn(oxyhydr)oxides are present in particulate phases and will be lost from the water column by sinking (**Figure 1.4**). Reaction times of a few

days were found for microbially mediated Mn(II) oxidation [Emerson et al., 1982; Sunda and Huntsman, 1987] compared to a reported Fe(II) half-life on the order of seconds to hours in oxic waters [Moffett, 2001], enabling Mn(II) to be present in oxic waters and leading to the precipitation of oxidized Fe species prior to oxidized Mn species in natural waters [Krauskopf, 1957; Vieira et al., 2018]. Additionally, the cycles of Fe and Mn might directly interact according to the following reaction [Postma, 1985]:

$$MnO_2 + 2Fe^{2+} + 4H_2O \longrightarrow Mn^{2+} + 2Fe(OH)_3 + 2H^+ \quad (1.2)$$

Postma (1985) found that MnO_2 can remove Fe from the water column via oxidation of Fe(II) to insoluble amorphous Fe(oxyhydr)oxide under conditions found in seawater, while producing reduced soluble Mn(II) species.

Furthermore, in the photic zone Mn is noticeably affected by photochemical processes. Especially, reductive dissolution processes of particulate Mn oxides are mediated by light, generating diurnally partitioning of Mn between the dissolved and particulate species [Sunda et al., 1983; Waite and Szymczak, 1993]. The photochemical reduction process keeps Mn in solution by prevention of Mn oxide formation with subsequent removal by sinking.

1.2 Trace metal determination in seawater

The determination of trace metal concentrations, and their speciation, in the pico- to nanomolar range in natural waters requires sensitive and accurate analytical techniques with appropriate detection limits in order to provide high quality data. Until the 1970s/80s dissolved trace metal concentrations in open ocean waters were reported at up to three orders of magnitude higher levels than nowadays [Achterberg et al., 2001; Varney, 2000] (**Figure 1.6**). This decrease in reported DFe concentrations (or in general trace metal concentrations) down to the pM range is rather a result of an improved understanding of potential contamination factors, better sample handling as well as the development of refined analytical techniques than a result of oceanographic processes. Therefore, it is inevitable to develop and comply with protocols for trace metal clean sample collection, handling and analysis, e.g. the GEOTRACES Cookbook, in order to obtain accurate and intercomparable measurements.

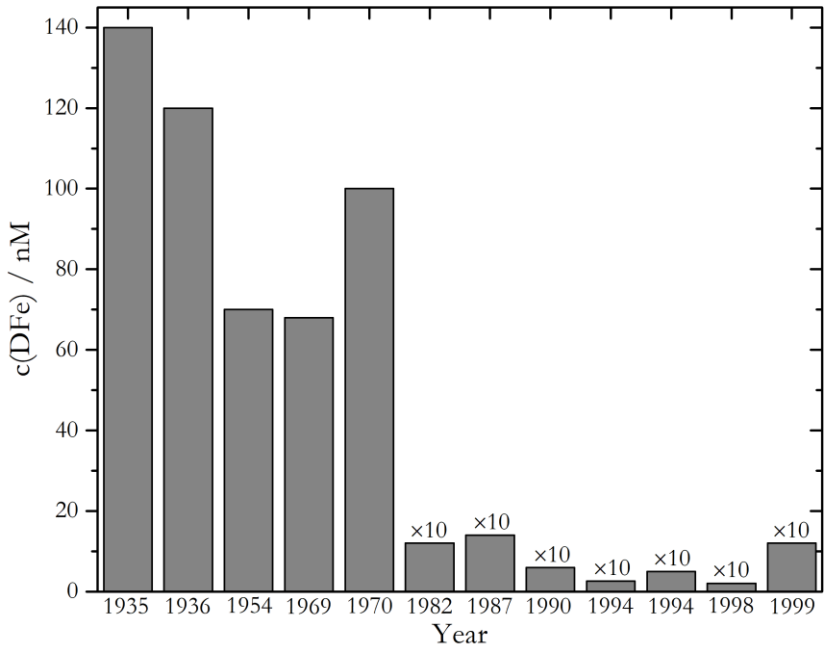

Figure 1.6: History of reported DFe concentrations determined with a variety of analytical methods in open ocean waters. In order to gain visibility values from 1982 onwards were multiplied by 10, values were taken from Achterberg et al. (2001).

1.2.1 Common analytical methods

The main analytical methods for the determination of Fe and Mn concentrations in seawater include atomic spectrometry, stripping voltammetry, spectrophotometry and chemiluminescence.

The most common technique for trace metal analysis in the 1970s and 80s was atomic spectrometry, in fact graphite furnace atomic absorption spectrometry (GFAAS) and more recently inductively coupled plasma mass spectrometry (ICP-MS) [Worsfold et al., 2014]. However, these methods require a pre-concentration or solvent extraction step prior to analysis in order to remove the seawater matrix [Bruland et al., 1979]. Solvent extraction methods were recently replaced by pre-concentration using solid-phase chelation with subsequent analysis via GFAAS [Bruland et al., 1994] or ICP-MS [Rapp et al., 2017]. Atomic spectrometry can provide high accuracy and precision with a detection limit down to the pM range [Achterberg et al., 2001]. A disadvantage of these techniques is that they do not allow for the determination of redox speciation and can be, in particular due to their bulkiness, just used in a controlled laboratory environment. However, GFAAS and ICP-MS are frequently used as reference method for ship board or *in situ* measurements of dissolved trace metal concentrations, as done in this work. Alternative analytical methods for the determination of Fe and Mn concentrations in seawater are provided by

voltammetry [Gledhill and van den Berg, 1995; Luther et al., 1999], spectrophotometry (see next section) and chemiluminescence [Bowie et al., 1998; Ussher et al., 2009] which can be used for both, shipboard as well as laboratory based measurement. All three methods generally do not require removal of the seawater matrix and allow redox speciation, with spectrophotometric techniques potentially being most suitable for *in situ* applications.

1.2.2 Spectrophotometric determination of iron and manganese in seawater

Spectrophotometry is probably the earliest used method for the determination of Fe in seawater with a first reported study from 1935 [Cooper, 1935]. It can be classified into two different groups, the derivatization method and the catalytic method [Achterberg et al., 2001]. Derivatization methods rely on the selective reaction of a certain redox state of Fe or Mn with a complexing agent, producing a colored complex with a high molar absorptivity. Due to the color formation the Fe or Mn-ligand complex can then be detected spectrophotometrically with the intensity of the color being proportional to the metal concentration (see section 2.1). This method allows the determination of total Fe or Mn concentrations by applying appropriate reducing reagents prior to the complex formation in order to have all the dissolved metal in a reduced form. The second spectrophotometric method utilizes the ability of metal ions to catalyze reactions that can be monitored spectrophotometrically due to a change of the absorption intensity. Common reagents which are used throughout the literature for Fe and Mn determination in seawater for both the derivatization as well as catalytic method are listed in **Table 2** and **Table 3**, respectively.

Table 2: Reagents commonly used for the spectrophotometric detection of Fe in seawater. The sensitivity of each reagent is given as molar absorptivity (ε) in $L \cdot mol^{-1} \cdot cm^{-1}$ (see section 2.1) at the absorption maximum. Grey cells indicate use in catalytic methods, and others are used in derivatization methods.

Compound	Sensitivity	Advantage	Disadvantage	References
Tiron	4,170 at 558 nm		− low sensitivity − absorption maximum depends strongly on pH	[Abe et al., 1986]
BPA	22,000 at 540 nm		− ethanol as solvent − hexanol extraction − low recovery and precision when organic matter is present	[McMahon, 1969; Pollock and Miguel, 1967; Verschoor and Molot, 2013]
TPTZ	22,300 at 594-595 nm	− little interferences − fast reaction	− autoreduction − expensive	[Verschoor and Molot, 2013] [Kremling et al., 2007]
Ferrozine	27,900 at 562 nm	− little interferences − fast reaction − wide pH range		[Stookey, 1970; Viollier et al., 2000]
Ferene	34,500 at 593 nm	− little interferences − fast reaction − wide pH range		[Hennessy et al., 1984; Meyer et al., 2012]
Morin	68,500 at 415 nm	− high sensitivity − fast reaction	− V(V), Fe(III), Al(III) interference − ethanol as solvent	[Ahmed and Roy, 2009]
DPD	$17 \cdot 10^6$ at 514 nm	− fast reaction time − high sensitivity	− no redox speciation possible	[Achterberg et al., 2001; Hirayama and Unohara, 1988]

Table 3: Reagents commonly used for the spectrophotometric detection of Mn in seawater. The sensitivity of each reagent is given as molar absorptivity (ε) in $L \cdot mol^{-1} \cdot cm^{-1}$ (see section 2.1) at the absorption maximum. Grey cells indicate use in catalytic methods, and others are used in derivatization methods.

Compound	Sensitivity	Advantage	Disadvantage	References
Formaldoxime	10,700 at 450 nm		− poor linearity − low sensitivity − interference with Fe, Ni, Co, Cu	[Chiswell and O'Halloran, 1991; Kremling et al., 2007]
PAN	44,000 at 562 nm	− high sensitivity − fast reaction	− surfactant needed − interference with Fe(III)	[Chin et al., 1992; Goto et al., 1977; Meyer et al., 2016]
T4CPP	95,400 at 468 nm	− high sensitivity − fast reaction	− toxic Cd^{2+} is used	[Chiswell and O'Halloran, 1991; Madison et al., 2011]
Leucomalachite green	Not reported	− very low detection limit	− pre-concentration necessary	[Massoth et al., 1998; Resing and Mottl, 1992]

1.2.2.1 Common complexing agents for iron analysis

DPD (N,N-Dimethyl-p-phenylenediamine) is by far the most sensitive spectrophotometric reagent for the quantitative determination of Fe in seawater, according to its molar absorptivity of $\varepsilon = 17 \cdot 10^6$ L·mol^{-1}·cm^{-1} [Hirayama and Unohara, 1988]. Its oxidation by hydrogen peroxide is catalyzed by Fe(III) and the formation of the oxidation product can be followed spectrophotometrically at 514 nm. However, the major disadvantage of this method is that it does not allow the determination of the redox speciation, which is possible with the use of Fe complexing agents for the derivatization method. All of the Fe ligands listed in **Table 2** selectively bind the divalent Fe(II) species. Here, Morin (2-(2,4-Dihydroxyphenyl)-3,5,7-trihydroxychromen-4-one) represents the most sensitive complexing agent for Fe(II), forming an Fe(II)-Morin$_2$ complex with a molar absorptivity of ε = 68,500 L·mol^{-1}·cm^{-1} at 415 nm. However, major drawbacks of this complexing agent are its interference with other cations and the need of organic solvents like ethanol due to its poor water solubility. This might create difficulties for *in situ* applications as the sensor materials can be susceptible to organic solvents. The same problem arises for BPA (4,7-Diphenyl-1,10-phenanthroline). Additionally an extraction step with hexanol is required to solubilize the formed Fe-BPA complex, which might be not applicable in automated systems. Furthermore, the BPA method provides a low recovery and precision when organic matter is present. The use of organic solvents is not required when using the water soluble ligand Tiron (Disodium 4,5-dihydroxy-1,3-benzenedisulfonate) as complexing agent. However, Tiron suffers from a low sensitivity for Fe with a molar absorptivity of just 4,170 L·mol^{-1}·cm^{-1} and a strong pH dependency at the absorption maximum. TPTZ (2,4,6-Tris(2-pyridyl)-s-triazine) seems to be an eligible candidate for Fe determination, providing a good sensitivity with ε = 22,300 L·mol^{-1}·cm^{-1}, few interferences and a fast reaction, but TPTZ is quite expensive and favors autoreduction of a considerable fraction of Fe(III) to Fe(II), producing an increase in absorbance with time and therefore overestimates Fe(II) concentrations. The effect of autoreduction is minor when using the structurally closely related water soluble ligands Ferene (3-(2-Pyridyl)-5,6-di(2-furyl)-1,2,4-triazine-5',5"-disulfonic acid disodium salt) and Ferrozine (FZ; 3-(2-Pyridyl)-5,6-diphenyl-1,2,4-triazine-p,p-disulfonic acid monosodium salt hydrate). They can form complexes with Fe(II) over a wide pH range and show few interferences from other cations, with a fast reaction rate. Their associated Fe(II) complexes provide good stabilities with logK values of 15.6 (FZ) and 14.9 (Ferene) [Hennessy et al., 1984] as well as a good sensitivity with a molar absorptivity of ε(FZ) = 27,900 L·mol^{-1}·cm^{-1} at 562 nm and

ε(Ferene) = 34,500 $L \cdot mol^{-1} \cdot cm^{-1}$ at 593 nm, making them suitable candidates for Fe detection in automated systems.

In order to determine the Fe(III) concentration, all Fe(III) can be reduced to Fe(II) using an appropriate reducing agent followed by spectrophotometric analysis. Fe(III) can then be determined by subtraction of the Fe(II) concentration obtained through analysis without a reducing agent from the Fe(II) concentration obtained with reducing agent.

1.2.2.2 Common complexing agents for manganese analysis

Compared to the various number of complexing agents which can be used for the determination of Fe, just a few can be found in the literature for the spectrophotometric Mn determination in seawater (**Table 3**). The formaldoxime method provides a moderate sensitivity towards Mn with a molar absorptivity of the Mn-formaldoxime complex of ε = 10,700 $L \cdot mol^{-1} \cdot cm^{-1}$ and poor linearity. Interference problems arise when other cations like Fe, Ni, Co or Cu are present. The PAN (1-(2-pyridylazo)-2-naphthol) method also suffers from interference problems, especially with Fe(III). However, this issue can be minimized by applying an Fe(III) masking agent. It has a good sensitivity towards Mn(II) with a molar absorptivity for the Mn(II)-PAN complex of ε = 44,000 $L \cdot mol^{-1} \cdot cm^{-1}$, although the formed complex as well as the PAN reagent itself is poorly water soluble. Therefore, a surfactant is introduced in order to form micelles and solubilize PAN and its associated Mn complex (see section 2.3). The most sensitive complexing agent for Mn(II) might be T4CPP (meso-tetrakis[4-(carboxymethyleneoxy)phenyl]porphyrin) with ε = 95,400 $L \cdot mol^{-1} \cdot cm^{-1}$ of the corresponding Mn(II) complex, which is formed instantaneously. However, a major disadvantage of this method is the use of Cd^{2+} in a metal substitution reaction as Cd^{2+} shows an acute toxicity for organisms [Qu et al., 2013]. A catalytic method is also available for Mn. It relies on the reaction of leucomalachite green with potassium periodate to malachite green catalyzed by Mn(II). This method provides a detection limit down to the pM range but requires also a pre-concentration step.

Currently the PAN method seems to be the best choice for the determination of Mn in seawater. Coincidentally, the absorption maximums of the Mn-PAN complex and that of the Fe-FZ complex are both located at 562 nm which might allow the determination of both, Fe and Mn, with the same automated hardware as will be evaluated throughout this work.

1.3 *In situ* approach

The marine environment is negatively affected by anthropogenic pressures especially in the coastal but also in the open ocean regions. Our understanding of the impacts of activities such as dumping of waste, use of fertilizer, shipping traffic, construction of harbors etc. on the environmental quality of our marine environment is still low and requires continuous monitoring of a wide range of biological, chemical and physical parameters under often harsh environmental conditions. Therefore, reliable *in situ* sensing approaches are highly demanded, also to improve our understanding of e.g. the essential biogeochemical processes, their interactions, the ocean's role in the global carbon cycle and its response to a changing climate.

1.3.1 Limitations of conventional sampling analysis approach

Oceanic processes can span a wide range regarding their temporal and spatial changes. Molecular processes for example take place in the centimeter and minute range, tidal processes occur in a diurnal pattern over tens to hundreds of kilometers, whereas oceanic gyre circulation can span decades with a spatial range up to thousands of kilometers [Prien, 2007]. In order to resolve all these processes a vast amount of data has to be acquired on a large temporal and/or spatial scale. Most of the characterization of the marine environment still relies on the conventional approach of collecting discrete water samples followed by their analysis either directly on the research vessel or in the home laboratory. However, this sampling and analysis approach leads to a prevalent undersampling of the oceans as it cannot meet the requirements of producing highly resolved data, preferentially remotely acquired. Ship-based oceanographic campaigns involve a high carbon-footprint as they require substantial logistical efforts with typical time delays of up to several months between sample collection and lab-based chemical analysis.

The undersampling problem is illustrated in **Figure 1.7** using the example of nitrate measurements in the Monterey Bay over a range of ~ 90 days. Here, the dynamics in nitrate concentration measured with a sensor on an hourly basis (upper panel) cannot be captured with the sampling analysis approach neither by collecting samples on a weekly basis nor at 3 day intervals (lower panel). Furthermore, the sampling analysis approach is expensive, time-consuming, demands good infrastructural conditions due to the required transport and storage of the collected samples. An additional problem linked to the

sampling analysis approach is the risk of contamination during sample collection, storage or treatment prior to analysis. Some compounds of interest might be labile and degrade over time in case the delay between sample collection and analysis is too long. Also the samples integrity might be compromised when collecting at depths and low temperatures and storing them under ambient pressure and temperature.

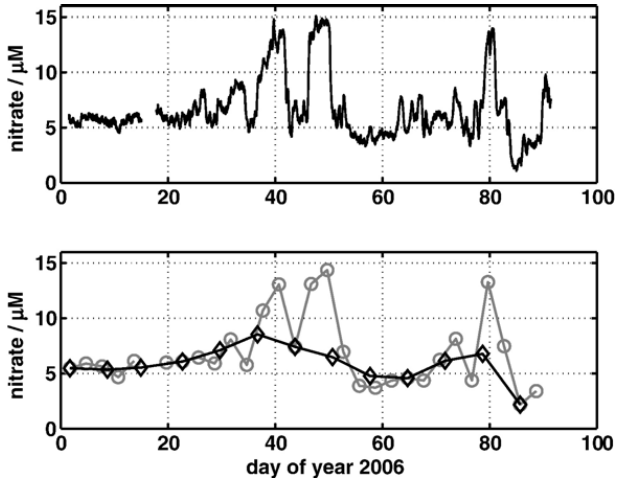

Figure 1.7: Nitrate concentrations in Monterey Bay measured hourly via the *in situ* sensing approach (upper panel) and using the sampling analysis approach with a sampling frequency of 7 days and 3 days (lower panel) [Prien, 2007].

1.3.2 Reported *in situ* analyzers for DFe and DMn species in seawater

Several automated systems and *in situ* analyzers for DFe and DMn, most of them based on spectrophotometry, have been developed in order to overcome the drawbacks of the laborious conventional laboratory based methods and to avoid time consuming and costly ship-based sample collection, handling, treatment and storage. A selection of those analyzers will be introduced chronologically in the following sections.

SCANNER

One of the earliest reported automated submersible analyzers for *in situ* observations in hydrothermal vent fields is the SCANNER, first designed for the determination of silicic acid and sulfide [Johnson et al., 1986] and later adapted for Fe and Mn measurements [Chin et al., 1994; Coale et al., 1991]. It relies on the unsegmented continuous flow of the sample mixed with the respective reagents, followed by on-line spectrophotometric detection. The FZ (+ ascorbic acid as reducing agent) and the PAN method were utilized in order to quantify the concentrations of DFe and DMn, respectively, with reported limits of detection of 25 nM for Fe and 22 nM for Mn. The SCANNER is able to perform *in situ* calibration with on-board blank and standard solutions. The flow is regulated by peristaltic

pumps, with a consumption of 0.8 mL·min^{-1} for sample, blank and standards, 0.15 mL·min^{-1} for PAN and FZ reagent and 0.2 mL·min^{-1} for the ascorbic acid.

SUAVE

The Submersible System Used To Assess Vented Emissions (SUAVE) represents a second generation of the SCANNER and is also capable of measuring DFe and DMn based on the spectrophotometric determination from a continuous-flow sample stream with injection of reagents [Massoth et al., 1995, 1998]. Different from the SCANNER, the SUAVE utilized catalytic analytical techniques with leucomalachite green and DPD, as described in section 1.2.2, for the detection of Mn and Fe, respectively. Detection limits of < 10 nM for DMn and < 5 nM for DFe were reported with a response time of 45 s. No information on the flow rates were found in the literature but it is expected that the sample and reagent consumption is comparable to the SCANNER.

Voltammetric *In situ* Profiler (VIP)

The VIP system is, in contrast to the above introduced analyzers, based around a submersible voltammetric probe and does not rely on the supply of reagents. It allows measurements of the trace metal fractions of Cu(II), Pb(II), Cd(II), Zn(II), Mn(II) and Fe(II) in natural waters down to the pM range using either square wave anodic stripping voltammetry or square wave cathodic sweep voltammetry [Tercier et al., 1998]. Reliable continuous real time monitoring was demonstrated in seawater for the determination of Cu(II), Pb(II) and Cd(II) [Braungardt et al., 2009, 2011; Tercier-Waeber et al., 1999], whilst studies for the quantification of Fe(II) and Mn(II) in seawater have not been reported.

Fe-OsmoAnalyzer

The submersible osmotically pumped analyzer Fe-OsmoAnalyzer was developed for the long-term continuous high resolution monitoring of Fe(II) and Fe(III) in hydrothermal vents using FZ as spectrophotometric reagent [Chapin et al., 2002]. The major advantage of the Fe-OsmoAnalyzer, compared to SCANNER and SUAVE, is its very low fluid consumption due to the use of osmotic pumps. Just 18 µL sample and 0.25 µL reagents were used per hour, with the analysis of one sample every 15 minutes, which allows deployments with a duration up to one year. A relatively high limit of detection of 100 nM was reported with a linear range up to 50 µM. But however, these values might be appropriate for the intended use in hydrothermal vents were Fe can be elevated up to the micro- to millimolar range [Douville et al., 2002; Gallant and Von Damm, 2006].

***In situ* dissolved Mn analyzer system**

In order to map the 3D spatial distribution of DMn in coastal waters an *in situ* DMn analyzer system was developed and interfaced to an autonomous underwater vehicle [Statham et al., 2003, 2005]. Similarly to the analyzers mentioned before, the *in situ* DMn analyzer system also relied on a continuous flow of the sample with the reagent (PAN) being injected into the sample stream. The flow was controlled with a peristaltic pump creating a combined flow of 1.6 $mL \cdot min^{-1}$, therefore capable of short-term deployments. The analyzer was able to perform *in situ* calibrations with on-board blank and standard and acquired DMn concentrations with a frequency of 0.1 Hz. The reported limit of detection was 25 nM.

ALCHIMIST

As most of the afore introduced *in situ* analyzers, the 'Analyseur chimique *in situ*' (ALCHIMIST) was developed for the determination of DFe concentrations in hydrothermal environments [Sarradin et al., 2005]. The ALCHIMIST was designed as flow injection analysis system with the injection of the sample and FZ reagent into a carrier stream (35 $g \cdot L^{-1}$NaCl). Flow rates were regulated with a peristaltic pump, 0.8 $mL \cdot min^{-1}$ for sample, blank, standards and carrier and 0.4 $mL \cdot min^{-1}$ for ascorbic acid and FZ reagent. The ALCHIMIST provided a high sampling frequency with 22 samples being analyzed within one hour and on-board calibration. The detection range was reported between 300 nM up to 100 μM.

CHEMINI

A similar setup to the ALCHIMIST was used for the *in situ* CHEmical MINIaturized analyzer (CHEMINI) which was also based on the FZ method for the detection of DFe in hydrothermal vent environments [Laes-Huon et al., 2014, 2016; Vuillemin et al., 2009]. As for the ALCHIMIST the limit of detection was 300 nM, with a detection range up to 100 μM DFe. On-board calibrations were performed before and after sample analysis using four internal standards.

METIS

The METals *In situ* analyzer (METIS) for the detection of DMn represents so far the latest developed *in situ* analyzer for the detection of trace metals in Baltic seawaters [Meyer et al., 2016]. It utilized the PAN method for the spectrophotometric detection of DMn in a multi-pumping flow-system. Instead of using peristaltic pumps, the reagent and sample

flow is regulated with solenoid pumps, producing a pulsed flow once activated. A detection limit of 77 nM was obtained with a highly linear calibration line.

1.3.3 Limitations of current *in situ* analyzers

Most of the above introduced wet chemical analyzers for Fe and Mn detection in seawater suffer from high reagent and sample/standard consumption up to several mL per minute. The high fluid consumption, which is typically also linked to a high power consumption due to the operation of the pumps, limits long-term deployments (weeks to months), unless a vast amount of liquids as well as an unlimited power supply is provided. The reported detection limits and ranges were adequate for the proposed use in hydrothermal environments with elevated Fe and Mn concentrations, however insufficient for measurements in regions with Fe and Mn concentrations in the lower nM regime, e.g. coastal waters. Furthermore, the physical size of many of the analyzers limits the portability and the user-friendliness. A modular design, where electronics manifold, fluid reservoirs or detection elements are physically separated into different modules might restrict the possibility of interfacing the analyzers to observing platforms, which are limited in space. Therefore, miniaturization is the key in developing the 'ideal' Fe and Mn analyzer and to overcome the above mentioned limitations of the up to the present developed Fe and Mn analyzers.

1.3.4 The 'ideal' sensing approach and quality assurance

In order to overcome the above mentioned problems associated with the sampling analysis approach *in situ* methods are required which measure the variables of interest directly in the marine environment. However, *in situ* devices need to meet a vast number of criteria to become suitable for their operation in the field, e.g. low limit of detection for the respective variable with a good selectivity, easy to maintain, low cost, low power consumption, portability, minimal direct operator intervention. An overview of all the criteria and aspects needed to be taken into account for the development of a theoretical 'ideal' sensor is given in **Figure 1.8**.

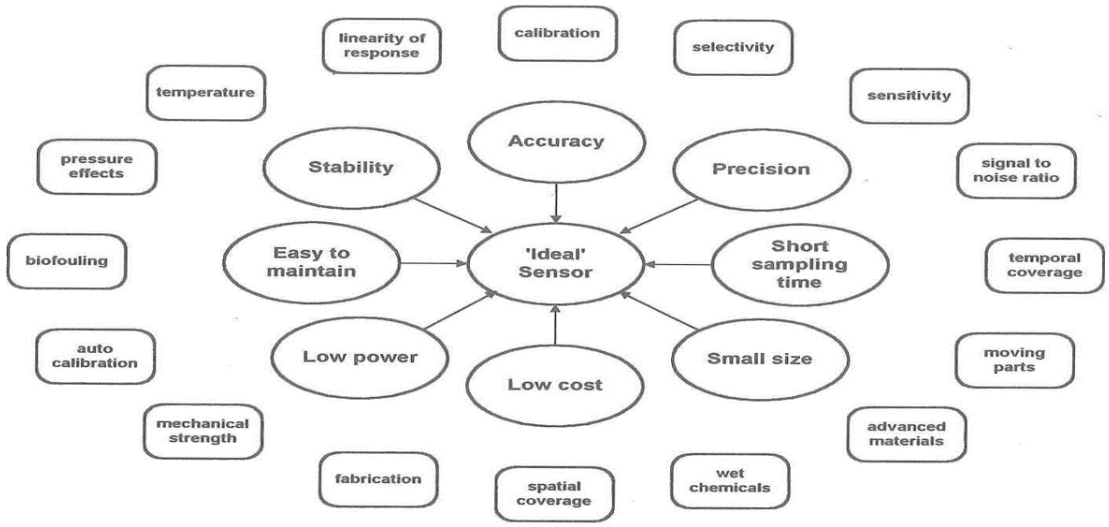

Figure 1.8: Specifications for an 'ideal' sensor for marine applications [Varney, 2000].

The development of a sensor towards a high technology readiness level (TRL) is a long process, starting from scratch to a final commercialization. Within these development phases the sensor needs to go through a careful validation process in order to test the reliability of the system and to confirm "by examination and the provision of objective evidence that the particular requirements for a specific intended use are fulfilled" [ISO/IEC 17025, 2005]. The validation of the method comprises several validation parameters, such as precision, accuracy, linearity, selectivity, limit of detection and quantification, reproducibility, robustness against external influences and cross-sensitivity against interferences from the sample matrix. Furthermore, the method has to be relevant to the customer's needs, e.g. it has to be taken into account on which platform the sensor should be deployed. For example, sensors on moving platforms such as ARGO floats or gliders need a high temporal resolution (preferably > 1 measurement min^{-1}), whereas sensors for the integration on a stationary cabled observatory should meet the requirement for long-term deployments. The quality assurance of a developed method or sensor should be performed using one or a combination of the following suggestions: (i) calibration using reference standards or reference materials, (ii) comparison of results achieved with other analytical methods, (iii) interlaboratory comparisons, (iv) systematic assessment of the factors influencing the result and (v) assessment of the uncertainty of the results based on scientific understanding of the theoretical principles of the method and practical experience [ISO/IEC 17025, 2005]. Additionally the metrology needs to be evaluated in order to gain and assure long-term confidence in the repeatability and reproducibility of measurements in order to make long-term and high precision comparisons for the understanding of oceanic processes and dynamics [Martinez et al., 2018].

1.3.5 Lab-on-chip technology

Microfluidic technology forms one of the most powerful approaches for the development of the 'ideal' Fe and Mn *in situ* analyzer in order to meet the criteria mentioned above. This approach utilizes the miniaturization of an analytical procedure, usually conducted in the laboratory with benchtop devices, for the integration on a micro scale chip device, therefore also called 'Lab-on-chip' (LoC). A LoC device integrates all steps of analysis (sampling, sample treatment, chemical reaction, detection, data processing) on a single instrument. Major advantages of this technology are the small size, portability, low power and reagent consumption (in the μL range) and its ability for long-term deployment on for example cabled observatories [Campos and da Silva, 2013; Nightingale et al., 2015]. This technology is already widespread and a useful tool in the bio-medicine [Giannitsis and Min, 2010; Wu et al., 2018]. In the recent years it was also adapted and optimized for nutrient analysis and pH measurements in marine environments by the 'Ocean Technology and Engineering Group' of the National Oceanography Centre Southampton [Beaton et al., 2011; Grand et al., 2017; Ogilvie et al., 2011; Rérolle et al., 2013; Yuecel et al., 2015]. Within the study presented in this work a LoC device is adapted for the detection of Fe and Mn, in a laboratory environment and finally tested and deployed in natural seawater environments.

1.4 Thesis objectives

Fe and Mn are both involved in crucial biogeochemical processes such as primary production and respiration. Their cycles interplay with other biogeochemical cycles such as oxygen, nitrogen or phosphorus as well as the global carbon cycle. In order to gain a better understanding of those processes it is inevitable to measure their concentrations, speciation and dynamics in the marine environment on well resolved temporal and spatial scales. However, due to their extended physico-chemical speciation (in terms of size fractions, different redox species, organically complexed etc.) exact determination of their concentrations is challenging. The conventional method of analyzing discrete samples via atomic spectrometry does not allow for the determination of redox speciation, is expensive and time-consuming. For the acquisition of highly resolved data *in situ* sensing is key. Here, spectrophotometry represents a good alternative due to the possibility of miniaturization and integration of the whole analysis procedure from sampling, chemical analysis to data processing into one device. Several *in situ* analyzers have been developed for Fe and Mn

analysis based on flow injection approaches mostly for the application in hydrothermal environments. Most of those devices suffer from high reagent and power consumption, high limits of detection, bulkiness or inability for long-term deployments (weeks to months).

Therefore, we present here a microfluidic LoC approach for the determination of Fe and Mn with the aim to overcome these issues and to contribute to the development of a global *in situ* observing system for trace metals. The overall research questions and objectives driving this work are the following:

- Adaptation of the FZ method for its use on an *in situ* system based around a microfluidic chip.

- Validation of the *in situ* FZ method in real seawater environment using discretely collected samples analyzed via ICP-MS as reference technique according to GEOTRACES protocol.

- What kind of adaptation measures, both chemical and physical, are necessary to improve the performance of the analyzer regarding the comparability of *in situ* determined DFe concentrations with those of discretely collected samples analyzed via ICP-MS?

- Adaptation and validation of the PAN method for *in situ* determination of DMn species using a LoC device.

- Which marine environments are suitable for the deployment of the analyzers in their current state considering their sensitivities?

The used FZ method for Fe and PAN method for Mn as well as the fabrication and operation of the LoC analyzers will be introduced in detail in chapter 2. Chapter 3 focusses on the validation and first test deployment in the Kiel fjord of the first version of the Fe analyzer. This chapter has been already published [Geißler et al., 2017]. The adaptation of the FZ method as well as the validation and test deployment of a second-generation analyzer with an implemented acidification step in order to improve recovery is presented in chapter 4. The first version of the Fe analyzers was adapted for the use of the PAN method for the detection of Mn. These results will be shown in chapter 5.

2 Methods and materials

2.1 Spectrophotometry

The experimental work in this thesis is mainly based on spectrophotometry. Therefore, the basic principle of this optical method is concisely explained in the following section.

Spectrophotometry relies on the interaction of photons with molecules. Upon absorption of electromagnetic radiation in the UV/VIS range (wavelengths between 200 nm and 800 nm) molecules can be excited into higher electronical states due to the transition of electrons. The energy which needs to be absorbed for the excitation from the ground state of the molecule to an energetically higher state reaches discrete values, also known as quantization of energy states. The energy difference ΔE of the two involved states (ground state E_1 and excited state E_2) can be described with the following resonance condition (2.1).

$$\Delta E = E_2 - E_1 = h \cdot \upsilon = h \cdot \frac{c_{light}}{\lambda} \tag{2.1}$$

When the energy of a photon, which is defined by the product of the Planck constant h with its frequency υ (or speed of light c_{light} divided by the wavelength λ of the photon), meets the resonance condition its energy can be absorbed by the molecule resulting in an electron transfer. It was empirically found that this absorption can be observed via a loss of light intensity while light of a certain wavelength is propagating through a solution of the concentration c over a certain length d. According to equation (2.2) the intensity I is decreasing exponentially, with the intensity I_0 of the incident radiation and the absorption coefficient ε' as proportionality constant.

$$I = I_0 \cdot e^{-\varepsilon' cd} \tag{2.2}$$

After mathematical transformation of the exponential equation (2.2) to a $\log_{10}$ scale a linear expression (2.3) for the dimensionless absorbance A, also known as Beer-Lambert law, is obtained:

$$A(\lambda) = -\log_{10}\left(\frac{I}{I_0}\right) = -\log_{10} T = \varepsilon(\lambda) \cdot c \cdot d, \tag{2.3}$$

where the absorbance is defined as negative logarithm to the base 10 of the transmission T. The molar extinction coefficient $\varepsilon(\lambda)$ in L·mol^{-1}·cm^{-1} is a property of the absorbing analyte and depends on the wavelength and temperature. The coefficient increases with the effective cross section for the absorbance of the analyte. It has to be noted that the Beer-Lambert law is linear over a limited range with respect to the concentration of the analyte [Mäntele and Deniz, 2017]. In case the analyte itself is not able to absorb light in the UV/VIS range, like it is for metal ions, a ligand which selectively forms a colored complex with the metal ion can be added, as introduced earlier in section 1.2.2.

2.2 Ferrozine method

The Ferrozine (FZ) method for the quantitative determination of Fe in aquatic samples was first developed by Stookey (1970) as a low cost alternative to reagents like TPTZ and BPA [Stookey, 1970]. These reagents are similar in their structure regarding the bidentate Fe(II) binding group, also referred to as the Ferroin group ($-N = C - C = N -$). This group binds the Fe(II) ion selectively via the two nitrogen atoms (**Figure 2.1**).

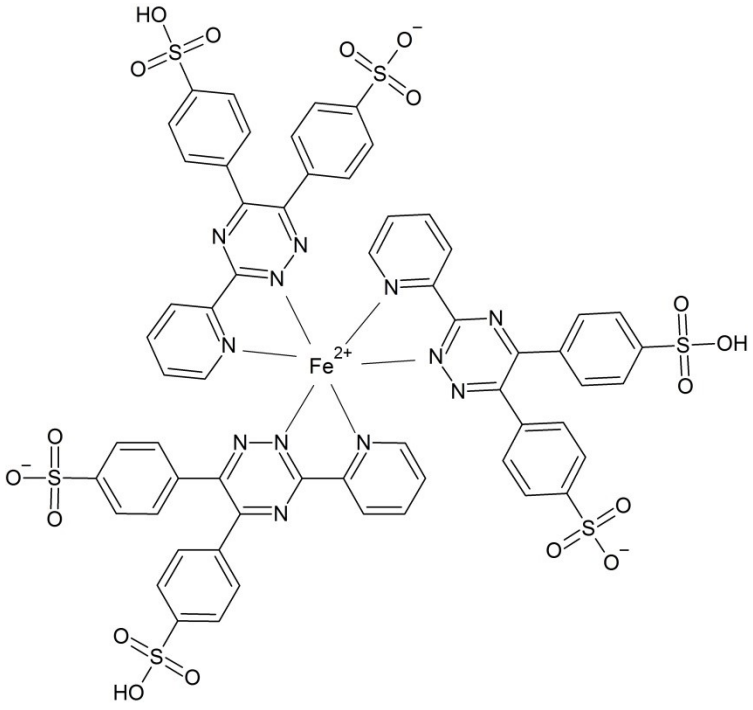

Figure 2.1: Chemical structure of the octahedral Fe(FZ)$_3$ complex which exhibits an absorbance maximum at λ = 562 nm.

As Fe(II) is coordinating six nitrogen atoms a molar ratio for FZ:Fe(II) of 3:1 is obtained for the octahedral FZ-Fe(II) complex ($Fe(FZ)_3$), as shown in **Figure 2.1**. The generated purple complex is highly water-soluble and stable between pH 4 and 8 with the highest absorbance values obtained in this pH range at the absorbance maximum of $\lambda = 562$ nm [Pascualreguera et al., 1997].

In order to determine the concentration of the total dissolved Fe pool (Fe(II) + Fe(III)), and to determine the Fe redox speciation, Fe needs to be present in its reduced Fe(II) form to generate a complex with FZ. For this purpose a reducing agent can be introduced to reduce the Fe(III) to Fe(II) with subsequent total DFe analysis. The reduction step requires a fast kinetic (in the order of seconds to minutes) as well as a high reduction rate under the optimal pH conditions for the complexation of Fe(II) with FZ. In the literature three different reducing agents have been reported for the reduction of Fe(III) to Fe(II) with subsequent determination of Fe(II): sodium sulfite, hydroxylamine hydrochloride and ascorbic acid. The use of sodium sulfite requires incubation times for efficient reduction of 15 min plus another 24 hours incubation with FZ [Farid et al., 2018]. Ussher et al. (2009) determined a completed reduction after 4 hours at room temperature and 20 min at 67 °C when using sodium sulfite. These long waiting periods as well as the use of a heating component are not ideal for *in situ* applications. Shorter incubation times for the reduction of Fe(III) to Fe(II) were found with hydroxylamine hydrochloride, ranging between 10 min [Viollier et al., 2000] and 1 hour [Boyle et al., 1977; Verschoor and Molot, 2013]. According to Verschoor and Molot (2013) hydroxylamine hydrochloride needs to be purified, in contrast to ascorbic acid, prior to its use for the reduction in order to minimize Fe contamination. However, in the vast majority of publications the use of ascorbic acid is described for an efficient reduction of Fe(III) to Fe(II) in natural water samples. In the reduction step, one molecule of ascorbic acid is able to reduce two Fe(III) ions to Fe(II), generating dehydroascorbic acid and two protons [Elmagirbi et al., 2012]. Most of the studies reported a nearly immediately completed reaction once ascorbic acid solution was applied to the sample (e.g. [Huang et al., 2009; Pascoa et al., 2009]). Whereas Elmagirbi et al. (2012) and Verschoor and Molot (2013) applied a reaction time of 5 min and 10 min, respectively, which is still an acceptable time scale for *in situ* measurements. Additionally, the use of a mixed reagent containing FZ and ascorbic acid [Huang et al., 2015], combining the two individual steps of Fe(III) reduction by ascorbic acid and Fe(II) complexation by FZ, has potential for *in situ* applications by simplifying the analyzers design. Based on this careful evaluation of the literature the use of ascorbic acid was chosen as reducing agent to continue with in our study.

2.2.1 Ferrozine reagent preparation

Prior to the preparation of the reagents and standard solutions all used plastic and glass ware was cleaned in a 2 % Citranox detergent bath (Sigma-Aldrich) followed by a 1.2 M HCl bath (reagent grade, Carl-Roth), both for periods of at least overnight. After thoroughly rinsing with de-ionized water (MilliQ, 18.2 MΩcm, Merck Millipore) the plastic and glassware was clean enough for further usage.

A 2 M sodium acetate/acetic acid buffer, containing 1.9 M sodium acetate and 0.1 M acetic acid, was prepared by dissolving 77.65 g sodium acetate (BioXtra, ≥ 99.0 %, Sigma-Aldrich) and 3.2 mL concentrated acetic acid (ultra purity acid grade, ROMIL) in de-ionized water up to a final volume of 500 mL. The buffer with pH ~ 6 was stored refrigerated in a transparent low density polyethylene (LDPE, Nalgene) bottle until use.

For the determination of the Fe(II) concentration a 10 mM FZ solution without any addition of ascorbic acid was prepared. Therefore, 1.25 g of FZ (3-(2-Pyridyl)-5,6-diphenyl-1,2,4-triazine-p,p-disulfonic acid monosodium salt hydrate, 97 %; Sigma-Aldrich) was dissolved in 100 ml of 2 M acetic acid/sodium acetate buffer and diluted to 250 ml with de-ionized water. When not in use the FZ reagent was stored refrigerated in a transparent high density polyethylene (HDPE, Nalgene) bottle, wrapped in aluminum foil in order to protect it from light.

In order to determine the total Fe (Fe(II)+Fe(III)) concentration ascorbic acid needs to be added as reducing agent to the 10 mM FZ reagent. Therefore, 1.25 g of FZ and 4.4 g of ascorbic acid (TraceSELECT, ≥ 99.9998 %, Sigma-Aldrich) were dissolved in 100 ml of 2 M acetic acid/sodium acetate buffer and diluted to 250 ml with de-ionized water, giving a final ascorbic acid concentration of 0.1 M and 40 % v/v of the 2 M acetic acid/sodium acetate buffer. For the analysis of acidified samples, a modified FZ/ascorbic acid reagent (FZ/AA) was used in order to increase the buffer capacity. For this purpose FZ and ascorbic acid were dissolved directly in 250 mL 2 M acetic acid/sodium acetate buffer without dilution with de-ionized water.
The reagents were prepared fresh on a weekly basis in order to avoid use of degraded ascorbic acid, notable in a color change from yellow to brownish due to the exposure to air. The degradation played a minor role in our deployments as the FZ/AA reagent was stored for this purpose in air tight flexible liquid storage bags (Flexboy Bags, Sartorius)

2.2.2 Iron standard preparation

The preparation of the Fe(II) standards requires special preservation to keep Fe(II) into solution and to prevent it from oxidation to Fe(III). Therefore, the standards were stabilized with an HCl and a sodium sulfite spike.

A 100 mM sodium sulfite stock solution was obtained by dissolving 1.26 g sodium sulfite (BioXtra, ≥ 98 %, Sigma-Aldrich) in 100 mL de-ionized water. A further dilution (1 mL of the 100 mM sodium sulfite stock made up to 100 mL with de-ionized water) yielded the 1 mM sodium sulfite working stock solution which was used for the stabilization of the Fe(II) standards. Sodium sulfite stock solutions were kept refrigerated in opaque HDPE bottles (Nalgene).

The Fe(II) stock solution was prepared by adding 0.7843 g ammonium iron(II) sulfate hexahydrate (99.997 % trace metals basis, Sigma-Aldrich) to 100 µL 1 mM sodium sulfite and 100 µL concentrated HCl (ultra purity acid grade, ROMIL) and made up to 100 mL with de-ionized water. This 20 mM Fe(II) stock solution was further diluted to 20 µM as follows: 1 mL 20 mM Fe(II) stock, 100 µL 1 mM sodium sulfite solution and 100 µL concentrated HCl (ultra purity acid grade, ROMIL) made up to 100 mL with de-ionized water. This 20 µM working stock solution was then used for the preparation of the standard solutions by further dilution to the required Fe(II) concentration. Every Fe(II) standard was stabilized with 0.1 % v/v 1 mM sodium sulfite solution and with 0.1 % v/v of concentrated HCl (ultra purity acid grade, ROMIL), giving a final concentration of 0.12 mM HCl and pH < 2. In order to obtain the same matrix for the Fe(II) blank the same spikes into de-ionized water were applied for the preparation of the blank solution.

Stock solutions of 20 mM Fe(III) were prepared by either dissolving 0.541 g iron(III) chloride hexahydrate (≥ 98 %, Carl Roth) or taking 558.5 µL of an 1000 ppm iron standard (TraceCERT, 1000 $mg \cdot L^{-1}$ Fe in 2 % nitric acid, Sigma-Aldrich), adding 100 µL concentrated HCl (ultra purity acid grade, ROMIL) and made up to 100 mL with de-ionized water. All other dilution steps (to 20 µM Fe(III) etc.) were conducted as done for Fe(II) without using the sodium sulfite spike. All stock solutions, both for Fe(II) and Fe(III), were kept refrigerated in transparent LDPE Nalgene bottles.

For benchtop experiments, the Fe(II) and Fe(III) standards were mixed with the FZ or FZ/AA reagent with the volumetric ratio of 9:1 in order to simulate the analyzers mixing

ratio. Absorbance spectra were acquired for experiments shown in chapter 3 with a single beam Agilent Cary 60 spectrophotometer between 400 nm and 800 nm using a 10 cm cylindrical quartz cuvette. The baseline corrected absorbance was processed at the peak maximum of 562 nm. Benchtop experiments shown in chapter 4 were conducted with a double beam Shimadzu UV-1800 spectrophotometer in 10 cm quartz cells. The absorbance was again processed at wavelength of 562 nm.

2.3 PAN method

The use of 1-(2-Pyridylazo)-2-naphthol (PAN) for the quantitative spectrophotometric determination of metal ions, such as the ions of Mn, Zn, Cd, Cu, Ni, Co, In, U, Ga, and Pd, is well established in the field of analytical chemistry [Marczenko and Balcerzak, 2000]. Depending on the prevalent pH of the solution three different forms of the PAN molecule with different degrees of protonation exist (**Figure 2.2**). In an acidic medium with pH < 2 PAN will be prevalent in the protonated form $HPAN^+$ with a positively charged pyridinium group. The dissociation of the proton occurs between pH values of 2 and 11 with a dissociation constant of $pK_1 = 2.6$ [Chiswell and O'Halloran, 1991] giving the water insoluble and uncharged PAN molecule. Further dissociation to PAN^- appears at pH > 11 with $pK_2 = 11.6$, attributed to the proton of the phenol group. The change in degree of dissociation causes a change of the electron system and therefore the three species appear different in their color, ranging from yellow-green to red for the protonated and deprotonated form, respectively and a yellow color of the uncharged molecule.

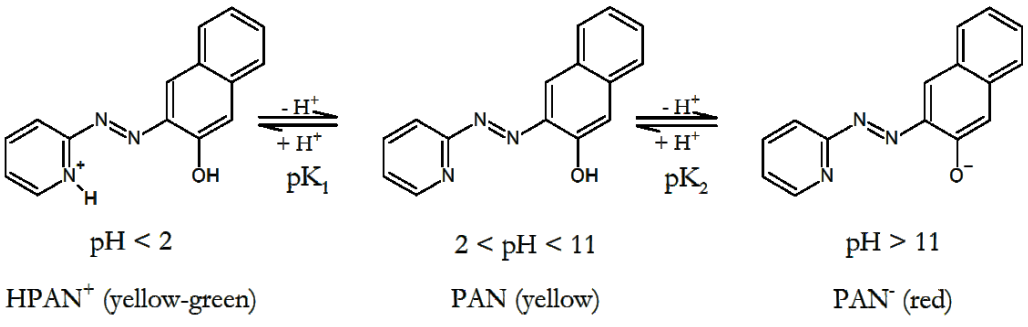

Figure 2.2: Structure of the PAN molecule at different pH values (adapted from [Coo et al., 1998]).

Also the complexing selectivity depends mainly on the pH of the solution. For example, the cations of Fe, Co and Ni are favorably complexed at pH = 4, whereas Mn, Zn and Cd

react with PAN at higher pH [Marczenko and Balcerzak, 2000], with pH = 9.5 being the optimum condition for the complexation of Mn(II) as well as for the spectrophotometric detection of Mn(II) [Chin et al., 1992]. For pH > 10 the absorbance of PAN itself is too dominant to allow a distinction between PAN and the Mn-PAN complex around 562 nm [Goto et al., 1977]. The tridentate ligand PAN forms with divalent cations, such as Mn(II), a 2:1 complex ($Mn(PAN)_2$; **Figure 2.3**) through the hydroxyl oxygen atom, a nitrogen of the azo group and the pyridinium group [Marczenko and Balcerzak, 2000; Safari et al., 2011]. As PAN and also metal-PAN chelate complexes are poorly water soluble, most spectrophotometric analyses were performed with an extraction step into chloroform or ether, or using solvents, as ethanol, methanol or acetonitrile or their corresponding aqueous-organic solutions [Coo et al., 1998; Marczenko and Balcerzak, 2000; Safari et al., 2011]. In order to overcome this drawback of using organic solvents and an additional extraction step (especially unfavorable for our aspired *in situ* application), Goto et al. (1977) developed a method where PAN as well as $Mn(PAN)_2$ is solubilized in the aqueous phase using the non-ionic surfactant Triton-X100. This molecule features a hydrophobic head group, 4-octylphenyl, and a hydrophilic tail, polyethoxylate (**Figure 2.4**). The critical micelle concentration (cmc) is 0.22 mM [Tiller et al., 1984]. If the concentration of Triton-X100 exceeds the cmc micelles will be formed in aqueous solutions with PAN or $Mn(PAN)_2$ incorporated in their centers (**Figure 2.5**), with van der Waals interactions prevalent between the hydrophobic hydrocarbon head groups of Triton-X100 and the PAN ligand. The hydrophilic tail group is directed towards the surrounding aquatic medium most probably via hydrogen bond attraction.

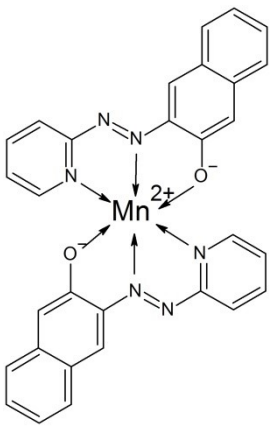

Figure 2.3: Chemical structure of the $Mn(PAN)_2$ complex

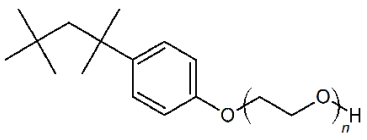

Figure 2.4: Chemical structure of the non-ionic surfactant Triton-X100 with n = 9 – 10.

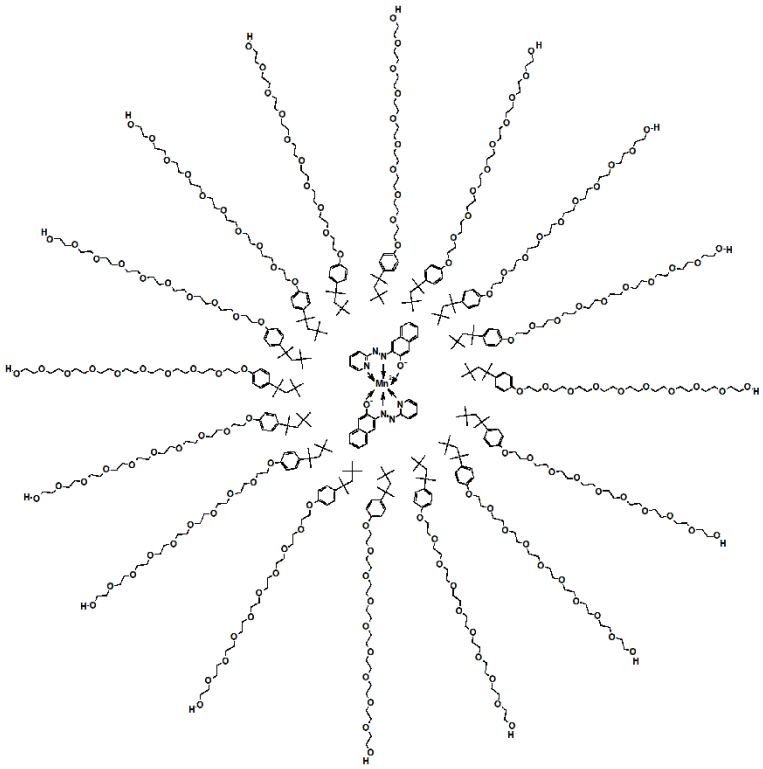

Figure 2.5: Schematic of a Triton-X100 micelle with a $Mn(PAN)_2$ complex in the center.

2.3.1 PAN reagent preparation

For the preparation of the PAN reagent, the method reported by Chin et al. (1992) was adapted for the purpose of our study as follows.

A borate buffer (pH ~ 10) was prepared by dissolving 0.618 g H_3BO_3 (99.99 %, trace metal basis, Acros Organics) and 0.4 g NaOH (98.5 %, Acros Organics) in 100 mL of de-ionized water, giving a concentration of 0.1 M for both boric acid and sodium hydroxide.

A mixture of 0.05 g of 1-(2-Pyridylazo)-2-naphthol (PAN) (general purpose grade, Fisher Scientific) and 5 mL of Triton-X100 (laboratory grade, Sigma-Aldrich) was added to approximately 50 mL of de-ionized water. The dispersion was stirred at 80 °C for at least 12 h until the PAN was dissolved completely. This mixture was then added to the 100 mL borate buffer and made up to 250 mL with de-ionized water. The final concentrations were 0.8 mM and 2 % v/v (equivalent to 33 mM) for PAN and Triton-X100, respectively, at pH ~ 10. Reagents were stored at room temperature in transparent borosilicate glass bottles. In order to verify the optimum concentration as well as composition of the surfactant, reagents were also prepared with 4 % v/v Triton-X100 and by using

polyvinylpyrrolidone (PVP) and the ionic surfactant sodium dodecyl sulfate (SDS) instead of Triton-X100.

2.3.2 Manganese standard preparation

A 100 μM Mn(II) working stock solution was prepared on a weekly basis by diluting 549 μL of a 1000 mg·L^{-1}Mn standard (1000 ppm Manganese for ICP, Inorganic Ventures) to 100 mL with de-ionized water. This stock solution was then used for another dilution step in order to obtain the required Mn(II) concentration for analysis/calibration. All stock solutions were kept at room temperature in opaque LDPE Nalgene bottles.

For benchtop experiments, the Mn(II) standards were mixed with the PAN reagent with the volumetric ratio of 9:1 in order to simulate the analyzers mixing ratio. Absorbance spectra were acquired with a double beam Shimadzu UV-1800 spectrophotometer between 400 nm and 800 nm using 10 cm quartz cuvettes The Absorbance was processed at the peak maximum of 562 nm.

2.4 Lab-on-chip analyzer

All Lab-on-chip (LoC) devices used in this work were designed, manufactured and assembled by the 'Ocean Technology and Engineering Group' of the National Oceanography Centre Southampton. In the following sections the hardware features as well as the measurement routine and data processing will be introduced in detail.

2.4.1 Hardware

The LoC analyzer comprises a microfluidic element which forms the top end cap of a polyvinyl chloride (PVC) housing (diameter: 12.5 cm, height: 19.5 cm) with a PVC tube (diameter: 15 cm, height: 45 cm) mounted on top (**Figure 2.6(A)**). The final dimensions of the analyzer ready for deployment are 15 cm in diameter and 56 cm in height.

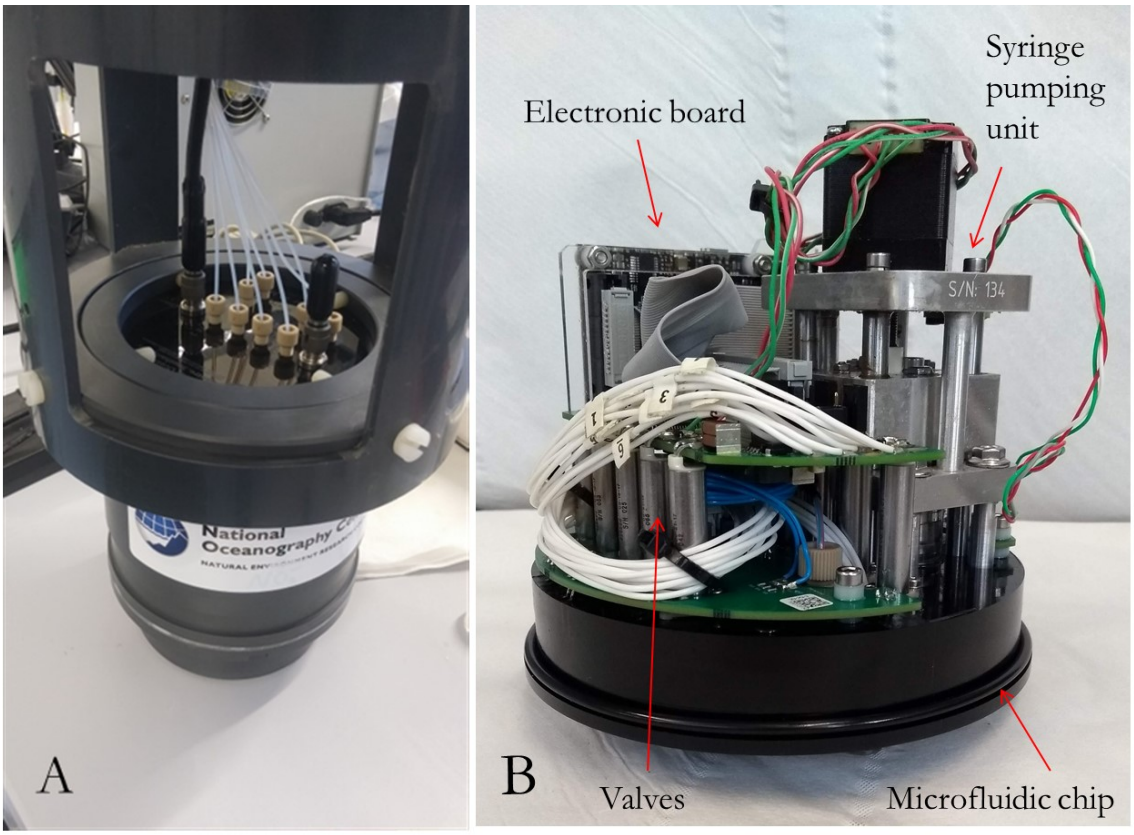

Figure 2.6: (A) LoC analyzer ready for deployment including PVC tube for reagent/standard bags and **(B)** microfluidic chip including all mechanical and electrical components (note the different orientation when mounted in PVC housing).

The PVC tube (not shown in its full length in **Figure 2.6(A)**) forms the housing for flexible liquid storage bags (Flexboy, Sartorius) in which reagents, blank, standards and waste are stored. Due to its open design, surrounding water can flow through and provide protection against external forces. The Luer-Lock fittings of the fluid storage bags are connected via polytetrafluoroethylene (PTFE) tubing with an inner diameter of 0.5 mm and ¼-28 flangeless fittings made of polyether ether ketone (PEEK) to the inlets on the chip. At the end of the sample inlet a 33 mm diameter polyether sulfone (PES) syringe filter with 0.45 µm or 0.22 µm pore size (Merck Millipore, Ireland) is mounted. In order to keep the dead volume of the sample inlet as small as possible a very short PTFE tubing (< 10 cm) is used.

The chip itself (**Figure 2.6(B)**) has a diameter of 11.9 cm and is manufactured from dark-tinted poly(methyl methacrylate) (PMMA), in order to enhance the linear range for absorbance measurements, reduction of the background illumination (e.g. originated from stray light and ambient light) and hence improving the sensitivity of the system when compared to transparent materials, as described in Floquet et al. (2011). Microfluidic channels with the dimensions of 160 × 300 µm as well as fluidic connectors and moldings

for light emitting diodes (LEDs) and photodiodes (PDs) were milled into an 8 mm thick PMMA layer using a computer numerical control micro mill (LPKF ProtoMat S100, Garbsen, Germany). A second PMMA sheet was prepared with aligned fluidic connector holes. After a thorough cleaning procedure with detergents, water and alcohols, the PMMA sheets were exposed to chloroform vapor in order to soften a thin surface layer (~ 2 µm). Both layers were then aligned and pressed together using a hot press. This bonding procedure reduces the surface roughness of the channels from 200 nm (after micro milling) to 15 nm (after solvent vapor exposure) and produces channel surfaces with an optical quality finish [Ogilvie et al., 2010]. **Figure 2.7** shows a simplified schematic (left) as well as the actual arrangement of the microfluidic channels using a computer-aided design draw tool (right) of the sensor version 'Iron 3.3a'.

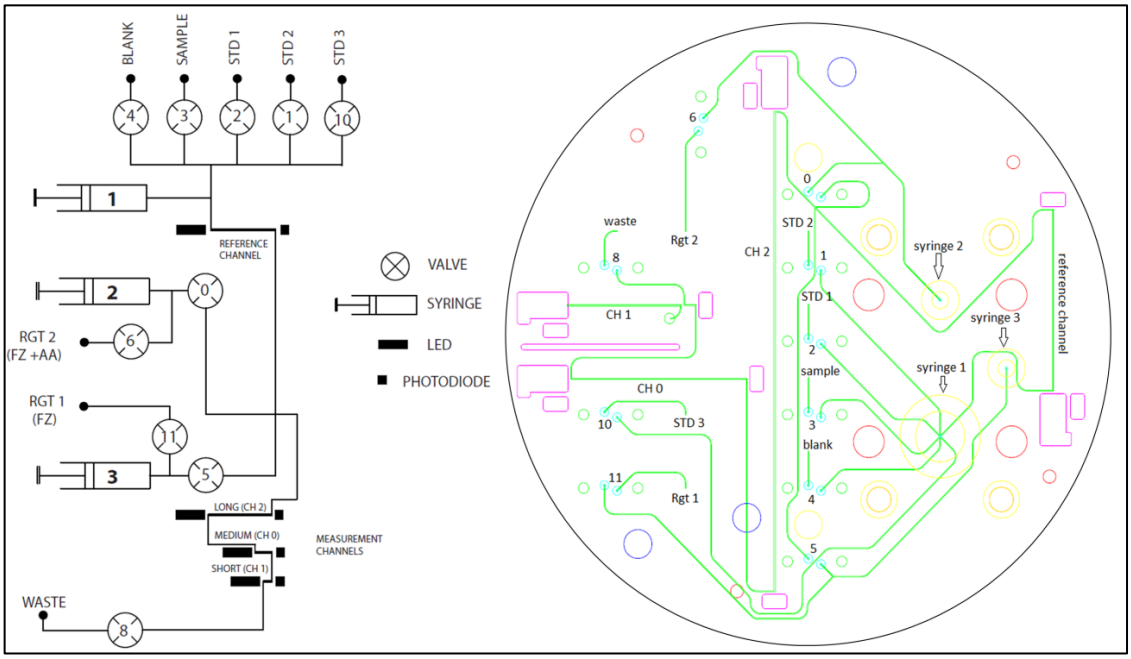

Figure 2.7: Microfluidic diagram of Iron Version 3.3a, simplified (left) and CAD draw (right). Large barrel (~560 µL) of the syringe pump unit is used for blank, sample and standards and labelled with **(1)**, the small barrels (~ 63 µL) **(2)** and **(3)** are used for the reagents.

In the course of this work a remodeled version 'Iron 3.3b' was used for DFe measurements. The design of this refined generation will be introduced in chapter 4. 'Iron 3.3a' comprises a custom-made syringe pump consisting of one ~ 560 µL (9.71 mm ID) and two ~ 63 µL (3.28 mm ID) glass syringes, all three connected to the same stepper motor (incl. two Hall effect sensors), ten micro-inert solenoid valves (LFNA1250325H, The Lee Company, USA), four LED light sources with a peak wavelength of 575 nm (AlGaInP, B5B- 433-20 LED, Roithner LaserTechnik GmbH, Austria), four photodiodes (TSLG257-LF, TAOS, USA) and custom-made electronic boards for control and data logging. All these components were mechanically linked to the bonded PMMA sheets

(**Figure 2.6(B)**). Full control of the fluid flow can be achieved by the closely linked processes of the movement of the syringe pump and the individual actuation of the solenoid valves (**Figure 2.7**). In the default state all valves are closed. Once power is applied to certain valves the fluidic path will be open. A detailed description of the measuring routine can be found in section 2.4.3. Due to the simultaneous movement of the plungers for all three glass syringe barrels, a reagent to analyte mixing ratio of 1:8.8 is generated. Absorbance measurements are conducted in three optical channels of different length labelled as 'long', 'medium' and 'short', with lengths of 9.16 cm, 3.46 cm and 0.25 cm, respectively. These channels are located downstream after the confluence point of analyte and reagent. A fourth channel labelled as 'reference' and with a length of 3.46 cm is located before the confluence in order to e.g. determine the absorbance of the analyte prior to the mixing with reagent. However, the reference channel was not used in this work as the background absorbance was determined in either the long, medium or short channel. All optical channels are equipped with a LED and a measuring photodiode at the opposite ends of the channels. Additionally, monitoring photodiodes are positioned perpendicular to the LEDs of the reference, long and medium channel in order to examine any temperature induced drift of the LED output and to correct for it, if needed, as described by Grand et al. (2017). The signal of the photodiodes is saved in real time with a frequency of 1 Hz on an on-board 2 GB flash memory card with individually accessible data sets for every channel. The device is operated whilst connected to a 12 V power supply. As the PAN method for the detection of Mn(II) and the FZ method for the detection of Fe(II) and DFe are both most sensitive at the same absorption maximum (λ_{max} = 562 nm) the same hardware can be used for their analysis.

2.4.2 Graphical user interface

For any measurement a measuring routine ('state machine') needs to be programmed by the user and saved on the LoC device. The 'wetchem.exe' GUI gives the user full control on all components integrated in the manifold as shown in **Figure 2.8**. For every single state, the settings can be edited individually, e.g. valves which need to be opened, the operation of the syringe pump in terms of pump speed, direction (withdraw or inject) and stop condition (timeout or Hall effect sensors) and the applied current to the LEDs. In addition to the control over the afore-mentioned electronical parts, the user can also generate a logical sequence of certain states (e.g. in order to iterate two consecutive states several times).

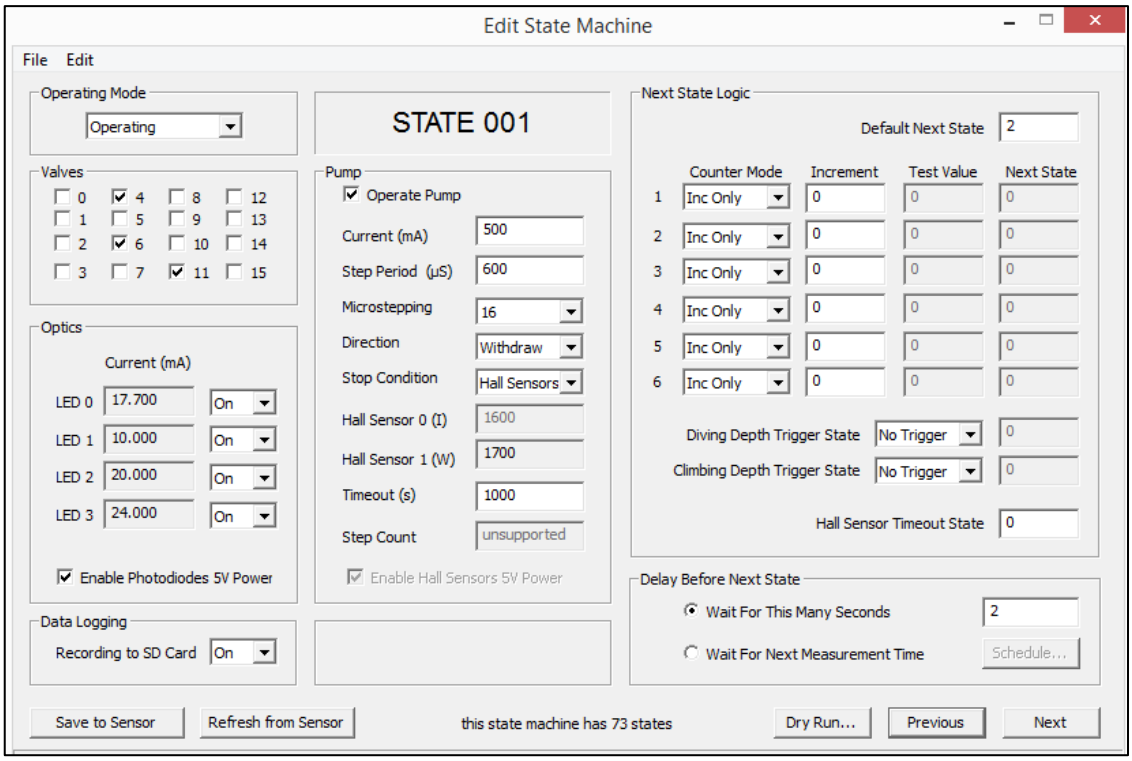

Figure 2.8: 'Wetchem.exe' GUI (version 2.7.7) to program state machines.

2.4.3 Measurement routine ('State machine')

The analysis routine is basically partitioned in four different sections, the blank, two standards and the sample measurement (**Table 4**). The state machine starts with state 0 where the starting command is defined. This can happen either manually or according to a specific set start time. The first sequence from state 1 to 9 handles the blank solution. Herein, state 1 to 3 is referred as flushing procedure including the withdrawal of blank and reagent in the respective syringe pump barrels (state 1) followed by the injection of the blank through the manifold (state 2). The valves which prevent the reagents from entering the manifold towards the optical cells are still closed, so that the reagents are pumped back into their reservoirs while the blank is injected. State 3 contains a loop which defines how often the flushing procedure has to be repeated. Usually five repetitions are programmed with a full pump stroke length, unless otherwise stated. After the flushing sequence, the blank and reagents are withdrawn (state 4) and the flow is stopped for five seconds (state 5) prior to the injection. The averaged signal of this reference state is used to determine the background signal (V_{BLK}^{R}) of the blank itself without any reagent added (see section 2.4.5). The blank together with one of the reagents is then injected in state 6 into the manifold towards the optical channels. The reagent which is not needed in this sequence is pumped back into its reservoir. State 7 is meant to be a space holder state in case the user decides

for whatever reason that one of the previous sequences needs to be repeated several times. Once the blank is injected together with the reagent a waiting period under stopped-flow condition is set in order to allow complete mixing of the fluids and full color development (state 8). Usually this time is set to 5 minutes for Fe(II) or DFe measurements and 15 minutes for Mn(II) measurements, unless otherwise stated. At the end of the waiting period the signal of additional 5 seconds (state 9) is averaged and used as V_{BLK} for the calculation of the absorbance of the blank solution (see section 2.4.5). When the blank sequence is completed the whole procedure is repeated for standard 1 (state 10 to 18), standard 2 (state 19 to 27) and finally for the sample (state 28 to 36). It should be noted that the flushing procedure for the standard solutions is programmed with a quarter of the full pump stroke length as it is the same matrix as the blank solution. Depending on the settings in state 36 the deployment stops at this point or continues with state 0 waiting for the next start command. Once the sensor is stopped a CSV file is created and saved on the onboard SD card. The file contains all important settings in the header as well as all acquired data (one data point per second) including elapsed time, state number, output of the measuring and monitoring PDs for all optical channels, relative position of the Hall effect sensors, on-chip temperature and a real-time clock.

Table 4: State machine as an example for a deployment using one blank and two standards for calibration. Numbering of valves according to Figure 2.7.

	State	State Description	Valves open	Executions
	0	Waiting for start command		
BLANK	1	Withdraw Blank and reagent	4, 6 , 11	5x flushed with blank
	2	Inject Blank, reagent is pumped back in reservoir	8, 6, 11	
	3	Decision state		
	4	Withdraw Blank and reagent	4, 6, 11	
	5	Reference Blank (V_{BLK}^{R})		
	6	Inject Blank + reagent	8, 6, 5	
	7	Decision state		
	8	Waiting period		
	9	Measurement state (V_{BLK})		
STANDARD 1	10	Withdraw STD 1 and reagent	2, 6, 11	5x flushed with STD 1
	11	Inject STD 1, reagent is pumped back in reservoir	8, 6, 11	
	12	Decision state		
	13	Withdraw STD 1 and reagent	2, 6, 11	
	14	Reference STD1 (V_{STD1}^{R})		

	State	State Description	Valves open	Executions
	15	Inject STD 1 and reagent	8, 6, 5	
	16	Decision state		
	17	Waiting period		
	18	Measurement state (V_{STD1})		
STANDARD 2	19	Withdraw STD 2 and reagent	1, 6, 11	5x flushed with STD 2
	20	Inject STD 2, reagent is pumped back in reservoir	8, 6, 11	
	21	Decision state		
	22	Withdraw STD 2 and reagent	1, 6, 11	
	23	Reference STD 2 (V_{STD2}^{R})		
	24	Inject STD 2 and reagent	8, 6, 5	
	25	Decision state		
	26	Waiting period		
	27	Measurement state (V_{STD2})		
SAMPLE	28	Withdraw Sample and reagent	3, 6, 11	5x flushed with sample
	29	Inject Sample, reagent is pumped back in reservoir	8, 6, 11	
	30	Decision state		
	31	Withdraw Sample and reagent	3, 6, 11	
	32	Reference Sample (V_{Sample}^{R})		
	33	Inject Sample and reagent	8, 6, 5	
	34	Decision state		
	35	Waiting period		
	36	Measurement state (V_{Sample})		

2.4.4 Characteristics of raw signal

The PD output of the measuring and monitoring PD of the long channel acquired for a full DFe measurement cycle according to **Table 4** is shown in **Figure 2.9** as an example for illustrating the characteristics of the raw signal.

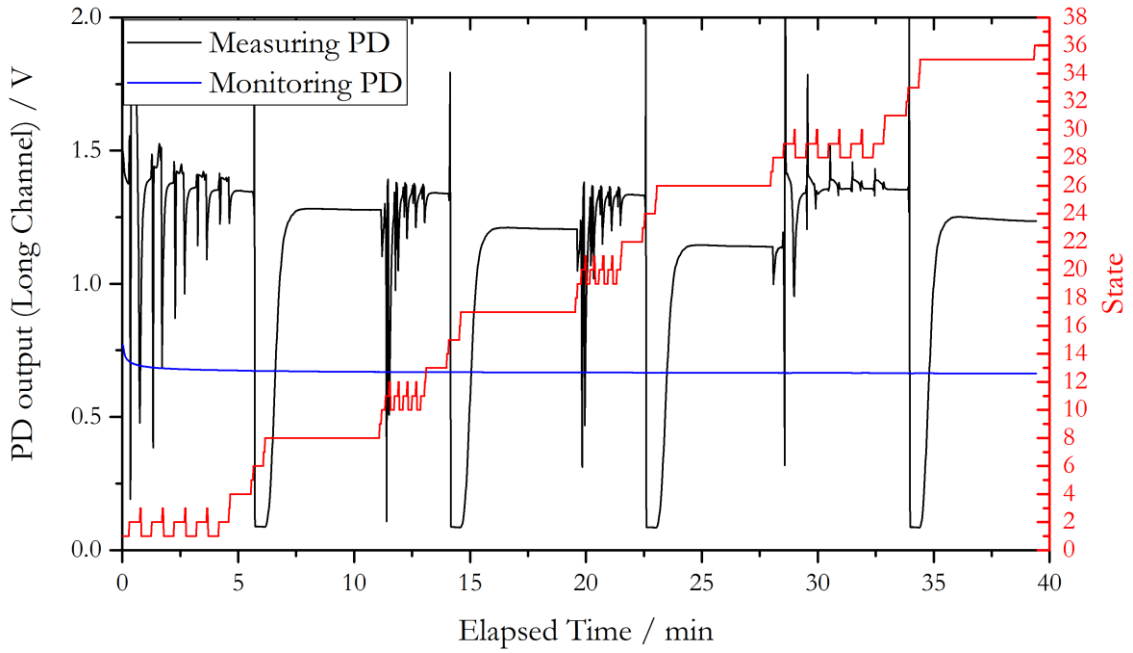

Figure 2.9: Raw signal of measuring and monitoring PDs for the long optical channel for a complete DFe measurement cycle including blank, two standards and a sample.

During the first five minutes, five flushing steps are conducted with the blank in order to avoid any carry-over of a previously measured sample. The spikes observed in the raw signal of the measuring PD are generated by the flow of the liquids and their relaxation when valves reopen. After the flushing procedure, the blank is injected together with the reagent. As laminar flow is prevalent in the microfluidic channels an interface between reagent and blank, as a consequence of their different chemical composition, is generated. Due to an increased degree of refraction of light at this interface (Schlieren effect), the signal decreases once both fluids enter the optical path. During the five minutes of waiting period diffusive mixing of the fluids results in an increase of the signal as the interface fades and complete mixing as well as full color development is achieved. The analysis procedure is then executed for the two standards, but with just a quarter of the full pump stroke length for the flushing procedure, and for the sample with full pump stroke length while flushing. According to an increased DFe concentration from blank towards standard 2, the signal (transmittance) at the end of the waiting period is highest for blank and lowest for standard 2. Ideally, the signal for the sample at the end of the waiting period should be in between those two values in order to cover the calibration range. Otherwise the concentrations of the standards require adaptation. In total the sequence including a blank, two standards and one sample measurement takes 39 minutes for Fe(II) and DFe and 79 minutes for Mn(II) with analyzer version 'Iron 3.3a'.

2.4.5 Data handling

As mentioned above in section 2.1, the absorbance is defined as the negative logarithm to the base 10 of the transmittance. As the PDs, which are integrated at the end of each measurement channel, are measuring the transmitted light emitted by the LEDs and propagated through the channel, the absorbance can be calculated as follows.

$$Absorbance = -\log_{10}\left(\frac{V_S}{V_{BLK}} \cdot \frac{I_{BLK}}{I_S}\right) - OPT_{corr} \tag{2.4}$$

with

$$OPT_{corr} = -\log_{10}\left(\frac{V_S^R}{V_{BLK}^R}\right) \tag{2.5}$$

Here, V_S and V_{BLK} represent the mean voltages of the measuring PDs during the last 5 seconds after the waiting period of standards/sample and blank, respectively (see also **Table 4**). Due to the warming up of the LEDs their illumination intensity and hence the detected signal of the PDs can drift throughout a measurement sequence between the blank measurement at the beginning and the sample measurement at the end. A change in temperature can be also related to natural effects during a deployment (e.g. day vs night). Therefore, the ratio I_{BLK}/I_S (monitoring PD voltages of the blank and standard/sample) is integrated in equation (2.4) as a scaling factor in order to correct for the drift of the LED illumination intensity caused by any temperature changes. When measuring natural seawater samples changes in salinity as well as the presence of colored dissolved organic matter has to be taken into account. Both parameters can change the background absorbance of the analyte and require compensation when processing the raw data using the optical correction term OPT_{corr} (see equation (2.5)). It can be computed during the 'reference state' (last step of the flushing sequence, **Table 4**) prior to the mixing of the blank (V_{BLK}^R) or sample (V_S^R) with the reagent. This approach for the calculation of the absorbance values, which is used in the 'wetchem.exe' software for processing the data, relates all absorbencies to the measurement of the blank. In case the blank measurement failed, for various reasons, the whole cycle cannot be taken into account for a time series. In order to determine the absorbencies of the blank, standards and sample individually (e.g. to identify and replace any outliers) and to use a more simplified algorithm, an alternative way of data processing can be applied, as shown in equation (2.6) using the example of a sample measurement.

$$Absorbance = -\log_{10}\left(\frac{V_{Sample}}{V_{Sample}^{R}} \cdot \frac{I_{Sample}^{R}}{I_{Sample}}\right) \quad (2.6)$$

Instead of relating V_{Sample} to the blank measurement (as done in equations (2.4) and (2.5)), V_{Sample} is related to the reference state of the sample (V_{Sample}^{R}) after the flushing procedure and prior to the mixing with the reagent. With this approach the matrix effect is already taken into account and every blank, standard and sample is referred to its own matrix, and no optical correction term needs to be implemented. These absorbencies (blank and standard(s)) are then used for a linear regression to compute the calibration curves. The Fe and/or Mn concentration was calculated by subtracting the intercept of the linear fit from the absorbance of the sample and finally dividing it by the slope of the calibration curve.

2.4.6 Salinity correction

The presence of colored dissolved organic matter as well as salinity gradients can affect the raw signal and therefore the processed data of real seawater samples. **Figure 2.10** shows the raw signal of the PD of the long optical channel for a blank and a 100 nM Fe(II) standard prepared at a salinity of 0 with de-ionized water and three 100 nM Fe(II) standards with a salinity of 7, 21, and 35. These standards were considered in this experiment as 'sample' and were prepared by diluting seawater from the South Atlantic Ocean which is very low in DFe (< 0.2 nM) with de-ionized water.

The output signal of the PD at the end of the flushing procedure of the 0 nM Fe(II) blank and the 100 nM Fe(II) standard both at zero salinity, after 200 s and 600 s, respectively, was here considered as baseline (indicated as red dashed line in **Figure 2.10**). Considering the PD output at the end of the flushing procedures for each individual 100 nM Fe(II) standard at S = 7, 21 and 35 it is obvious that this signal is increasing with increasing salinity. A possible explanation for a salinity induced increase of the background signal is the change of refraction indices with ionic strength. Snell's law indicates that the ratio of the sines of the angle of incident and refraction between two different media (in our case PMMA as optical window and salt solution) is equivalent to the reciprocal of the refractive indices of the respective media. As the refractive index of a salt solution is increasing with increasing concentration [Aly and Esmail, 1993], it approaches the refractive index of PMMA of $n = 1.4912$ at 575 nm (fitted data from Sultanova et al. (2009); accessed via [www.refractiveindex.info]). According to Snell's law this results in a reduced grade of

refraction at the interface between optical window and fluid of the light emitted by the LED. Therefore, a salinity induced increase in signal (as shown in **Figure 2.10**) is equivalent to a reduced loss of light intensity due to refraction.

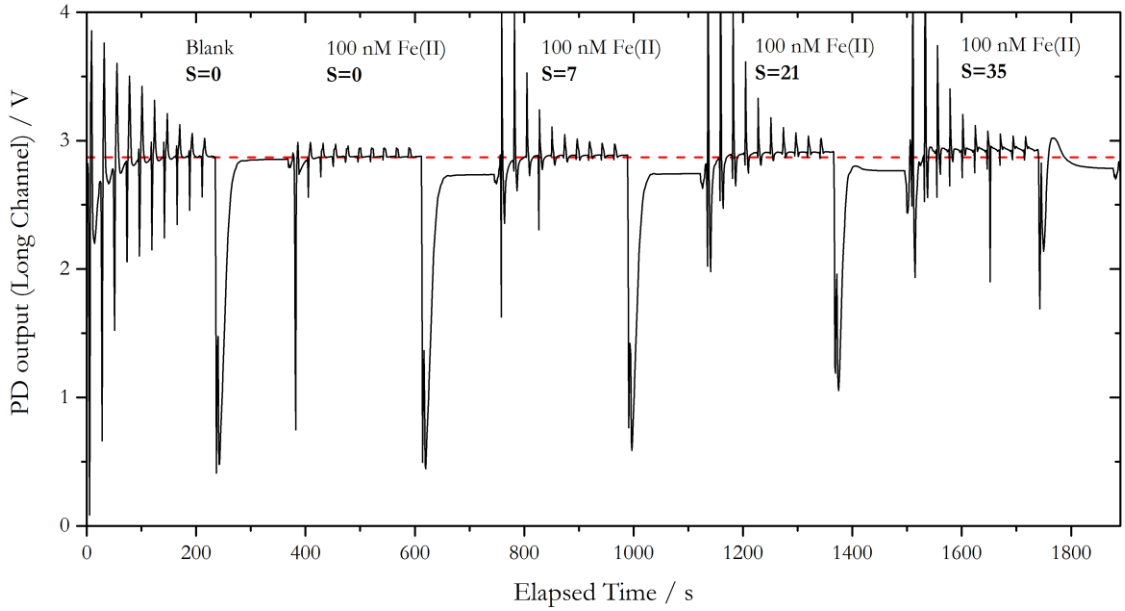

Figure 2.10: Raw signal of the PD from the long channel for a 0 nM Fe(II) blank and 100 nM Fe(II) standards at different salinities. The red dashed line indicates the position of the 'zero salinity baseline'.

The shift in the background signal also affects the signal at the end of each waiting period after complete mixing of standard with reagent and full color development compared to the 100 nM Fe(II) standard at S = 0. In order to determine how a salinity gradient between blank/standards and sample influences the computed Fe(II) concentrations and to validate the salinity correction, the raw data were processed using three different approaches: equation (2.4) with and without the optical correction term as well as equation (2.6), as shown in **Figure 2.11**. When the raw data were processed according to equation (2.4), but without any optical correction term, the computed Fe(II) concentration was under-estimated by more than 40 nM for S = 35 to a Fe(II) concentration of ~ 60 nM. However, these under-estimated concentrations can be corrected using the optical correction term in equation (2.4) or by using equation (2.6). Both yielded comparable results (**Figure 2.11**).

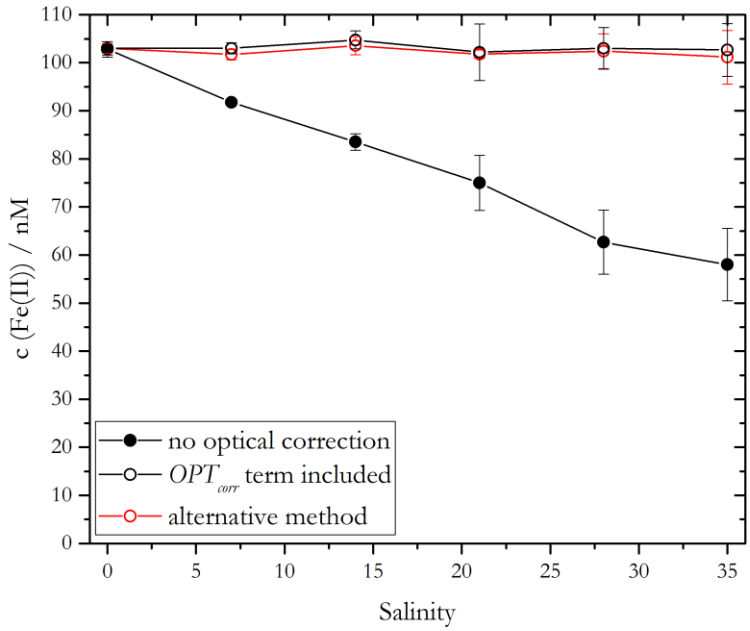

Figure 2.11: Computed Fe(II) concentrations of 100 nM Fe(II) samples at different salinities based on the calibration with a 0 nM Fe(II) blank and a 100 nM Fe(II) standard at S = 0. Raw data were processed using equation (2.4) without any optical correction (filled black circle), with optical correction (open black circle) and with equation (2.6) as alternative method (open red circle).

In addition to the previously described salinity induced shift of the PD output signal, high salinities also affect the kinetics of the chemical reaction between analyte and reagent. This is best visible in **Figure 2.10** when comparing the signal for the 100 nM Fe(II) standards at S = 0 with this of S = 35 after mixing with reagent. For the zero salinity standard the signal increases while mixing and stays at the maximum after complete mixing without any change, indicating that the reaction is already completed. In contrast, the signal of the standard prepared with a salinity of 35 increases due to mixing and decreases again after the maximum (complete mixing) is reached, indicating that the FZ is still reacting with Fe(II) and the absorbance is increasing with time. This longer reaction time at high ionic strength can be explained with the Debye-Hückel theory, as it proposes that the activity of an ion is decreasing with increasing ionic strength [Liang et al., 2007; Lin and Kester, 1992]. Lin and Kester (1992) also proposed that the overall complexation constant depends on parameters like the FZ concentration, pH, temperature and ionic strength, where the ionic strength being the major component causing a decrease of the complexation rate with increasing salinity. Another contributor to a longer reaction time could be an increased concentration of dissolved organic matter for high salinity standards because a larger volume of natural seawater was used for the preparation compared to low salinity standards. Dissolved organic matter can possibly complex Fe(II) as a concurring reaction to the complexation with FZ. Therefore, it is recommended to prepare the standards and blank in the same salinity range as expected for the sample.

2.5 Deployment and discrete samples

Following the analyzers characterization through laboratory experiments, field measurements in natural waters were conducted in order to validate their performance under real environmental conditions. Therefore, the analyzers were deployed from a pontoon in the Kiel fjord, Germany, mounted on a stainless steel frame together with other wet chemical analyzers and hydrographic sensors (**Figure 2.12**) in 2 m depth in September 2016, August 2018 and October/November 2018. Detailed descriptions of the deployments are given in the respective chapters.

Figure 2.12: Deployment frame with LoC analyzers, optical nitrate sensors and SeapHOx attached (photo credit: M. Nehir).

2.5.1 Discrete sample collection

In order to validate the analyzer's performance during the deployments in natural waters in terms of observed trace metal concentrations, discrete samples were collected on a regular basis (three to four samples per day). Sample collection for dissolved metals, dissolved organic carbon and nutrients was conducted using either an acid cleaned 5 L GO-FLO sampling bottle (General Oceanics Inc, USA) on a nylon line or using a Masterflex L/S

series peristaltic pump (Cole-Palmer GmbH, Germany) with an acid cleaned 6.4 mm ID Masterflex C-Flex tubing (Cole-Palmer GmbH, Germany) attached. Water samples collected with the GO-FLO bottle were subsampled in a clean laboratory through a 60 mL syringe (Henke-Sass, Wolff GmbH, Germany) equipped via Luer-Lock connection with a 0.45 μm PES syringe filter (Merck Millipore Ltd, Ireland) into 125 mL LDPE Nalgene bottles, and acidified to pH < 2 by the addition of 150 μL conc. HCl (ultra purity acid grade, ROMIL) for trace metal analysis. Dissolved organic carbon samples were subsampled by using the same syringe/filter into 20 mL pre-combusted glass vials and acidified with 20 μL conc. HCl (ultra purity acid grade, ROMIL). Filtered nutrient samples were kept in a freezer at -20 °C in 15 mL polypropylene centrifuge vials until analysis.

For the sample collection using the peristaltic pump, the inlet of the C-Flex tubing was positioned on the stainless steel frame at the same water depth as the sample inlet of the deployed analyzers. At the outlet of the C-Flex tubing a 0.2 μm PES filter capsule including a 0.8 μm pre-filter (AcroPak 500, Pall GmbH, Germany) was attached in order to sample directly at the deployment site into 125 mL LDPE Nalgene bottles for trace metal analysis. The samples were then acidified to pH < 2 by the addition of 180 μL conc. HCl (ultra purity acid grade, ROMIL) in a clean laboratory. Dissolved organic carbon samples and nutrient samples were directly filtered into 20 mL pre-combusted glass vials and 15 mL polypropylene centrifuge vials, respectively. Dissolved organic carbon samples were acidified with 20 μL conc. HCl in a clean laboratory and kept in the fridge until analysis. Nutrient samples were kept frozen until analysis.

Before their usage, all LDPE trace metal sample bottles were thoroughly pre-cleaned in 2 % Mucasol detergent for one day, one week in a 1.2 M HCl bath, one week in 1.2 M HNO_3 bath and three de-ionized water rinses after each stage. Dissolved organic carbon vials were soaked overnight in 1.2 M HCl bath, thoroughly flushed with de-ionized water and combusted for 8 h at 500 °C wrapped in aluminum foil. No special cleaning procedure was applied for nutrient vials. Prior to the final filling of the sample bottles with seawater all bottles were flushed for at least three times with the same seawater.

2.5.2 Hydrographic data acquisition

In order to continuously record hydrographic data during field measurements, an EXO2 sonde (YSI Inc., USA) or a SeapHOx unit (Sea-Bird Electronics, USA) was deployed simultaneously with the analyzers at the same depth as the analyzers' sample intakes.

The multiparameter EXO2 sonde was used for a deployment in September 2016 in the Kiel fjord (see chapter 3) and equipped with a conductivity sensor, a dissolved oxygen sensor, a temperature probe and a turbidity probe. Data for all units were acquired every minute.

The SeapHOx unit was deployed for field measurements conducted in the Kiel fjord in August 2018 and October/November 2018. It comprised a SeaFET pH sensor and a SBE 37-SMP-ODO MicroCAT CTD+DO sensor for the integrated data collection of pH, temperature, salinity and dissolved oxygen concentration. Data were collected every 10 minutes.

3 Evaluation of a ferrozine based autonomous *in situ* lab-on-chip analyzer for dissolved iron species in coastal waters

Felix Geißler[1], Eric P. Achterberg[1,2], Alexander D. Beaton[3], Mark J. Hopwood[1], Jennifer S. Clarke[1], André Mutzberg[1], Matt C. Mowlem[3], Douglas P. Connelly[3]

Published in *Frontiers in Marine Science*

DOI: 10.3389/fmars.2017.00322

[1]Chemical Oceanography, Marine Biogeochemistry, GEOMAR Helmholtz Centre for Ocean Research Kiel, Kiel, Germany

[2]University of Southampton, National Oceanography Centre, Southampton SO14 3ZH, United Kingdom

[3]National Oceanography Centre, Southampton SO14 3ZH, United Kingdom

Abstract

The trace metal iron (Fe) is an essential micronutrient for phytoplankton growth and limits, or co-limits primary production across much of the world's surface ocean. Iron is a redox sensitive element, with Fe(II) and Fe(III) co-existing in natural waters. Whilst Fe(II) is the most soluble form, it is also transient with rapid oxidation rates in oxic seawater. Measurements of Fe(II) are therefore preferably undertaken *in situ*. For this purpose an autonomous wet chemical analyzer based on lab-on-chip technology was developed for the *in situ* determination of the concentration of dissolved (< 0.45 μm) Fe species (Fe(II) and labile Fe) suitable for deployments in a wide range of aquatic environments. The spectrophotometric approach utilizes a buffered ferrozine solution and a ferrozine/ascorbic acid mixture for Fe(II) and labile Fe(III) analyses, respectively. Diffusive mixing, color development and spectrophotometric detection take place in three separate flow cells with different lengths such that the analyzer can measure a broad concentration range from low nM to several μM of Fe, depending on the desired application. A detection limit of 1.9 nM Fe was found.

The microfluidic analyzer was tested *in situ* for nine days in shallow waters in the Kiel Fjord (Germany) along with other sensors as a part of the SenseOCEAN EU-project. The analyzer's performance under natural conditions was assessed with discrete samples collected and processed according to GEOTRACES protocol (acidified to pH < 2 and analyzed via inductively coupled plasma mass spectrometry (ICP-MS)). The mechanical performance of the analyzer over the nine day period was good (consistent high precision of Fe(II) and Fe(III) standards with a standard deviation of 2.7 % (n = 214) and 1.9 % (n = 217), respectively, and successful completion of every programmed data point). However, total dissolved Fe was consistently low compared to ICP-MS data. Recoveries between 16 % and 75 % were observed, indicating that the analyzer does not measure a significant fraction of natural dissolved Fe species in coastal seawater. It is suggested that an acidification step would be necessary in order to ensure that the analyzer derived total dissolved Fe concentration is reproducible and consistent with discrete values.

3.1 Introduction

Over the past few decades the biogeochemical cycling of the trace metal iron (Fe) in the ocean has been subject to intense research interest. As a micronutrient with a low oceanic concentration in the pM – low nM range [Johnson et al., 1997], Fe is essential for marine primary production and is widely considered as a limiting co-factor for the growth of phytoplankton [Coale et al., 1996; Kolber et al., 1994; Moore et al., 2013]. Widespread Fe limitation of marine primary production links the biogeochemical Fe cycle with the global carbon cycle by affecting the efficiency of the ocean's biological carbon pump and thus atmospheric pCO_2 [Martin, 1990]. In coastal environments, there are multiple Fe sources including riverine runoff [Boyle et al., 1977], submarine groundwater discharge [Windom et al., 2006] and atmospheric deposition [Jickells et al., 2005]. Relatively high concentrations of natural organic matter compared to the open ocean, combined with multiple Fe sources, creates a highly dynamic Fe cycle in estuarine and coastal waters. This leads to a multitude of coexisting dissolved Fe species including dissolved Fe(II), Fe(III) complexes, and less bioavailable iron oxyhydroxide colloids [Rose and Waite, 2003b].

Fe(II) is a particularly challenging fraction of total dissolved Fe (DFe, Fe(II)+Fe(III)) to quantify because it is a transient species with a typical oxidation half-life of only minutes in surface seawater [Sarthou et al., 2011]. Furthermore, Fe(II) concentrations and oxidation rates are sensitive to multiple physical/chemical parameters including pH, temperature, light intensity and O_2, H_2O_2 and DOC concentrations [Davison and Seed, 1983; Millero et al., 1987]. This means that Fe(II) sample collection and analysis via conventional oceanography rosette based approaches are non-ideal for determining Fe(II) concentrations in natural waters. In order to resolve the high spatial/temporal Fe variability in coastal waters, and to minimize analytical errors due to the short residence time of Fe(II), *in situ* measurements are preferably undertaken for the determination of Fe(II) and DFe. Therefore, the development of precise Fe sensors and analyzers is a high priority target within the field of trace metal biogeochemistry [Tagliabue et al., 2017]. Remote real-time analysis has many potential advantages over discrete sampling including: replacement of laborious sample collection and analysis procedures; reduction of the contamination risk and alteration of samples during collection, handling and storage; and a potentially enhanced spatial and temporal resolution which cannot be achieved with manual sampling procedures [Prien, 2007; Varney, 2000].

The Fe concentrations in natural waters can be determined spectrophotometrically with ferrozine (FZ) which forms a purple colored $Fe(FZ)_3$ complex with Fe(II) [Stookey, 1970]. This approach is cheap, easy to operate, has a good sensitivity [Gibbs, 1976] and is adaptable to *in situ* measurements of Fe(II) as well as DFe after addition of a reducing agent like ascorbic acid [Huang et al., 2015; Pascualreguera et al., 1997].

Within the last three decades, several *in situ* flow injection devices based on the FZ method have been developed and deployed in hydrothermal environments, where elevated Fe concentrations can be found. These include the submersible chemical analyzers, SCANNER [Chin et al., 1994; Coale et al., 1991], ALCHIMIST [Le Bris et al., 2000; Sarradin et al., 2005] and CHEMINI [Laes-Huon et al., 2016; Vuillemin et al., 2009]. The most recent Fe analyzer capable of *in situ* measurements is the IonConExplorer, but for this device experiments in natural waters have not yet been reported [Jin et al., 2013]. The limits of detection (LOD) and measurement ranges of the above mentioned FZ based *in situ* analyzers are suitable for deployments in hydrothermal environments with elevated Fe concentrations, but not sensitive enough for Fe measurements in coastal waters with concentrations in the low nM regime. Additionally, autonomous long-term deployments of the flow injection devices are presently impeded by the high liquid and power consumption as peristaltic pumps are needed to provide continuous flow of carrier solution, reagents and sample. In contrast, microfluidic stopped flow devices can use integrated syringe pumps. These enable long-term deployments because of their energy efficiency and minimal fluid consumption. They are also free from drift in the injected flow volume [Nightingale et al., 2015].

Here we present the laboratory characterization and an *in situ* deployment of a new Fe lab-on-chip (LoC) analyzer based on microfluidic technologies [Beaton et al., 2012; Legiret et al., 2013; Rérolle et al., 2013], which is designed to measure Fe(II) and DFe over a broad concentration range (from low nM to several µM Fe). Basing the system around a microfluidic chip provides advantageous reductions in power consumption, reagent use and physical size of the analyzer. It has previously been reported that the FZ method may underestimate Fe concentrations at high dissolved organic matter (DOM) concentrations due to slow kinetics of the release of Fe from colloids and complexes [Luther et al., 1996]. Therefore, we evaluate whether a FZ based analyzer design is capable of producing DFe data in coastal seawater comparable to DFe concentrations determined in discrete samples and analyzed after acidification via inductively coupled plasma mass spectrometry (ICP-MS) according to GEOTRACES protocol.

3.2 Materials and methods

3.2.1 Lab-on-chip analyzer design and specifications

The system presented here is the second generation of a previously developed LoC device for the determination of Fe as described by Milani et al. (2015). A schematic of the microfluidic chip, where reagents are injected and mixed and the spectrophotometric measurements are conducted, is presented in **Figure 3.1**.

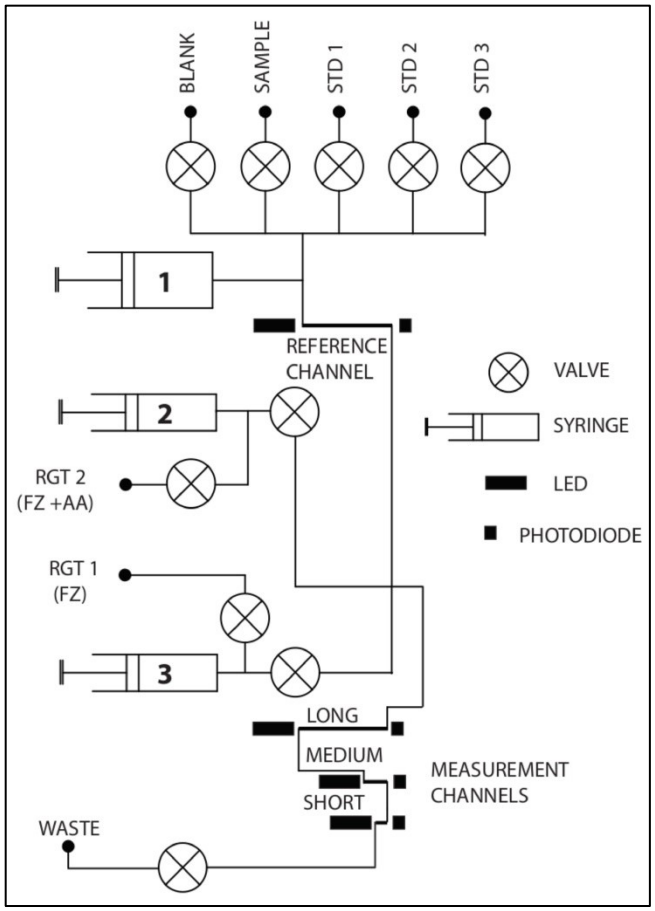

Figure 3.1: Schematic of the microfluidic manifold illustrating the design of the chip. Absorbance measurements are conducted in three optical cells of different length, labelled as long (91.6 mm), medium (34.6 mm) and short (2.5 mm). The syringe pumping unit comprises a large barrel (1) with 9.71 mm ID for blank, sample and standards and two small barrels (2 and 3) with 3.28 mm ID for the FZ/ascorbic acid mixture (RGT 2) and the FZ reagent (RGT 1). Solenoid valves are used for fluidic control.

The chip was manufactured from tinted poly(methyl methacrylate) (PMMA) [Floquet et al., 2011] and consists of three 8 mm thick layers into which microfluidic channels (160 μm wide, 300 μm deep) were milled using a CNC micromill (LPKF ProtoMat S100, Garbsen, Germany). The layers were bonded using an in-house developed solvent bonding method, which also has the effect of reducing surface roughness caused by the milling process,

leaving an optical quality finish [Ogilvie et al., 2010]. The final dimensions of the chip were 119 mm in diameter and 24 mm in thickness. Three on-chip optical absorbance cells (lengths 91.6 mm, 34.6 mm and 2.5 mm) are used to detect the absorbance of the $Fe(FZ)_3$ complex. The LED light source for each cell (AlGaInP, B5B-433-20 LED, Roithner LaserTechnik GmbH, Austria) provides a peak wavelength of 575 nm and a luminous intensity of 4.5 cd. The transmitted light intensity is measured by a photodiode (PD, TSLG257-LF, TAOS, USA) at the end of each optical cell. A custom built three channel syringe pump is directly mounted onto the chip for sample and reagent withdrawal from the reservoirs and injection into the microfluidic channels. The pumping unit comprises two barrels (3.28 mm ID) for FZ and FZ /ascorbic acid mixture (FZ/AA) and one barrel (9.71 mm ID) for sample, blank and standard solutions. All three plungers are moved simultaneously, with the ratio of the injection volume between FZ reagent and sample/standards/blank fixed at 1:8.8. Hall-effect sensors enable the exact determination of the position of the syringe and therefore the adjustment of the total withdrawn and injected volume. Fluidic control is achieved by using micro-inert solenoid valves (LFNA1250325H, The Lee Company, USA) mounted directly onto the PMMA chip. PTFE tubing (0.5 mm ID) is used to connect the fluid reservoirs to the inlets on the microfluidic chip via ¼-28 flangeless fittings (IDEX Health & Science LLC, USA). The chip forms the top endcap to an air-filled cylindrical underwater polyvinyl chloride (PVC) housing (140 mm in diameter, 170 mm in height).

For the characterization of the analyzer in the laboratory it was connected to a benchtop power supply adjusted to 12 V. The measurement cycles were programmed such that the large barrel of the pumping unit and the fluidic channels were flushed five times with 140 µL of the respective fluid (sample, blank or standards) to prevent carry-over effects. For the optimization of this flushing procedure, see section 3.3.1.2. After the flushing procedure, 560 µL of sample, blank or standards and 56 µL of FZ or FZ mixed with ascorbic acid were injected and, after a waiting period of five minutes (to allow complete mixing and stable color formation), the absorbance was measured with the PDs as an average of the signal over 3 s. For the *in situ* deployment, the measurement order for one cycle was programmed as follows: blank, Fe(II) standard, sample (Fe(II)), sample (DFe), DFe standard, blank. This resulted in a measurement frequency of one pair of data points (Fe(II) and DFe) every 45 minutes. A primed 0.45 µm membrane filter (Millipore, polyethersulfone (PES)) was attached to the sample inlet. Reference measurements were conducted in each of the optical cells prior to the addition of color-forming reagents to correct for background absorbance of the sample (sample blank). The concentrations of

Fe(II) and DFe were automatically calculated by the onboard microcontroller using a linear fit according to the Beer-Lambert Law using the reagent blank (color-forming reagent + blank solution) and standard intensity measurements. The simultaneously acquired data sets for all three measurement channels were stored on a built-in 2 GB flash memory card and were individually accessible for processing the data.

The analyzer's sensitivity in laboratory based experiments was evaluated against a benchtop Agilent Cary 60 spectrophotometer using the FZ method in a 10 cm quartz cell. The absorbances at 562 nm obtained with the benchtop device were multiplied by the factor 0.916 to correct for the different cell lengths.

3.2.2 Chemical assays

All glass and plastic ware was cleaned prior to use with ~2 % v/v Citranox acid detergent (Sigma-Aldrich), followed by soaking in a 1.2 M HCl bath (reagent grade, Carl Roth) over night and then rinsed with de-ionized water (MilliQ, 18.2 MΩcm; Merck Millipore) at least three times. Reagents and standards were all prepared and diluted with de-ionized water, except where stated otherwise.

For the detection of Fe(II) a 10 mM FZ solution (3-(2-Pyridyl)-5,6-diphenyl-1,2,4-triazine-p,p'-disulfonic acid monosodium salt hydrate, 97 %; Sigma-Aldrich) was prepared with a 2 M acetate buffer (pH ~ 6) consisting of 0.1 M acetic acid (ultra purity acid grade, ROMIL) and 1.9 M sodium acetate (BioXtra, ≥ 99.0 %, Sigma-Aldrich) giving a final concentration of 0.8 M of the acetate buffer in the FZ reagent. For analysis of DFe the FZ reagent additionally contained 0.1 M ascorbic acid (TraceSELECT, ≥ 99.9998 %, Sigma-Aldrich) acting as a reducing agent to reduce Fe(III) to Fe(II). FZ solutions were prepared weekly and stored at 4 °C in high density polyethylene (HDPE) bottles wrapped in aluminum foil to protect them from light. Ammonium iron(II) sulfate hexahydrate (99.997 % trace metals basis, Sigma-Aldrich) and iron(III) chloride hexahydrate (≥ 98 %, Carl Roth) were used to prepare 20 mM stock solutions of Fe(II) and Fe(III), respectively. These stock solutions were further diluted to 20 µM which was then used for the preparation of the Fe(II) and Fe(III) working standard solutions. All stock and working solutions were stabilized by the addition of concentrated HCl (ultra purity acid grade, ROMIL) giving an HCl concentration of ~12 mM. To prevent the Fe(II) solutions from oxidizing the standards were stabilized using 1 µM sodium sulfite (BioXtra, ≥ 98 %, Sigma-

Aldrich). Stock solutions were made fresh on a weekly basis and stored in opaque HDPE bottles at 4 °C. Working standards were prepared daily for the use in the laboratory.

South Atlantic seawater ([DFe] < 0.2 nM) was used for the preparation of the blank and standard solutions for the *in situ* deployment (50 nM Fe(II) and 100 nM Fe(III)) and diluted with de-ionized water to obtain a salinity of 18, which approximately mimicked the conditions in the Kiel Fjord. All FZ reagents, Fe standards and the blank solution for the *in situ* deployment were stored in 150 mL and 500 mL transparent flexible bags (Flexboy-Bag, Sartorius) covered with dark tape to prevent sun light induced degradation. The bags were suspended inside a PVC tube (length 440 mm, diameter 200 mm), which was attached to the top of the main analyzer housing.

3.2.3 Deployment site and discrete sampling

As part of the SenseOCEAN EU project the Fe LoC analyzer was tested together with other microfluidic analyzers for nitrate, phosphate and pH as well as several optodes *in situ* in the Baltic Sea at 54°19'48.7"N 10°08'59.5"E (inner Kiel Fjord) in the period from September 12 to 20, 2016. The inner Kiel Fjord forms the southernmost part of the Kiel Bay, is extensively used for shipping, has extensive dockyards and a population of ca 250,000 in the surrounding areas. Kiel Fjord has a mean depth of ~13 m, and a maximum tidal range of 4 cm. During the deployment a variation in water height of ± 0.2 m was observed, attributed to winds and pressure gradients over the Baltic Sea. A residence time of a few days has been reported for waters in Kiel Fjord during periods with strong winds [Javidpour et al., 2009]. The major source of freshwater input is rainwater from Kiel and the surrounding areas, which drains into the fjord, and the Schwentine River, located at the eastern shore of the inner Kiel Fjord.

All microfluidic analyzers and part of the optodes were electrically integrated using a central Modbus hub (Chelsea Instruments Ltd) which logged data and provided power. All connected instruments were mounted on two stainless steel frames which were lowered from a pontoon to 2 m water depth. The frames were raised every one to two days in order to inspect the functionality of the sensor packages (e.g. bio-fouling, condition of filters etc.) and to download the data. An EXO2 sonde (YSI Inc., USA) was deployed from September 14 onwards, in order to continuously record hydrographic parameters (salinity, water temperature and oxygen saturation).

Directly next to the deployment site discrete samples were collected three to four times per day using a trace metal clean 5 L GO-FLO sampling bottle (General Oceanics, Inc.) on a nylon line at 2 m water depth. Subsampling was conducted in a clean laboratory and completed within 30 minutes of sample collection.

Dissolved oxygen samples were collected in Winkler glass bottles (nominal volume of 60 mL) in duplicate and analyzed at the end of each day by Winkler titration [Carpenter, 1965].

Samples for the determination of the dissolved inorganic carbon (DIC) and total alkalinity (TA) were collected in 250 mL ground-glass stoppered borosilicate bottles and spiked with 50 µL saturated $HgCl_2$ solution. DIC was analyzed by coulometric titration using a single-operator multiparameter analyzer (SOMMA) [Johnson et al., 1993]. The TA was measured by potentiometric titration using a VINDTA 3S [Mintrop et al., 2000]. Measurements were calibrated using certified reference material (batch 142) obtained from A.G. Dickson (Scripps Institution of Oceanography, USA).

The *in situ* pH was calculated on the free scale from DIC and TA using CO2SYS [van Heuven et al., 2011]. The carbonic acid dissociation constants of Mehrbach et al. (1973) refitted by Dickson and Millero (1987), the boric acid dissociation constant of Dickson (1990), the bisulphate ion acidity constant of Dickson (1990a) and the boron-to-chlorinity ration of Lee et al. (2010) were used.

DFe samples were syringe filtered through 0.45 µm PES filters, which were pre-cleaned with 1 M HCl and rinsed with de-ionized water prior to use. Samples were collected in pre-cleaned (Mucasol detergent for one day, one week in 1.2 M HCl, one week in 1.2 M HNO_3 with three de-ionized water rinses after each stage) 125 mL low density polyethylene (LDPE, Nalgene) bottles. Total dissolvable Fe (TdFe) samples were collected as per DFe samples, but without filtration. TdFe and DFe samples were then acidified to pH < 2 by the addition of 150 µL concentrated HCl (ultra purity acid grade, ROMIL) and stored for 6 months prior to analysis. Samples were then diluted using 1 M distilled HNO_3 (Spa grade, Romil, distilled using a sub-boiling PFA distillation system, DST-1000, Savillex), and subsequently analysed by high resolution ICP-MS (ELEMENT II XR, ThermoFisherScientific) with calibration by standard addition. Analysis of the Certified Reference Materials NASS-7 and CASS-6 yielded Fe concentrations of 6.21 ± 0.62 nM (NASS-7, certified 6.29 ± 0.47 nM) and 26.6 ± 0.71 nM (CASS-6, certified 27.9 ± 2.1 nM), respectively.

For the determination of dissolved organic carbon (DOC), fjord water was syringe filtered (using pre-cleaned 0.45 µm PES filters) into pre-combusted glass vials. The DOC samples

were acidified to pH < 2 with 50 µL conc. HCl (trace metal grade, Carl Roth) per 20 mL seawater. DOC was then analyzed as non-purgeable organic carbon (NPOC) using a high temperature catalytic combustion approach (Shimadzu TOC-L CPH) with direct aqueous injection [Spyres et al., 2000].

Meteorological data (e.g. solar irradiation, wind speed, wind direction) next to the deployment site were obtained from the GEOMAR weather station.

3.3 Results and discussion

3.3.1 Laboratory characterization

3.3.1.1 Calibration and analyzer sensitivity

In order to investigate the response of the *in situ* analyzer, calibration experiments with Fe standards of different concentrations were conducted in the laboratory (**Figure 3.2**). Molar extinction coefficients of 27,200 ± 380 $L \cdot mol^{-1} \cdot cm^{-1}$ and 22,100 ± 240 $L \cdot mol^{-1} \cdot cm^{-1}$ were obtained with the benchtop spectrophotometer (at 562 nm) and the LoC analyzer, respectively. Whilst the coefficient determined using the spectrophotometer was in close agreement with the reported value of 27,900 $L \cdot mol^{-1} \cdot cm^{-1}$ [Stookey, 1970], the coefficient obtained with the *in situ* analyzer was notably lower (**Figure 3.2(A)**). This reduced sensitivity of the analyzer was most likely the result of the use of LEDs with a peak wavelength of 575 nm, whereas the absorption maximum of the $Fe(FZ)_3$ complex is located at 562 nm.

Nevertheless, the microfluidic Fe LoC device is able to detect Fe concentrations with a mean LOD of 1.9 nM for the long cell (calculated as three times the standard deviation of the blank, n = 23). This is significantly lower than other Fe *in situ* analyzers with reported LODs of 25 nM (SCANNER; Chin et al., 1994; Coale et al., 1991), 70 nM (ALCHMIST; Sarradin et al., 2005), 300 nM (CHEMINI; Vuillemin et al., 2009) and 27.25 nM (IonConExplorer; Jin et al., 2013). This enables measurements of DFe concentrations in the low nM regime typically found in coastal waters. Fe standards with concentrations higher than 5 µM exceeded the linear detection range of the long measurement cell (**Figure 3.2(B)**). Whereas, the medium cell (**Figure 3.2(B)**) is capable of measuring elevated Fe concentrations, up to 20 µM, with a linear response. The calibration data recorded with the short measurement cell are not presented here since the range of this cell far exceeds Fe concentrations expected in the water column. Possible applications for the short cell could

be Fe analyses in sediment pore waters, where Fe concentrations in the order of several hundred µM can be found [Burdige, 1993]. Due to the combined use of three different cell lengths, the analyzer is flexible with respect to deployment environments, and thus could potentially be employed in regions with high and variable Fe concentrations.

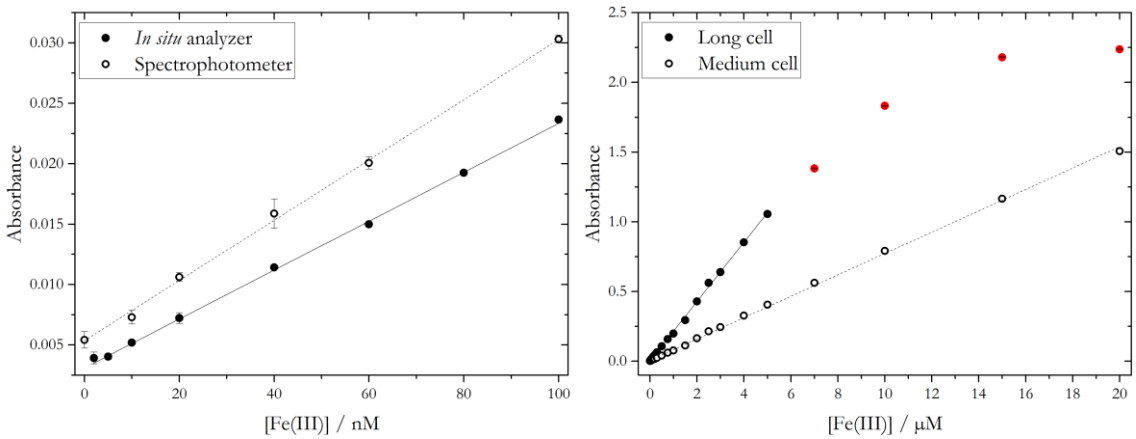

Figure 3.2: Calibration and detection range of the *in situ* analyzer. **(A)** Calibration curves for Fe(III) standards obtained with the long cell of the *in situ* analyzer produced a molar extinction coefficient of 22,100 ± 240 L·mol^{-1}·cm^{-1} (n = 4, filled circles plotted ± standard deviation, R^2 = 0.999) compared to a benchtop spectrophotometer derived molar extinction coefficient of 27,200 ± 380 L·mol^{-1}·cm^{-1} (n=3, open circles plotted ± standard deviation, R^2 = 0.999). **(B)** The linear range for Fe detection with the long (filled circles) and medium (open circles) cells of the analyzer (n = 4), error bars are within the symbols. Data points above the linear response are presented in red.

3.3.1.2 Flushing procedure of microfluidic device

In order to minimize carry-over between standards or samples the required number of flushing steps was determined. For this purpose, the experimental routine was to flush the system first with a 1 µM Fe(II) standard and a pump stroke duration of 6 s (equivalent to 140 µL) followed by the injection with a pump stroke duration of 24 s (equivalent to 560 µL) for the final absorption measurement (red data points in **Figure 3.3**). At least two flushing steps were required to obtain a maximum absorbance signal. The system was then flushed with de-ionized water to determine the required number of flushing steps to prevent carry-over of the Fe(II) standard (blue data points in **Figure 3.3**). Five repetitions of a pump stroke with a duration of 6 s was found to be appropriate to completely flush the system of the previous solution prior to the next analysis. The flushing experiments were also performed with pump stroke durations of 12 s and 24 s (280 µL and 560 µL, respectively). The same results were produced with all three settings. Therefore, carry-over is more dependent on the number of flushes, rather than the total flushing volume. This is likely because much of the volume that needs to be flushed is situated in the bottom of the

large syringe barrel, rather than the fluidic channels of the chip. Thus, prior to each absorbance measurement (both during the deployment and the characterization in the laboratory) 5 × 6 s flushing steps were applied with the respective fluid, followed by a final injection with a pump stroke duration of 24 s for the absorbance measurements during which time the FZ reagent (56 µL) was also injected. Consequently, 1.26 mL of each blank, standard and sample and 168 µL FZ reagent were consumed for each full measurement cycle consisting of one blank, one standard and one sample analysis.

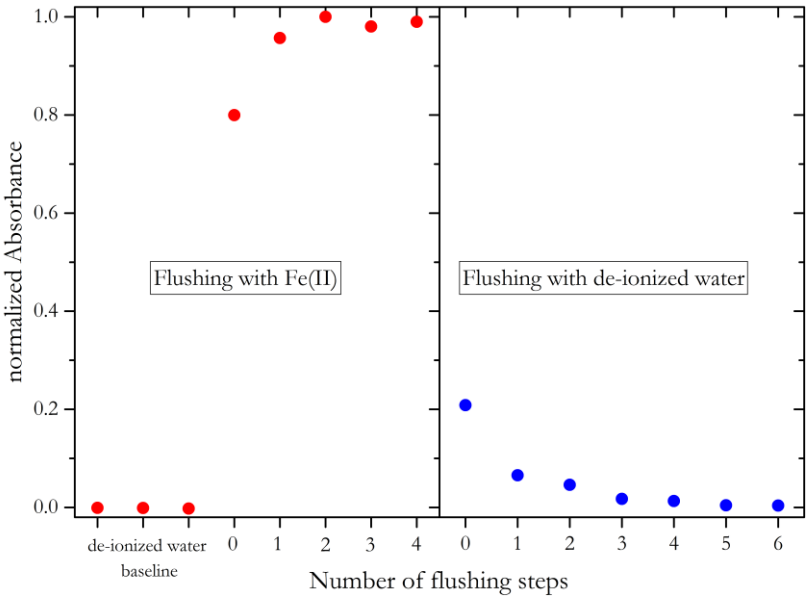

Figure 3.3: Required flushing steps to avoid a carry-over of reagents and standards. The x-axis shows how many flushing steps with a pump stroke duration of 6 s have been applied prior to the injection of the reagents with a pump stroke duration of 24 s for the final absorption measurements. Red data points indicate flushing and absorption measurements with a 1 µM Fe(II) standard, whereas blue data points represent de-ionized water. The first three data points refer to de-ionized water measurements and were set as 0. The maximum absorbance for the Fe(II) standard was normalized to 1.

3.3.1.3 Response time of analyzer

Continuous flow devices rely on turbulent mixing of reagents with blank, standard or sample solutions, which takes place in integrated mixing columns or reaction coils as in SCANNER [Chin et al., 1994] and ALCHIMIST [Sarradin et al., 2005], respectively. In contrast, the microfluidic LoC analyzer was designed as a stopped flow manifold, where the mixing of the reagent with blank, standards and sample is reliant mainly on diffusive processes, and laminar flow conditions are dominant. The results of tests to determine the required time for complete mixing at three different temperatures are shown in **Figure 3.4**.

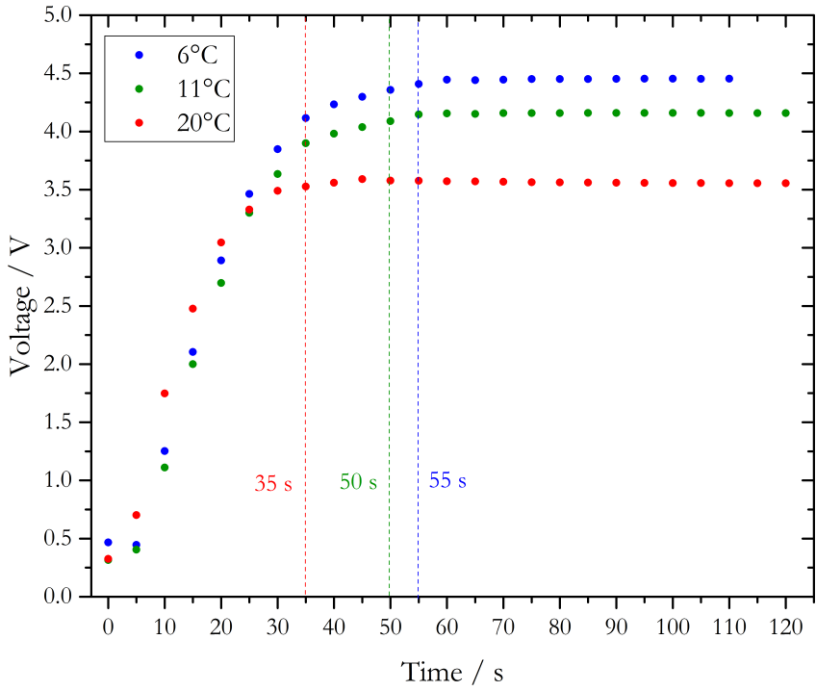

Figure 3.4: Required time to allow complete mixing and stable color development of a 40 nM Fe(II) standard with 10 mM FZ in a de-ionized water matrix using the long measurement cell. The raw voltage signal of the PD of the long cell is shown here (inversely proportional to absorbance). Response times are given as τ_{99}, when the detector output corresponds to 99 % of the maximum signal. Differences in the final recorded voltage for the three applied temperatures after stable signals are obtained due to the temperature dependent signal output of the PDs.

The time which defines complete mixing was calculated as τ_{99}, where the signal reached 99 % of a stable PD output. It was assumed that the time required for full color development is limited by diffusion (seconds to minutes) rather than by the chemical reaction when an Fe(II) spike is added to a FZ solution in a de-ionized water matrix because a stable signal was obtained once mixing was completed (for $t > \tau_{99}$). (To confirm this assumption an experiment with a benchtop spectrophotometer at temperatures between 10 °C and 25 °C was conducted, using an Fe(II) standard manually mixed with FZ. After manual mixing, which occurred within 15 seconds, the absorbance was constant for all applied temperatures.) Due to the inverse relationship between temperature and diffusion coefficient the mixing process in the microfluidic device at 20 °C is faster than at 11 °C or 6 °C with τ_{99} of 35 s, 50 s and 55 s, respectively (**Figure 3.4**). Directly after the injection the light passing through the measurement cell was almost completely attenuated (very low signal), and the light intensity reaching the PD increased with time. This is because a boundary layer is generated when fluids with varying densities and refractive indices are not well mixed (the Schlieren effect). This fluidic interface can act as liquid lens resulting in a loss of light intensity along the optical path [Dias et al., 2006; Zagatto et al., 1990]. The boundary layer disappears with time by diffusive mixing.

However, an additional problem is raised by the speciation of Fe in natural waters where DFe will be present as organic complexes and colloids due to the presence of dissolved organic matter (DOM) [Gledhill and Buck, 2012]. This will affect the reduction rate for DFe measurements and the kinetics of the chemical reaction between Fe(II) and FZ due to a slow release of Fe from its complexes/colloids [Box, 1984; Hopwood et al., 2014]. Consequently, a waiting period of less than one minute may be sufficient to detect only the free/unbound Fe species and may underestimate the total DFe concentration. Taking into account the above issues (temperature, the Schlieren effect, presence of DOM) a waiting period of five minutes prior to the absorption measurements during the deployment was implemented as an attempted compromise between measurement frequency and minimizing the underestimation of DFe species.

3.3.1.4 Measurement frequency and fluid consumption

The settings established in the previous sections (required number of flushing steps and waiting period for complete mixing/reaction) combined to a single measurement duration of ca. 7.5 minutes. As the deployment measurement sequence consisted of six individual measurements (2× blank, 2× standards, 1× Fe(II) sample, 1× DFe sample), one complete cycle for the *in situ* determination of the concentration of Fe(II) and DFe took approximately 45 minutes. This was a much lower measurement frequency than continuous flow analyzers can provide (e.g. 22 samples per hour for the ALCHIMIST analyzer [Sarradin et al., 2005]), but sufficient for the purpose of long-term *in situ* monitoring where other constraints, such as reagent consumption, are also important design considerations. Additionally, if required, the measurement frequency of the LoC analyzer can be increased by programming the sequence such that blanks and standards are analyzed less frequently than every measurement cycle, for example once per hour, resulting in a measurement frequency of eight Fe(II) or DFe samples per hour and less fluid consumption.

A major drawback of continuous flow analyzers is a limited operational lifetime due to their power and reagent consumption [Nightingale et al., 2015]. For example, the ALCHIMIST analyzer consumes 36 mL sodium chloride carrier solution, 18 mL FZ reagent and 18 mL reducing agent over 45 minutes, or normalized per sample: 2.2 mL carrier solution, 1.1 mL of FZ reagent and reducing agent, respectively, excluding standard and blank solution [Sarradin et al., 2005]. Whereas, the fluid consumption of our microfluidic approach within 45 minutes was approximately 2.5 mL of blank and standard solutions and approximately 170 µL of the FZ and the FZ/AA reagent. Normalized per

sample, excluding standard and blank measurements, a consumption of 56 µL of color-forming reagent follows from above. The resulting total fluid consumption for a nine day deployment was therefore a relatively modest 730 mL of blank and sample, 360 mL of each standard and 50 mL of FZ and FZ/AA reagent.

3.3.2 Deployment in Kiel Fjord

3.3.2.1 Standard stability and time series

For the *in situ* deployment of the Fe LoC analyzer two standards, 50 nM Fe(II) and 100 nM Fe(III), were used to determine the Fe(II) and DFe concentrations in Kiel Fjord. Both standards showed a very good stability with no significant drift over the nine days (**Figure 3.5**), resulting in a precision of 2.7 % (n = 214) for measurements of the Fe(II) standard (black data points) and 1.9 % (n = 217) for the Fe(III) standard (red data points).

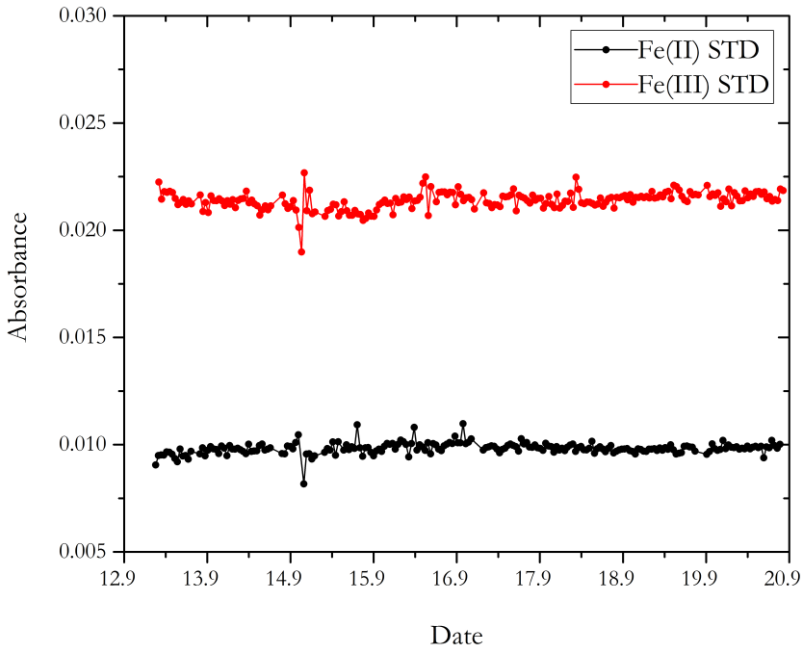

Figure 3.5: Stability of two Fe standard solutions, 50 nM Fe(II) (black line) and 100 nM Fe(III) (red line) over the duration of the nine day deployment in Kiel Fjord.

A linear fit according to the Beer-Lambert Law between each reagent blank and standard measurement was used to calculate the *in situ* concentration of Fe(II) and DFe. As shown in **Figure 3.6**, a maximum of 42 nM (September 18, evening) and a minimum of 17 nM (September 13, morning) was determined for Fe(II) during the nine day deployment with a mean *in situ* concentration of 28 ± 5 nM. The nine day mean of the DFe concentration was

39 ± 6 nM with a maximum of 57 nM (September 13, evening) and a minimum of 27 nM (night between September 13 and 14).

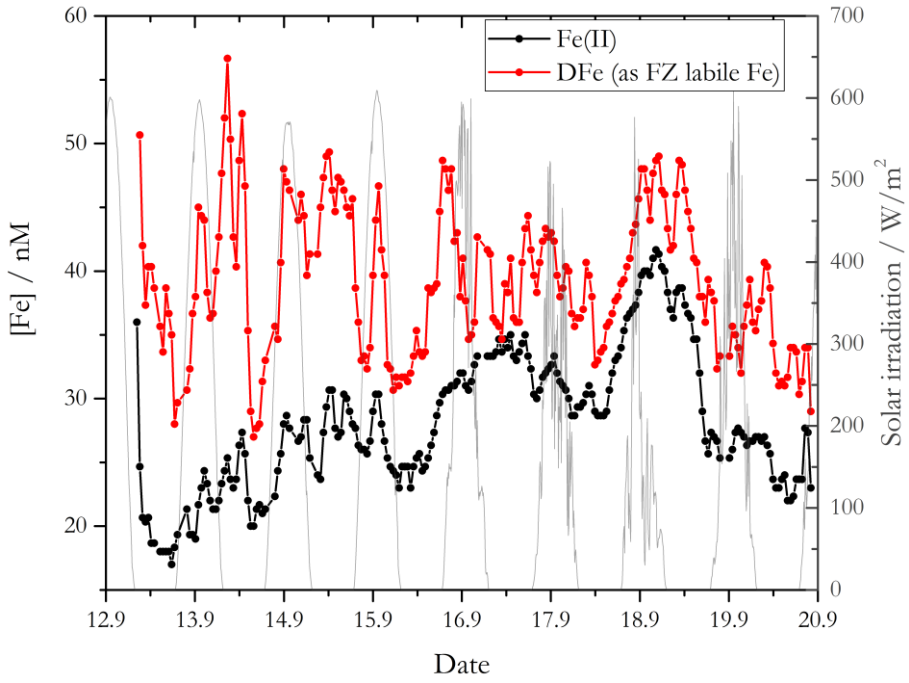

Figure 3.6: Nine day time series of Fe(II) and DFe obtained with the *in situ* analyzer in Kiel Fjord together with the recorded solar irradiation (grey line) next to the deployment site.

Sunlight induced photochemical processes may affect the concentrations of Fe(II) and DFe, but there was no clear evidence of a diurnal trend within this data series over the whole nine deployment days. Sunlight was measured as solar irradiation with a peak irradiation of ~ 600 $W \cdot m^{-2}$ (grey line, **Figure 3.6**). For the first three days of the deployment (September 13 to 15) stable weather conditions were experienced with low cloud cover and clear water conditions with the frame visible from the pontoon in 2 m water depth. On these sunny days there is an indication for a semidiurnal trend of both Fe(II) and DFe, with increasing concentrations during the morning, maximum concentration near noon and reduced levels in the evening. These variations may be linked to photochemical processes [Fan, 2008; Weber et al., 2005]. Increased concentrations during the night may be related to sediment resuspension. From September 16 to 19 it was partly cloudy, with the lowest solar irradiance recorded on September 18. The wind direction was almost exclusively from the northeast (from the estuary of the Schwentine River heading towards the deployment pontoon) with elevated speeds up to 9 $m \cdot s^{-1}$. From September 16 to 19 shallow sediments around the fjord were re-suspended producing very turbid water with high light attenuation. The water temperature at 2 m depth generally showed a diurnal cycle ranging from approximately 19.5 °C – 20.5 °C daily until

September 17. A nearly constant water temperature of ~ 19 °C was recorded for the last three deployment days. The salinity ranged from 18.6 (September 17, noon) to 20.2 (September 19, morning) with a mean salinity of 19.5. The calculated *in situ* pH ranged between 7.8 - 8.2, which is within the range expected for the Kiel Fjord in September [Wahl et al., 2015]. A mean dissolved oxygen concentration of 257 µM, with a minimum of 197 µM O_2 (September 19, morning) and a maximum of 308 µM O_2 (September 15, afternoon) was observed for the manually collected samples. The DOC concentration showed a lower dynamic range, with DOC concentrations between 242 µM and 277 µM over the whole deployment.

The Spearman rank correlation test was used to identify correlation/anti-correlation between the above mentioned variables and the *in situ* obtained Fe(II) and DFe concentrations. The results are summarized in **Table 5**, with shaded cells indicating statistically significant results ($p < 0.05$). A strong statistically significant anti-correlation was found between wind speed and salinity at the deployment site ($p = 2.0 \times 10^{-7}$). The high wind speeds produced low salinities next to the pontoon, which implies the predominance of a wind driven freshwater transport. The *in situ* analyzer showed increasing Fe(II) and DFe concentrations at low salinities/high wind speeds with a strong statistical significance as would generally be expected in any estuarine system with enhanced Fe levels in the freshwater endmember and a loss of DFe and Fe(II), mainly via flocculation, with increasing salinity [Boyle et al., 1977; Huang et al., 2015].
The *in situ* determined Fe(II) concentration tended to decrease with increasing oxygen saturation, measured with the probe situated next to the analyzer, with a statistical significance of $p = 0.021$. This is most likely because Fe(II) is thermodynamically unstable under oxic conditions and rapidly oxidized to Fe(III), with an anticipated Fe(II) half-life ranging from 0.5 min to 6.2 min under the conditions measured in the Kiel Fjord (estimated using oxidation rate constants from Millero et al., 1987).

Table 5: Spearman correlation, variables which correlate/anti-correlate ($p < 0.05$) are highlighted. Cell contents: 1. Correlation coefficient, 2. P Value, 3. Number of samples. Calculations were conducted in SigmaPlot 13.

	$[Fe(II)]_{In\ situ}$	$[DFe]_{In\ situ}$	$[DFe]_{ICP\text{-}MS}$	Recovery	pH	Salinity	Oxygen	Temp.	DOC	Wind speed
$[DFe]_{In\ situ}$	0.492 2.0×10^{-7} 214		0.038 0.847 27	0.029 0.890 25	0.159 0.425 27	-0.424 1.7×10^{-8} 166	-0.111 0.153 166	0.161 0.038 166	-0.401 0.071 21	0.204 0.002 217
$[DFe]_{ICP\text{-}MS}$	-0.357 0.067 27	0.038 0.847 27		-0.908 2.0×10^{-7} 25	-0.632 4.1×10^{-4} 27	0.447 0.054 19	-0.495 0.009 27	-0.093 0.640 27	-0.512 0.008 26	-0.555 0.003 27
Recovery	0.549 0.005 25	0.029 0.890 25	-0.908 2.0×10^{-7} 25		0.503 0.011 25	-0.517 0.028 18	0.333 0.172 18	0.013 0.949 25	0.327 0.117 24	0.588 0.002 25
pH	0.029 0.885 27	0.159 0.425 27	-0.632 4.1×10^{-4} 27	0.503 0.011 25		-0.346 0.144 19	0.869 2.0×10^{-7} 27	0.537 0.004 27	0.246 0.222 26	0.521 0.005 27
Salinity	-0.379 5.9×10^{-7} 166	-0.424 1.7×10^{-8} 166	0.447 0.054 19	-0.517 0.028 18	-0.346 0.144 19		-0.447 2.1×10^{-9} 166	-0.418 2.8×10^{-8} 166	-0.552 0.017 18	-0.791 2.0×10^{-7} 19
Oxygen	-0.180 0.021 166	-0.111 0.153 166	-0.495 0.009 27	0.333 0.172 18	0.869 2.0×10^{-7} 27	-0.447 2.1×10^{-9} 166		0.814 2.0×10^{-7} 166	0.184 0.364 26	0.605 0.006 19
Temp.	-0.090 0.249 166	0.161 0.038 166	-0.093 0.640 27	0.013 0.949 25	0.537 0.004 27	-0.418 2.8×10^{-8} 166	0.814 2.0×10^{-7} 166		0.123 0.546 26	0.412 2.9×10^{-10} 219
DOC	0.094 0.644 26	-0.401 0.071 21	-0.512 0.008 26	0.327 0.117 24	0.246 0.222 26	-0.552 0.017 18	0.184 0.364 26	0.123 0.546 26		0.485 0.012 26
Wind speed	0.371 1.9×10^{-8} 214	0.204 0.002 217	-0.555 0.003 27	0.588 0.002 25	0.521 0.005 27	-0.791 2.0×10^{-7} 19	0.605 0.006 19	0.412 2.9×10^{-10} 219	0.485 0.012 26	

3.3.2.2 Evaluation of the ferrozine method

Despite the reasonable observed trends and correlations between dissolved Fe(II) and DFe concentrations and other hydrographic parameters, the Fe(II) fraction was unexpectedly high for oxic water conditions. A Fe(II) fraction of 45 % of the total *in situ* determined DFe pool was observed on the first day of the deployment, rising to an average fraction of 80 % for September 16 – 20 with a maximum of 97 % in the evening of September 16. Other studies report much lower fractions, ranging from 7 % to 30 % for estuaries using a similar FZ based method [Hopwood et al., 2015]. Our elevated *in situ* Fe(II) fractions could be generated by either an overestimation of Fe(II) concentrations or an underestimation of DFe concentrations by the FZ based microfluidic system. An overestimation of the Fe(II) concentration may be produced by an undesired reaction of labile Fe(III) with FZ contributing to the final absorption of the colored $Fe(FZ)_3$ complex [Viollier et al., 2000]. It was reported that FZ tends to shift the Fe redox speciation through the reduction of Fe(III) to Fe(II), with a reaction half-time of several hours to days at pH = 5, depending on the Fe(III) and FZ concentrations [Mao et al., 2015]. The sample to FZ reagent mixing ratio in the *in situ* analyzer produces a final pH of ~ 5.3. Thus, at this reaction pH and with a mixing time of only five minutes, the potential for overestimation of Fe(II) is limited. However, the rate of FZ induced Fe(III) reduction in natural waters may be accelerated in the presence of DOM [Hopwood et al., 2014].

3.3.2.2.1 Comparison of the *in situ* DFe measurements with ICP-MS

To validate the *in situ* DFe measurements and to examine the extent of a possible underestimation, discrete samples (n = 27) were manually collected, acidified and measured via ICP-MS according to the GEOTRACES protocol for analysis of DFe concentrations in seawater. The DFe concentration of the discrete samples showed a high variability (**Figure 3.7(A)**) ranging from 61 nM (September 18, noon) to 235 nM (September 19, morning). Critically, the *in situ* time series and the discrete samples do not show a significant relationship ($p = 0.847$, see **Table 5**). Furthermore, in contrast to the analyzer, a strong anti-correlation between the DFe concentration of the discrete samples and the seawater pH was obtained ($p = 4.1 \times 10^{-4}$), which is most likely due to the removal of Fe(III) from the dissolved phase at high seawater pH values as a consequence of its precipitation as particulate Fe-oxyhydroxides [Byrne and Kester, 1976; Rose and Waite, 2003b]. While the *in situ* measurements showed a strong anti-correlation with salinity, and a correlation with

wind speed, the ICP-MS data are weakly correlated with salinity and anti-correlated with wind speed, with $p = 0.054$ and $p = 0.003$, respectively. These differences cannot be attributed to any mechanical failure of the analyzer. The lack of a relationship between DFe concentrations measured *in situ* and via ICP-MS strongly suggests that the analyzer does not measure some DFe species in coastal seawater using the current physical and chemical setup. While the ICP-MS analyses provided the total DFe concentration, it can be assumed that the analyzer with the setup and conditions used here only measures kinetically labile Fe species including weak complexes and colloids [Hopwood et al., 2014], where labile refers to the lability of the Fe species to the FZ/AA reagent over a period of 5 minutes.

Curiously, previous work contrasting FZ based Fe analyzers deployed in hydrothermal environments with discrete samples has not reported such underestimations. For the ALCHIMIST analyzer it is reported that the DFe concentrations obtained were in good agreement with ICP atomic emission spectroscopy (ICP-AES) measurements of the discrete samples [Sarradin et al., 2005]. Similarly, excellent agreement was also reported between *in situ* measurements from the SCANNER analyzer and discrete samples analyzed both via graphite furnace atomic absorption spectroscopy (GFAAS) [Coale et al., 1991] and flow injection analysis [Chin et al., 1994]. However, for both deployments there was a difference in the filtered size fractions. The *in situ* SCANNER samples were drawn through 10 μm [Coale et al., 1991] or 20 μm filters [Chin et al., 1994], whereas the discrete samples were filtered at 0.2 μm. Whether or not this difference matters depends on the size distribution of labile Fe/Fe(II) species in a specific natural water body. Where the concentration of labile Fe in the size range 0.2 – 20 μm is negligible compared to the Fe concentration < 0.2 μm, it would be expected that a change in filtration size would not significantly affect a comparison of *in situ* and discrete Fe data. However, where the concentration of labile Fe in the size range 0.2 – 20 μm is non-negligible comparable to the concentration < 0.2 μm, it is still possible that a similar Fe concentration could be obtained comparing sensor determined $Fe_{< 20\,\mu m}$ and ICP determined $Fe_{< 0.2\,\mu m}$, because the sensor determined $Fe_{< 20\,\mu m}$ is strictly the true concentration multiplied by a recovery factor (see Section 3.3.2.2.2). Thus, in an environment where the analyzer design results in a recovery factor of significantly less than 100 %, equivalence between sensor determined $Fe_{< 20\ \mu m}$ and ICP determined $Fe_{< 0.2\,\mu m}$ in isolation does not necessarily demonstrate that the sensor is producing data comparable to acidified ICP samples. Furthermore, the ALCHIMIST and SCANNER analyzers were both primarily tested in hydrothermal vent plumes where Fe speciation is very different from that expected in coastal seawater. Within the vicinity of

hydrothermal vents only a small fraction of DFe is present as organically associated complexes or colloids [Bennett et al., 2008; Hawkes et al., 2013], whereas, in estuarine and near-shore coastal waters Fe speciation is dominated by interaction with DOM [Buck et al., 2007; Gerringa et al., 2007; Rose and Waite, 2003a]. Thus, given the slower kinetics of the reaction between FZ and Fe-DOM species compared to the free Fe(II)/Fe(III) ions, the Fe recovery of a FZ based analyzer in estuarine or coastal seawaters may be considerably less than if the same sensor were deployed within a hydrothermal vent plume.

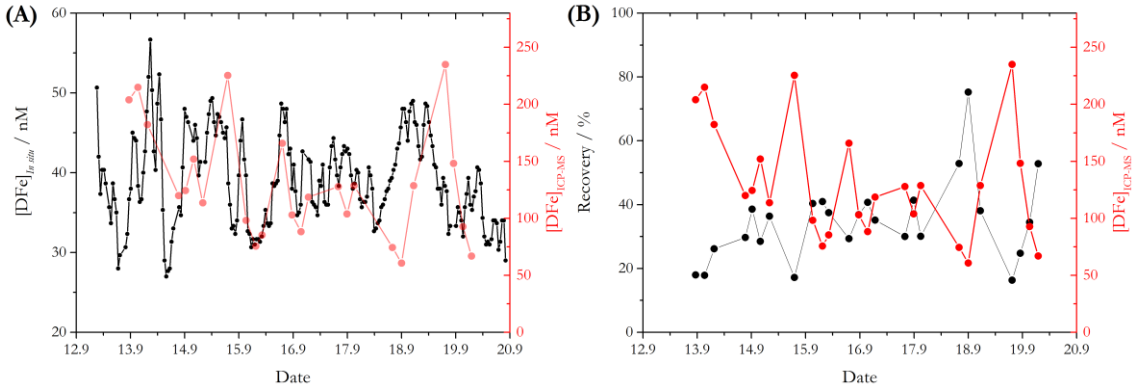

Figure 3.7: (A) Time series of the DFe *in situ* measurements (black, as FZ labile Fe) and discrete samples analyzed via ICP-MS (red). Note the different scales of the y-axes. **(B)** The analyzer's recovery (black) together with $[DFe]_{ICP\text{-}MS}$ (red). For recovery calculations the moving average of the two closest *in situ* data points to each discrete sample was used.

3.3.2.2.2 DFe recovery

The determined DFe concentrations of the discrete samples were used to calculate how well the *in situ* analyzer recovered DFe in the Kiel Fjord (**Figure 3.7(B)**, equation (3.1)).

$$Recovery = \frac{[DFe]_{In\ situ}}{[DFe]_{ICP-MS}} \times 100\ \% \qquad (3.1)$$

Recoveries ranged from 16 % to 75 % of the total DFe pool with a correlation with Fe(II) concentrations ($p = 0.005$), pH ($p = 0.011$), DOC concentrations ($p = 0.006$) and wind speed ($p = 0.002$), and an anti-correlation with salinity ($p = 0.028$). As shown in **Figure 3.7(B)**, a high recovery is achieved for low $DFe_{ICP\text{-}MS}$ concentrations, e.g. 75 % for $[DFe]_{ICP\text{-}MS}$ = 61 nM (September 18, noon), and low recoveries for high DFe concentrations, e.g. 17 % for $[DFe]_{ICP\text{-}MS}$ = 225 nM (September 15, morning), resulting in a very strong statistically significant anti-correlation between recovery and $DFe_{ICP\text{-}MS}$ concentration ($p = 2.0\times10^{-7}$). This may be produced as a consequence of a kinetic effect, as

shown in **Figure 3.8**. Here, the five minutes waiting period after reagent injection in the microfluidic manifold (to allow complete mixing of the reagent and stable color development) is shown for *in situ* determined DFe data points giving a high (black line) and a low recovery (red line). The mixing process of the two phases (FZ/AA reagent and sample) was completed after 50 – 60 s, where both curves show the maximum light intensity reaching the PD detector, indicating an homogenous mixture without the presence of any measurable Schlieren effect (see Section 3.3.1.3). After complete mixing was achieved, the intensity of the transmitted light through the long measurement cell decreased exponentially due to a progressing $Fe(FZ)_3$ complex formation and thus color development. As expected, the curve for the data with a low recovery (high $[DFe]_{ICP\text{-}MS}$) had a stronger exponential decay than the data with a high recovery (low $[DFe]_{ICP\text{-}MS}$). Also, both curves continued to decrease after 300 s of the waiting period, and did not reach their final stable intensity value. This means that the selected time of five minutes to allow color development for DFe measurement is insufficient for the Fe(III) reduction/$Fe(FZ)_3$ complex formation process in natural waters if Fe is present as species other than kinetically labile Fe, causing an underestimation of DFe.

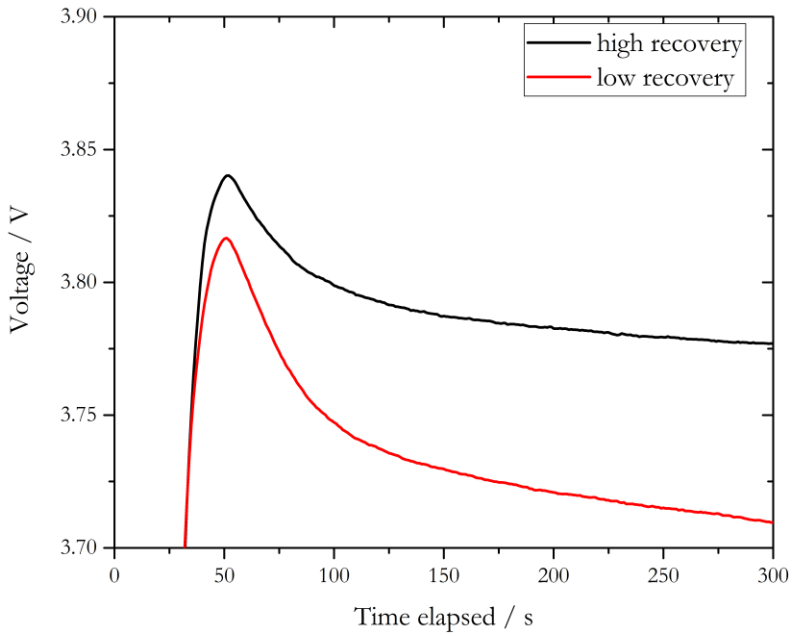

Figure 3.8: Raw signal during the five minutes waiting period to allow complete mixing as well as Fe(III) reduction and complexation with FZ. Data points with a high (September 18, noon, black line) and a low recovery (September 14, noon, red line) are shown.

3.3.3 Implications for future analyzer designs

To improve the DFe recovery of the *in situ* device using the FZ method the waiting period for the color development should be prolonged to release strongly bound Fe from their

complexes and to obtain a constant absorption signal. A second, and probably more analytically robust, option would be an in line acidification step according to the GEOTRACES protocol to pH < 2 prior to the injection of the FZ/AA reagent. This would shift the Fe speciation towards truly dissolved non-complexed Fe phases [Box, 1984; Huang et al., 2015]. However, for both suggested options further investigation is needed to determine whether complete recovery can be achieved within a timescale (minutes – hours) useful for *in situ* deployments.

3.4 Conclusions

In this study an *in situ* microfluidic LoC analyzer for the determination of Fe(II) and DFe in natural waters based on the FZ method was tested to determine the required number of flushing steps (5 × 6 s), required mixing time to achieve a homogenous mixture of components (less than one minute) and LOD (1.9 nM). It was found that the analyzer was able to detect dissolved Fe species across a broad concentration range, from 1.9 nM to more than 20 μM. This facilitates *in situ* deployments in a broad range of marine environments including, for example, estuaries, near-shore coastal waters, benthic boundary waters and hydrothermal vent plumes. The viability of long-term deployments was demonstrated by a nine day deployment in a turbid environment with continuous and successful generation of data.

However, whilst both Fe(II) and DFe time series showed expected relationships to hydrographic variables such as salinity, dissolved oxygen saturation, temperature and to solar irradiation; discrete samples analyzed via ICP-MS revealed a low and highly variable recovery of DFe. A recovery between 16 % and 75 % attributed to an incomplete reaction between organically-complexed Fe species and the FZ/AA reagent meant there was no statistically significant correlation between sensor derived and discrete DFe concentrations. It is therefore suggested that the current waiting period of five minutes to allow full color development is not sufficient. Such a flaw in FZ based *in situ* Fe analyzer designs has not previously been widely discussed, likely because similar analyzers have been primarily developed for hydrothermal vent plumes, where organic complexation is a less prominent feature of DFe speciation. Further experiments should be undertaken to investigate the viability of a longer waiting period and the addition of an acidification step to the present design of the FZ based *in situ* analyzer. Such improvements may facilitate reproducible DFe data in marine environments comparable to datasets obtained from manual sample collection.

Whilst this study describes an estuarine surface deployment, the LoC analyzer is based on a microfluidic platform capable of long-term deployments in environments with highly variable Fe concentrations. Future work will look at validating the analyzer in a range of these environments, ranging from rivers to the deep sea.

Acknowledgements

We thank Chris Cardwell, John Walk, Greg Slavik, Allison Schaap, Urska Martincic, Robin Pascal, Maxime Grand and other members of the Ocean Technology and Engineering Group (OTEG) at NOC. SenseOCEAN colleagues are thanked for assistance with the sensor deployment. We finally thank the three reviewers for their constructive comments

4 Novel lab-on-chip method for *in situ* dissolved Fe analysis in coastal waters

Felix Geißler[1], Eric P. Achterberg[1], Alexander D. Beaton[2], Mark J. Hopwood[1], Mario Esposito[1], Matt C. Mowlem[2], Douglas P. Connelly[2]

In preparation for submission

[1]Chemical Oceanography, Marine Biogeochemistry, GEOMAR Helmholtz Centre for Ocean Research Kiel, Kiel, Germany

[2]National Oceanography Centre, Southampton SO14 3ZH, United Kingdom

Abstract

Iron (Fe) is an essential micronutrient for marine organisms, is fundamentally involved in biogeochemical cycles of other elements and is affecting the productivity and ecology of our oceans; but it is also relatively scarce in marine waters. The dissolved Fe pool (DFe) represents the most bioavailable Fe species. Due to its transient nature, its bioavailability is closely linked to the presence of natural organic ligands. Those ligands form organic complexes with Fe, retaining Fe in the dissolved phase. However, in an earlier study we hypothesized that the spectrophotometric quantification of DFe in natural water samples, using the Ferrozine (FZ) method *in situ* on a lab-on-chip device, is mainly influenced by the presence of those natural Fe complexes, leading to an underestimation of *in situ* determined DFe concentrations compared to discretely collected samples analyzed via inductively coupled plasma mass spectrometry (ICP-MS). Within the here presented study, we demonstrate that acidification (supply of protons) of a natural water sample collected from the Kiel Fjord (Germany) prior to benchtop spectrophotometric detection facilitates the liberation of Fe from its natural complexes, make it therefore accessible for FZ and improve finally the recovery of the method. We found recoveries of ~ 90 % and 96 % when storing the sample for four weeks at pH values of ~ 3 and ~ 2, respectively. Full recovery was achieved after a reaction time of two to three days when acidifying to pH ~ 1. Thus, we re-designed an existing autonomous *in situ* LoC system for the purpose of on-line acidification to pH ~ 1. During *in situ* field tests in August and October/November 2018 of the adapted analyzer in the Kiel Fjord, a period of two hours prior to FZ addition was applied to allow reaction between sample and hydrochloric acid, as a compromise between temporal resolution and recovery. According to Spearman rank correlation test, a significant positive correlation, with a correlation coefficient of 0.55 ($p \leq 0.05$), between the *in situ* determined time series using the acidification approach and DFe concentrations from discretely collected samples and analysis via ICP-MS as validation tool was found. However, an overestimation of the *in situ* time series of ~ 85 nM on average (equal to 180 % recovery) was found when compared to discrete samples. However, as the *in situ* time series showed reasonable significant correlations with other hydrographic parameters, such as dissolved oxygen concentrations, pH value, temperature and salinity, the presented analyzer in its current state might be a useful tool to allow estimations of temporally well resolved relative DFe trends.

4.1 Introduction

The transition metal iron (Fe) is with ~ 4.32 % the 4th most abundant element in the earth's crust [Wedepohl, 1995] but relatively scarce in marine waters and therefore referred as a trace metal. Dissolved Fe (DFe; < 0.45 μm / < 0.2 μm) concentrations of the order of hundreds of nM can be found in coastal waters and estuaries, mainly introduced via riverine and continental runoff [de Baar and de Jong, 2001; Ussher et al., 2004]. Open ocean waters exhibit relatively low Fe concentrations in the range 10^{-12} moles per liter (pmol·L^{-1}) to 10^{-9} moles per liter (nmol·L^{-1}) [Boyd and Ellwood, 2010]. Iron is scarce in marine waters, but plays a pivotal role as a micronutrient in microbial processes, and is closely linked to the biogeochemical cycles of other elements [Raiswell and Canfield, 2012]. The availability of phosphorus, for example, is considered to be regulated by Fe due to the high adsorption capacity of iron(oxyhydr)oxide phases for phosphate [Ruttenberg and Sulak, 2011]. Iron is also fundamentally involved in the marine nitrogen cycle, being an essential part of nitrogenase enzyme complexes which are required for the transformation of di-nitrogen gas into ammonium (nitrogen fixation) [Morel and Price, 2007; Whittaker et al., 2011]. Furthermore, a limited availability of Fe is affecting the productivity and ecology of the world's oceans especially in 'high nitrate low chlorophyll' (HNLC) regions [Martin et al., 1991], as Fe is involved in important cellular processes like photosynthesis and respiration [Sunda, 2001]. The supply of bioavailable Fe is supposed to stimulate phytoplankton growth in HNLC areas thus linking Fe to the global carbon cycle as phytoplankton forms a major sink for atmospheric carbon dioxide [Basu and Mackey, 2018; Breitbarth et al., 2010].

In natural waters the DFe fraction is supposed to be the most bioavailable form of Fe, with Fe being prevalent in the oxidation states +II and +III. Fe(II) is mainly present as free ions but tend to oxidation to the thermodynamically more stable Fe(III) under oxic conditions [Raiswell and Canfield, 2012]. However, Fe(III) is poorly soluble at pH values found in the marine environment (pH ~ 8) [Stumm and Morgan, 1995]. Therefore, it mainly exists as Fe(oxyhydr)oxides and as organic Fe complexes with ligands such as siderophore type molecules or humic substances [Raiswell and Canfield, 2012]. In coastal waters and estuaries ca. 70 – 95 % of DFe, supplied through river outflows or resuspension of sediments, is removed via flocculation along the salinity/pH gradient towards open ocean waters, scavenging onto particles or biological uptake [Ussher et al., 2004]. Therefore, and as result of the transient nature of Fe species with respect to redox processes, the quantification of DFe requires measurements undertaken at high temporal and spatial

resolution. Conventionally, the determination of trace metals in natural waters, such as Fe, is undertaken using laborious sampling and analysis approaches. This involves sample collection, handling, transport, pre-treatment and analysis, and therefore extensive logistical efforts. Furthermore, this classical approach is slow, expensive, of low spatial and temporal resolution and the risk of contamination and alteration of the samples is relatively high. Therefore, the future direction for the determination of trace metals in natural waters is the development of remote real-time analysis methods using *in situ* technologies. The major advantages of *in situ* measurements are the minimization of the risks of sample contamination and alteration while ensuring the integrity of the analyzed water body and gaining reproducibility, enhanced spatial and temporal resolution compared to manual sampling procedures, with the possibility of long-term deployments in remote areas [Prien, 2007; Varney, 2000]. Here microfluidic approaches using lab-on-chip (LoC) technology are a potentially powerful tool for the *in situ* determination of DFe in natural waters [Geißler et al., 2017; Hopwood et al., 2014; Milani et al., 2015]. These submersible analyzers enable the wet-chemical spectrophotometric analysis of natural waters on a micro-scale chip integrating all steps of the analytical procedure (sampling, sample treatment, chemical reaction, detection, data processing) on a single instrument. Lab-on-chip analyzers feature low power and reagent/sample consumption (in the μL range), portability due to their small size as well as capability for long-term deployments (weeks to months), as successfully demonstrated for nutrient analysis and pH measurements in marine environments [Beaton et al., 2011; Grand et al., 2017; Rérolle et al., 2013; Yuecel et al., 2015].

The spectrophotometric analysis of DFe in natural waters can be performed via the reduction of Fe(III) to Fe(II) by a reducing agent followed by the formation of a colored Fe(II) complex with an adequate Fe(II) complexing agent such as Ferrozine (FZ) [e.g. Huang et al., 2015; Pullin and Cabaniss, 2001]. This approach requires Fe(III) to be present in the free ionic form as a reactive species. However, Fe(III) in natural waters exists mainly as species with limited reactivity due to the formation of colloidal Fe(oxyhydr)oxides or organic complexes which might lead to an underestimation of DFe with a recovery remarkably lower than 100 %, especially when bound to strong Fe(III) ligands [Farid et al., 2018; Geißler et al., 2017; Lunvongsa et al., 2006]. In order to liberate Fe(III) from its colloids and complexes a sample treatment is required prior to the spectrophotometric analysis. In literature two pre-treatment measures are suggested for the determination of dissolved trace metal concentrations using sampling and analysis approaches, UV irradiation as well as acidification to pH < 1.9 and sample storage for at least one month

prior to analysis [Bruland and Rue, 2001]. The use of UV light aims to destroy photochemically labile organic ligands and accelerates the liberation of Fe(III). The acidification of the water sample causes a change in Fe speciation through competition by protons for the complexing sites of the ligands and thereby releasing Fe(III) into solution. Furthermore, the acidification shifts the solubility equilibrium from Fe(oxyhydr)oxides towards free Fe(III) and prevents their reformation as well as a re-complexation of dissociated Fe(III) by organic ligands [Farid et al., 2018].

Within the here presented study the acidification approach was evaluated and adapted to a previously reported *in situ* LoC analyzer in order to gain full DFe recovery [Geißler et al., 2017]. The acidification approach was preferentially chosen in the scope of this work as the implementation of an UV irradiation step would require a major conceptual change of the analyzers design. Laboratory experiments were conducted with natural water samples to determine the optimal pH and reaction time required for sample acidification prior to spectrophotometric detection with FZ. The findings were then adapted to the LoC approach in order to evaluate whether on-line acidification can provide *in situ* DFe time series in coastal seawaters comparable to those obtained using collection of discrete samples analyzed via inductively coupled plasma mass spectrometry (ICP-MS).

4.2 Methods and materials

4.2.1 Standard and reagent preparation

All used glass and plastic ware was cleaned prior to use in a ~ 2 % v/v acidic detergent bath (Citranox, Sigma-Aldrich) bath followed by a 1.2 M HCl (reagent grade, Carl Roth) bath, both at least overnight. After each treatment in the respective cleaning bath, the glass and plastic ware was thoroughly rinsed with de-ionized water (MilliQ, 18.2 MΩcm, Merck Millipore).

Stock solutions of Fe(II) and Fe(III) (20 mM, 100 mL) were individually prepared with 0.7843 g ammonium iron(II) sulfate hexahydrate (99.997 % trace metals basis, Sigma-Aldrich) and 558.5 µL of an 1000 ppm iron standard (TraceCERT, 1000 mg·L^{-1} Fe in 2 % nitric acid, Sigma-Aldrich), respectively, and made up to 100 mL with de-ionized water. The 20 mM stock solutions were further diluted to the required Fe(II) and Fe(III) standard concentrations. Additionally, every Fe(II) stock and standard solution was spiked with 0.1 % v/v of a 1 mM sodium sulfite solution (BioXtra, ≥ 98 %, Sigma-Aldrich), and of concentrated HCl (ultra purity acid grade, ROMIL) in order to prevent Fe(II) oxidation.

Each Fe(III) stock and standard solution contained a 0.1 % v/v spike of concentrated HCl to keep Fe(III) in solution.

The Ferrozine/ascorbic acid reagent (FZ/AA) was prepared as follows: 1.25 g of FZ (3-(2-Pyridyl)-5,6-diphenyl-1,2,4-triazine-p,p-disulfonic acid monosodium salt hydrate, 97 %; Sigma-Aldrich) and 4.4 g of ascorbic acid (TraceSELECT, ≥ 99.9998 %, Sigma-Aldrich) were dissolved together with 38.83 g sodium acetate (BioXtra, ≥ 99.0 %, Sigma-Aldrich) and 1.6 mL of concentrated acetic acid (ultra purity acid grade, ROMIL) in de-ionized water and made up to 250 mL. This yielded a FZ/AA reagent with a concentration of 10 mM and 0.1 M, respectively. In contrast to a previously reported study [Geißler et al., 2017], where the FZ/AA reagent was prepared in a 0.8 M sodium acetate/acetic acid buffer (using 40 % v/v of a 2 M buffer), the final buffer concentration of the FZ/AA reagent was increased here to 2 M. This higher concentration was necessary in order to improve the buffer capacity of the FZ/AA reagent due to sample acidification.

Natural water samples were acidified prior to the addition of FZ/AA reagent with dilutions of concentrated HCl (ultra purity acid grade, ROMIL) to the required pH values.

4.2.2 Laboratory acidification experiments

Laboratory acidification experiments of a water sample collected in Kiel fjord with subsequent spectrophotometric analysis (FZ method) were conducted in order to evaluate the effect of pH and duration of acid treatment on the recovery of DFe in natural waters. A volume of 20 L of fjord water (S = 10) was sampled with a polycarbonate canister (Nalgene Clearboy) and stored unacidified for one day in the laboratory. The storage time allowed for temperature equilibration and also equilibration of trace metals with the container walls. The sorption of trace metals in unacidified samples onto the container walls results in their loss from solution which happens most prominent directly after sampling [Subramanian et al., 1978]. After one day, a Tygon tubing was connected to the 20 L canister and nine 1 L subsamples were collected into acid washed 1 L opaque low density polyethylene (LDPE, Nalgene) bottles, with filtration using a 0.2 µm polyether sulfone (PES) filter capsule including a 0.8 µm pre-filter (AcroPak 500, Pall GmbH, Germany). Filtered subsamples were also collected in triplicate in 125 mL LDPE bottles and acidified with 150 µL concentrated ultra-pure HCl; these samples were analyzed using ICP-MS in order to validate the spectrophotometric Fe analysis. The nine 1 L subsamples were directly acidified to pH values of ~ 1, 2 and 3 (each pH value in triplicates) by addition of 10 mL, 1.5 mL and 350 µL, respectively, of concentrated ultra-pure HCl. All

samples were stored and handled at room temperature under a laminar flow hood. Spectrophotometric determination of DFe concentrations in the 1 L subsamples was performed after acidification in fixed intervals over a period of four weeks. For this purpose, 3.4 mL of FZ/AA reagent and 30 mL of acidified sample were mixed in high density polyethylene (HDPE, Nalgene) bottles in triplicates. After five minutes reaction time, the solution was transferred into a 10 cm quartz cell (SUPRASIL, Hellma Analytics). The absorption spectrum was acquired between 400 nm and 800 nm against a sample blank (acidified sample without the addition of FZ/AA) using a double beam spectrophotometer (Shimadzu UV-1800) in order to account for the background absorbance of the water. Individual calibration curves were obtained using Fe(III) standards prepared at pH 1, 2 and 3 and at S = 10 with diluted South Atlantic Seawater ([DFe] < 0.2 nM). The absorbance value at a wavelength of 562 nm was used for the calculation of the DFe concentrations in the samples.

4.2.3 Lab-on-chip analyzer and deployment

4.2.3.1 Chip design

A previously reported design of the LoC analyzer ('Iron 3.3a') [Geißler et al., 2017] was adapted in order to allow *in situ* on-line acidification of a water sample. It required an additional reagent barrel within the syringe pumping unit and a microfluidic reservoir, where the reaction between sample and acid can take place. In principle, all implemented hardware components and overall dimensions of the modified version 'Iron 3.3b' were consistent with version 'Iron 3.3a'. As shown in **Figure 4.1**, an additional connector (RGT 1) as well as an additional small barrel (4) with the same dimensions as the barrels for the FZ (2) and FZ/AA reagents (3) (volume of ~ 63 µL) was integrated into the syringe pumping unit for acid supply. The plunger was attached to the same moving board as the plungers of the three other barrels, which enables a synchronized movement. Control of the movement direction of the acid is achieved via the solenoid valves (0) and (6). A microfluidic inertial flow mixer with the same dimensions as the rest of the microfluidic channels (160 × 300 µm) was milled into the dark-tinted poly(methyl methacrylate) (PMMA) chip between the confluence points of sample with acid and sample with FZ/AA reagent. The added part enhanced mixing of sample and HCl by the introduction of Dean vortices [Al-Halhouli et al., 2015; Howell, Jr et al., 2004], and created an extra volume of 8.42 µL where the reaction between acid and sample was allowed to take place prior to the

addition of FZ/AA reagent. In order to save space on the 11.9 cm wide chip, the length of the long detection channel (CH 2) was reduced from 9.16 cm to 8.58 cm resulting in a volume of 4.12 µL. The dimensions of the medium (CH 0) and the short channel (CH 1) were kept as in LoC version 'Iron3.3a' with a length of 3.46 cm (1.66 µL) and 0.25 cm (0.12 µL), respectively. A light emitting diode (LED) with a peak wavelength of 574 nm (AlGaInP, B5B- 433-20 LED, Roithner LaserTechnik) as light source and a photodiode (PD, TSLG257-LF, TAOS) as detection unit were mounted at the opposite ends of the measurement channels. Additional PDs were positioned perpendicular to each LED to monitor and compensate for any temperature induced drift of the LED output.

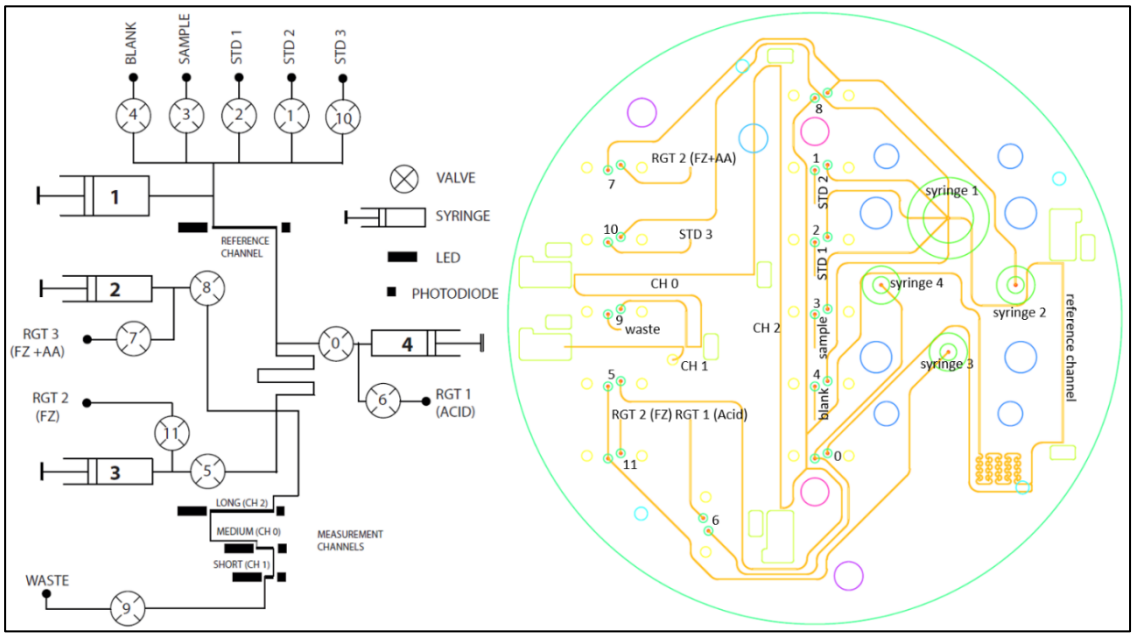

Figure 4.1: Microfluidic diagram and design of the microfluidic chip ('Iron 3.3b') with a schematic (left) and a detailed CAD draw of the actual layout (right). Color code for the CAD draw: orange – microfluidic channels, red – fluid thru holes, small green circles – solenoid valves, green double circles – syringe pump barrels, light green – LEDs and PDs, pink – communication ports, all other circles represent filling, mounting and thermistor holes.

Flexible liquid storage bags (Flexboy, Sartorius) for the supply of standard solutions and reagent were connected via polytetrafluoroethylene (PTFE) tubing with an inner diameter of 0.5 mm and ¼-28 flangeless fittings made of polyether ether ketone (PEEK) to the respective inlets on the chip. The sample was withdrawn through a 0.22 µm PES filter (Merck Millipore) connected via a Luer-Lock fitting to a short (< 10 cm) PTFE tubing in order to minimize dead volume.

4.2.3.2 Deployment measurement routine

Two field campaigns were conducted in Kiel Fjord at 2 m depth, in August and October/November 2018, in order to test the capability of the analyzer to perform accurate DFe measurements in a natural water body. For the deployment the analyzer was programmed such that one analytical cycle for the determination of the DFe concentration was acquired every three hours. This resolution is limited by the time required for on-line acidification but also regarded as sufficient to capture changes associated with the diurnal cycling of light, tidal cycles and changes in weather, all of which either directly affect Fe chemistry, or induce significant changes in the state of the water column and thereby indirectly affect Fe cycling. Each cycle contained five individual parts in the following order: the analysis of a blank, a low Fe(III) standard (STD 1), a high Fe(III) standard (STD 2), a sample without acidification followed by the analysis of an acidified sample (see **Table 6**). Prior to each analysis the system was flushed with the respective standard/sample to avoid any carry over effects of the previous medium. For the blank and sample, five flushing cycles were applied with a full pump stroke length (5 × ~ 560 µL), as the change of matrix required a more rigorous rinsing cycle. The flushing procedure for the standards comprised five flushing cycles with a shorter pump stroke length of 6 s (5 × ~ 130 µL) as the solutions were prepared in the same matrix as the blank. The FZ/AA reagent (RGT 3) was pumped back and forth between syringe barrel and reservoir during flushing. After the flushing procedure, the respective fluid was injected together with the FZ/AA reagent towards the detection channels. In order to allow complete mixing and color formation, the solution was held for five minutes in a stopped flow condition. After the reaction time the output of the photodiode was acquired for the determination of the absorbance which was undertaken using equation (2.6).

The on-line acidification of the sample required a simultaneous injection of a seawater sample and 1.6 M HCl. The mixture was kept for 2 h in the holding/mixing loop to allow Fe(III) dissociation from its organic complexes. Afterwards the acidified sample together with the FZ/AA reagent was slowly propelled (with a reduced pump speed of up to 1/1000 of the original speed) into the detection channels. The reduced pump speed was necessary to ensure that the 8.42 µL of acidified sample is pushed precisely towards the detection channel. The volume of the acidified sample (8.42 µL) is close to that of the sum of the long and medium measurement cell plus the connecting fluidic channel (~7 µL). Therefore, the injection time and speed was chosen in such a way that the analysis was performed in either the long or the medium measurement cell as dispersion could affect a

precise determination. Again, after five minutes reaction time of acidified sample with FZ/AA reagent under stopped flow condition the PD output was obtained and used for the determination of the absorbance according to equation (2.6) After a full analysis cycle of ca. 170 minutes, an idle time of 10 minutes was programmed before the start of the next cycle in order to obtain a sampling frequency of one sample analysis every three hours.

Table 6: Measurement routine for deployment with LoC analyzer version 3.3b in order to determine DFe concentrations of unacidified samples and after *in situ* acidification. Valves are numbered according to **Figure 4.1**.

	State	State Description	Valves open	Executions
	0	Waiting for start command		
BLANK	1	Withdraw Blank and reagent	4, 6 , 7, 11	5x flushed with blank
	2	Inject Blank, reagent is pumped back in reservoir	6, 7, 9, 11	
	3	Decision state		
	4	Withdraw Blank and reagent	4, 6, 7, 11	
	5	Reference Blank (V_{BLK}^{R})		
	6	Inject Blank + reagent	6, 8, 9, 11	
	7	Decision state		
	8	Waiting period		
	9	Measurement state (V_{BLK})		
STANDARD 1	10	Withdraw STD 1 and reagent	2, 6 , 7, 11	5x flushed with STD 1
	11	Inject STD 1, reagent is pumped back in reservoir	6, 7, 9, 11	
	12	Decision state		
	13	Withdraw STD 1 and reagent	2, 6 , 7, 11	
	14	Reference STD1 (V_{STD1}^{R})		
	15	Inject STD 1 and reagent	6, 8, 9, 11	
	16	Decision state		
	17	Waiting period		
	18	Measurement state (V_{STD1})		
STANDARD 2	19	Withdraw STD 2 and reagent	1, 6, 7, 11	5x flushed with STD 2
	20	Inject STD 2, reagent is pumped back in reservoir	6, 7, 9, 11	
	21	Decision state		
	22	Withdraw STD 2 and reagent	1, 6, 7, 11	
	23	Reference STD 2 (V_{STD2}^{R})		
	24	Inject STD 2 and reagent	6, 8, 9, 11	
	25	Decision state		

	State	State Description	Valves open	Executions
	26	Waiting period		
	27	Measurement state (V_{STD2})		
SAMPLE	28	Withdraw Sample and reagent	3, 6, 7, 11	5x flushed with sample
SAMPLE	29	Inject Sample, reagent is pumped back in reservoir	6, 7, 9, 11	5x flushed with sample
SAMPLE	30	Decision state		5x flushed with sample
SAMPLE	31	Withdraw Sample and reagent	3, 6, 7, 11	
SAMPLE	32	Reference Sample (V^R_{Sample})		
SAMPLE	33	Inject Sample and reagent	6, 8, 9, 11	
SAMPLE	34	Decision state		
SAMPLE	35	Waiting period		
SAMPLE	36	Measurement state (V_{Sample})		
Acidified SAMPLE	37	Withdraw Sample and reagent	3, 6, 7, 11	5x flushed with sample
Acidified SAMPLE	38	Inject Sample, reagent is pumped back in reservoir	6, 7, 9, 11	5x flushed with sample
Acidified SAMPLE	39	Decision state		5x flushed with sample
Acidified SAMPLE	40	Withdraw Sample and reagent	3, 6, 7, 11	
Acidified SAMPLE	41	Inject Sample and HCl	0, 7, 9, 11	
Acidified SAMPLE	42	Waiting period (2 hours)		
Acidified SAMPLE	43	Reference acidified Sample (V^R_{Sample})		
Acidified SAMPLE	44	Inject Sample and reagent at 1/1000 speed	6, 8, 9, 11	
Acidified SAMPLE	45	Waiting period		
Acidified SAMPLE	46	Measurement state (V_{Sample})		

Additionally, the Fe analyzer 'Iron3.3a' was deployed together with 'Iron3.3b' for the *in situ* determination of Fe(II). Analytical procedures for the detection of Fe(II) using 'Iron3.3a', including the used standards and reagents are explained elsewhere [Geißler et al., 2017].

4.2.3.3 Discrete sampling and acquisition of hydrographic data

Discrete samples for trace metals, dissolved organic carbon (DOC) and nutrients were taken up to four times per day at the deployment site (inner Kiel fjord, Germany). Manual sample collection was undertaken at the time the *in situ* sample was drawn by the analyzer in order to facilitate direct comparison of *in situ* data and discrete samples. A peristaltic pump (Masterflex L/S series, Cole-Palmer) with an acid cleaned 6.4 mm ID tubing

(Masterflex C-Flex, Cole-Palmer) and a 0.2 µm PES filter capsule including a 0.8 µm pre-filter (AcroPak 500, Pall GmbH, Germany) was used for sample collection from 2 m depth and in-line filtration.

Dissolved trace metal samples were collected in 125 mL transparent LDPE bottles (Nalgene) and acidified to pH < 2 by addition of 150 µL concentrated HCl (ultra purity acid grade, ROMIL). Samples were stored for three months prior to ICP-MS analysis. The samples were diluted 1:10 using 1 M distilled HNO_3 (distilled using a sub-boiling PFA distillation system from SPA grade acid, ROMIL) prior to ICP-MS analysis and analyzed by high resolution ICP-MS (ELEMENT II XR, ThermoFisherScientific). Dissolved Fe concentrations were obtained from the raw data using a linear calibration curve from standards prepared from a multi-element stock solution spiked into 1 M HNO_3. Analysis of NASS-7 and CASS-6 certified reference materials yielded Fe concentrations of 5.91 ± 0.39 nM (certified 6.29 ± 0.47 nM) and 26.8 ± 2.8 nM (certified 27.9 ± 2.1 nM). DOC samples were collected into 20 mL pre-combusted glass vials and acidified with 25 µL concentrated HCl (ultra purity acid grade, ROMIL) and analyzed as non-purgeable organic carbon (NPOC) using a high temperature catalytic combustion approach (Shimadzu TOC-L CPH). Filtered nutrient samples were collected into 15 mL Falcon centrifuge tubes and kept frozen until analysis. Macronutrients were analyzed using a segmented flow autoanalyzer (QuAAtro, SEAL Analytical).

A SeapHOx unit was deployed at the same depth as the LoC analyzers. It comprised of a SeaFET pH sensor and a SBE 37-SMP-ODO MicroCAT CTD+DO sensor for the integrated data collection of pH, temperature, salinity and dissolved oxygen concentration. Data were collected every 10 minutes.

4.3 Results and discussion

4.3.1 Laboratory acidification experiments

Two individual experiments were conducted in order to investigate the effect of an acidification step on the spectrophotometric DFe analysis compared to results obtained via ICP-MS; (1) the color formation over time in an acidified sample after adding FZ/AA reagent was compared to an unacidified sample and (2) the required pH and duration of acid treatment to gain full recovery was determined. **Figure 4.2(A)** shows the change of absorbance over time measured at 562 nm of an unacidified (black) and an acidified (pH ~ 1; red) sample. Here it has to be noted that the x-axis expresses different times for

both sample types. For the unacidified sample it corresponds to the time after mixing of the sample with FZ/AA reagent. The x-axis for the acidified sample corresponds to the time after acid addition. Absorbance spectra of the acidified sample were then measured five minutes after adding the FZ/AA reagent. The absorbance after 35 minutes of acid treatment followed by five minutes reaction with FZ/AA reagent equals the absorbance value obtained after three hours treatment of the unacidified sample with FZ/AA reagent. This suggests that the supply of protons helps effectively to liberate Fe(III) from their colloids and organic complexes into solution, which provides free Fe(III) ions easily accessible for the reduction with ascorbic acid and subsequent complexation of Fe(II) by FZ. Without acidification Fe(III) is just slowly released as a slightly acidic pH of ~ 4.5 is prevalent due to the applied buffer.

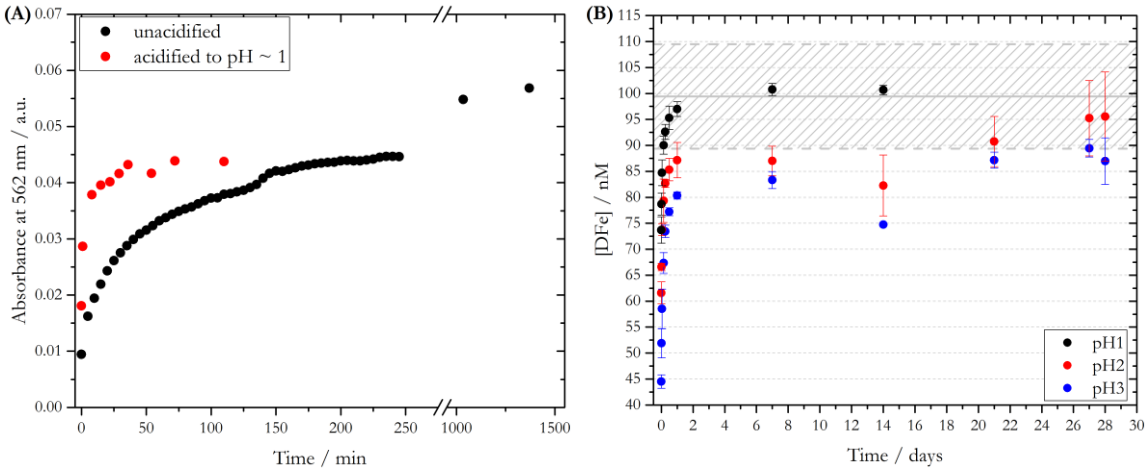

Figure 4.2: (A) Absorbance at 562 nm over time for an unacidified and an acidified (pH ~ 1) fjord water sample, the different expression of the x-axes is explained in the text. **(B)** Spectrophotometrically determined DFe concentration of a fjord water sample acidified to different pH values prior to FZ/AA addition over storage time. Grey line indicates results from analysis via ICP-MS.

The effect of different levels of acidification of a natural sample on the spectrophotometrically determined DFe concentration is shown in **Figure 4.2(B)**. Filtered subsamples from a 20 L water sample from the Kiel fjord were collected and acidified to pH1 = 0.96 ± 0.03 (black), pH2 = 1.88 ± 0.02 (red) and pH3 = 3.03 ± 0.09 (blue) using different amounts of concentrated HCl. After varying time intervals of acid treatment (represented by the x-axis), the samples were mixed with FZ/AA reagent and measured after five minutes. A DFe concentration of 99.1 ± 10.1 nM of the fjord water sample was obtained with ICP-MS analysis as reference technique (grey line), therefore regarded as 100 % recovery. The DFe concentration was fully recovered when storing the sample for one week at pH 1, and subsequent spectrophotometric analysis (**Table 7**). By extrapolation, it can be estimated that full recovery was achieved after three to four days.

Liberation of Fe(III) at pH 2 was almost complete after four weeks storage resulting in a recovery of ~ 96 % compared to ICP-MS analysis. This is in close agreement with the recommendation of GEOTRACES trace element research groups performing DFe measurements to store the sample prior to analysis at pH ~ 1.7 for at least one month [Bruland and Rue, 2001]. When acidifying the natural water sample to pH 3 just ~ 90 % of prevalent DFe was recovered after four weeks; comparable with the recovery achieved after ca. three hours at pH 1. It can be argued that the reduced proton concentration is not adequate to liberate organically complexed Fe. It may also be the case that at higher pH, Fe is more easily adhered to the LDPE bottle surfaces and thus lost from solution.

Table 7: Recoveries of spectrophotometrically determined DFe concentrations compared to ICP-MS analysis for three different pH values over the period of up to four weeks of storage.

Time	Recovery [%]		
	pH1	pH2	pH3
5 min	74.4	62.2	44.9
20 min	79.4	67.2	52.4
1 h	85.5	74.4	59.0
3.5 h	90.8	80.1	68.0
6 h	93.4	83.4	74.1
12 h	96.2	86.1	77.9
1 day	97.9	87.9	81.1
7 days	101.7	87.8	84.1
14 days	101.6	83.0	75.4
21 days	--	91.5	87.9
27 days	--	96.1	90.3
28 days	--	96.4	87.8

Our results show that the Fe liberation from its organic Fe complexes and colloidal Fe phases can be accelerated when applying a pH lower than 1.7 as recommended in GEOTRACES protocols, here pH1 = 0.96 ± 0.03. However, a reasonable compromise between duration required for acid treatment and recovery has to be made when implementing the acidification step to the *in situ* approach. A reproducible high recovery is most desirable, but conversely so is the shortest possible time delay between acidification and analysis in order to obtain highly temporally resolved DFe data. It could be hypothesized that the degree of acidification to pH values lower than the in our study selected pH1 further reduces the storage time required for full DFe recovery. However, in

order to ensure the integrity of the analyzer's internal components a lower pH is not recommended.

4.3.2 Adaptation of acidification step to lab-on-chip analyzer

For the above described benchtop acidification experiments an aliquot of concentrated HCl was used to reduce the pH value of the natural fjord water sample prior to spectrophotometric DFe detection. However, for the purpose of an on-line acidification, the integrity of the components of the LoC analyzer cannot be ensured when exposed to concentrated acid. Furthermore, the volumetric ratio of the sample, acid spike and FZ/AA reagent is fixed to 8.8:1:1 due to the dimensions of the syringe barrels. Therefore, the concentration of the stock acid solution needed to be adapted in a manner that a sample pH similar to pH 1 for the benchtop experiments (e.g. ~ 0.90 to 1.00) after on-line acidification, and a pH > 4.00 after the addition of FZ/AA reagent can be achieved. For pH values lower than 4.00, the performance of the FZ method is impaired [Stookey, 1970]. The use of a 1.6 M HCl and FZ/AA reagent prepared in 2 M acetic acid/sodium acetate buffer is appropriate to meet these pH criteria.

Table 8 shows pH values of a natural fjord water sample after acidification using three different HCl concentrations and after the addition of two different FZ/AA reagents. Although the spike of the natural water sample with a 3.2 M HCl reduced the pH of the sample to 0.50, the integrity of the components of the LoC analyzer cannot be assured when applying this relatively high concentrated acid. Therefore, the use of the moderately concentrated 1.6 M HCl was favored for the on-line acidification step.

Table 8: pH matrix for the addition of 1 mL HCl at different concentrations and 1 mL of two differently prepared FZ/AA reagents to 9 mL of a fjord water sample. RGT1 and RGT2 contained 0.8 M and 2 M acetic acid/sodium acetate buffer, respectively. The initial pH of the fjord water sample was 8.00.

		pH after adding x M HCl		
		0.6 M HCl	1.6 M HCl	3.2 M HCl
9 mL fjord water	+ 1 mL HCl	1.30	0.90	0.50
	+ 1 mL HCl + 1 mL RGT1	3.79	1.26	0.64
	+ 1 mL HCl + 1 mL RGT2	4.71	4.45	-

4.3.3 *In situ* testing phase

The LoC analyzer version 'Iron 3.3b' was first tested in the field in August 2018 in Kiel fjord for a period of nine days. At the beginning of each analysis cycle a calibration with a blank and two Fe(III) standards was performed followed by the analysis of an unacidified sample and an acidified sample. A waiting period of two hours was chosen for the *in situ* treatment with 1.6 M HCl as a compromise between recovery and sampling frequency. At the same location a deployment was conducted in September 2016, and yielded DFe concentrations, as FZ labile Fe, ranging between 27 and 57 nM without *in situ* acidification, and a recovery of 16 to 75 % compared to discrete samples analyzed with ICP-MS [Geißler et al., 2017]. As both deployments were conducted at similar periods of the year, similar DFe concentrations are expected. The *in situ* DFe time series for August 2018 of both unacidified and acidified samples is illustrated in **Figure 4.3**.

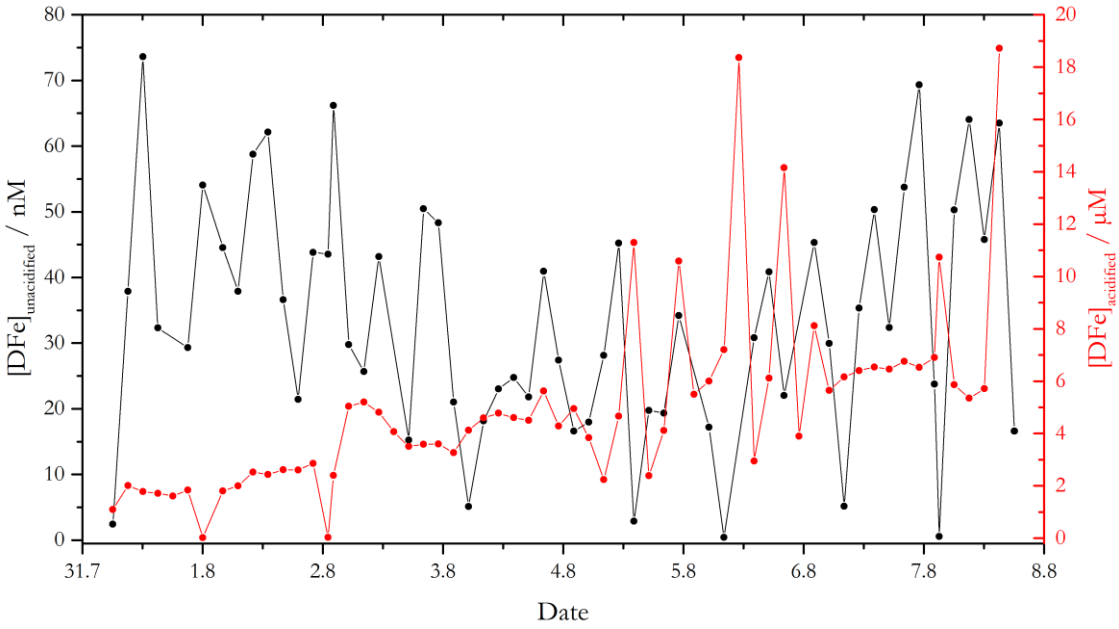

Figure 4.3: Processed DFe concentrations acquired with the DFe LoC analyzer after *in situ* acidification step (red circles / right axis) and of unacidified samples (black circles / left axis) from deployment in the Kiel fjord in August 2018. Note the different scales of the y-axes.

The processed concentrations of the unacidified samples (black circles), which were thus analyzed in the same manner as reported in Geißler et al. (2017), show high variability with a minimum concentration of ~ 1 nM and a maximum of 75 nM. A similar range as for the September 2016 time series was obtained. In contrast, the processed DFe concentrations after a two hour *in situ* acidification step (red circles in **Figure 4.3**) were much higher. At the first two days of the deployment DFe concentrations of ~ 2 µM were measured *in situ* increasing within the period of the deployment up to a maximum of 19 µM and showing a

high variability. Those high concentrations exceed the linear range of the long measurement cell for the detection of Fe [Geißler et al., 2017] resulting in a PD output close to zero due to the high absorbance of the light emitted by the LED as illustrated in **Figure 4.4**.

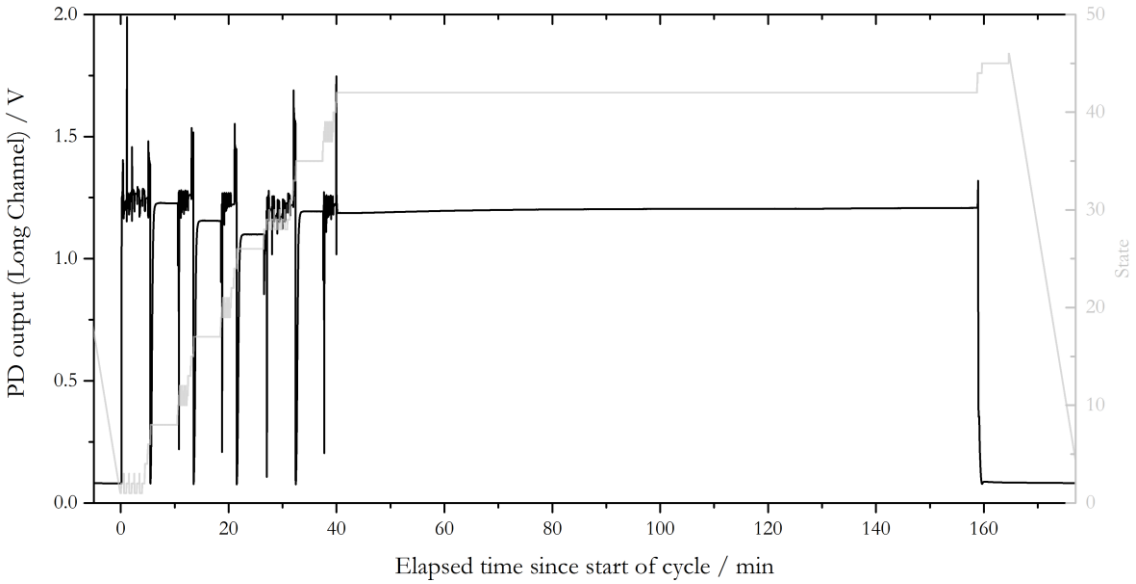

Figure 4.4: Raw PD output of the long measurement channel for one complete cycle of analysis during the deployment in Kiel Fjord in August 2018, including a blank (minute 0 to 11 / state 1 to 9), a 100 nM Fe(III) standard (minute 11 to 19 / state 10 to 18), a 200 nM Fe(III) standard (minute 19 to 27 / state 19 to 27), a sample without acidification (minute 27 to 38 / state 28 to 36) followed by a sample with *in situ* acidification step (minute 38 to 165 / state 37 to 46).

Here, the PD output after complete color development for the unacidified sample at minute 38 is equivalent to a DFe concentration of 63 nM and is thus located within the calibration range. When the acidified sample is introduced after two hours of acid treatment into the measurement channel together with the FZ reagent at minute 160 the PD signal dropped instantaneously to a value of 0.1 V which was equivalent to a DFe concentration of 5.7 µM when applying the previously determined calibration curve of this cycle. Additionally, a purple coloring, which is typical for the $Fe(FZ)_3$ complex, of the waste reservoir attached to the analyzers outlet was observable.

4.3.4 Evaluation of the flushing procedure with hydrochloric acid

In order to assess whether internal leaching of Fe from sensor components induced by the used HCl was responsible for the high Fe concentrations (and the increase with time over the deployment, as seen in **Figure 4.3**), the HCl flushing procedure was evaluated. It has to be noted that the HCl onboard of the analyzer was injected into the analyzers serpentine

mixer towards the measurement channels just for the purpose of the *in situ* acidification step in state number 41 (see **Table 6**). During all other states of the deployment state machine, including the flushing procedures with standards and sample, the analyzers HCl syringe barrel was loaded with HCl when withdrawn and emptied back towards the HCl reservoir bag during the injection movement of the stepper motor. However, a careful evaluation of the flushing procedure was undertaken after the August 2018 deployment (**Figure 4.5**). It was tested whether the flushing routine including or excluding HCl affects the raw output of the PD after mixing the sample with FZ/AA reagent.

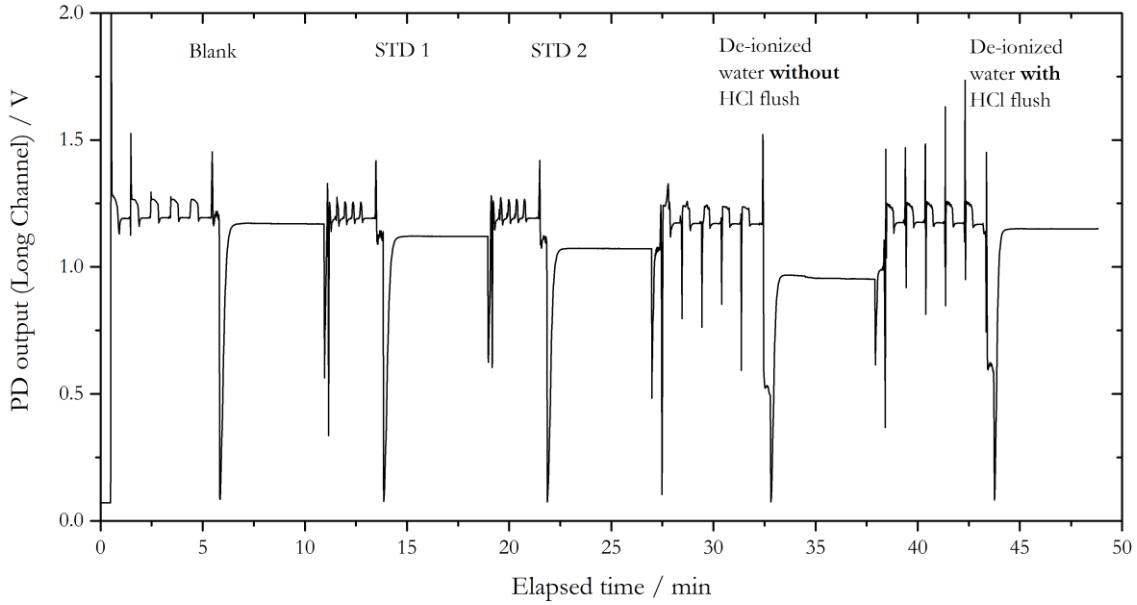

Figure 4.5: Post-deployment laboratory tests for the evaluation of the HCl flushing procedure for the *in situ* acidification step. The analysis cycle included a blank, a 100 nM Fe(III) standard (STD 1), a 200 nM Fe (III) standard (STD 2) and two analyses of de-ionized water with on-line HCl addition. The flushing procedure between minute 27 and 32 was performed just with de-ionized water, whereas HCl flushes together with de-ionized water were applied between minute 38 and 42.

A blank solution and two standards were analyzed as done during the deployment, with HCl pumped in between syringe barrel and reservoir bag, followed by the analysis of a sample (here de-ionized water). This analysis comprised the flushing of the system with de-ionized water (minute 27 to 32) and the injection of the de-ionized water together with HCl and FZ/AA reagent followed by a waiting period to allow full color development (minute 32 to 38). Hereafter, the analysis of de-ionized water was repeated. Distinct to the previous analysis, the system was here flushed with de-ionized water together with HCl (minute 38 to 42) in order to provide 'fresh' HCl for the subsequent analysis with FZ/AA reagent (minute 42 to 48). Compared to the blank and standard solutions, the signal of the PD output for the long measurement cell, shown in **Figure 4.5**, reveals a much lower signal (higher absorbance) after mixing with FZ/AA reagent when HCl is excluded from the

flushing procedure. However, when HCl was included into the flushing procedure a PD output similar to that of the blank solution was obtained after mixing with FZ/AA reagent (minute 42 to 48). Thus, it seems likely that Fe is somehow leached out from the analyzers components (either from the PMMA walls of the microfluidic channels or from the plungers used in the syringe barrels or solenoid valves) induced by the relatively high concentrated HCl while pumped forth and back during the analysis cycles of blank and standard solutions. The Fe accumulated in the HCl falsified therefore the absorbance reading when not included into the flushing procedure and produced the high absorbance values seen during the August 2018 deployment. As a consequence for future deployments a flushing procedure including HCl prior to the *in situ* acidification step is required in order to provide 'fresh' HCl and was therefore implemented into the state machine used for subsequent deployments.

4.3.5 DFe time series and evaluation of analyzers performance

A second field campaign with the analyzer was conducted from October 17 to November 19, 2018 in the Kiel fjord, with HCl being flushed through the system together with the sample to minimize any contamination risk. Again, each analysis cycle started with a calibration sequence including standards with three different Fe(III) concentrations followed by the analysis of an unacidified as well as an acidified sample with a sampling frequency of one sample per three hours. A total number of 197 *in situ* data points were acquired and 80 discrete samples were collected. The analyzer needed to be recovered after two weeks of deployment due to a malfunction of its pumping unit. Opening of the analyzer revealed that all mechanical metal parts of the pumping unit were corroded, assuming a leakage of HCl. After maintenance and careful cleaning of the affected parts the analyzer was re-deployed but the performance was still not acceptable. Therefore, *in situ* data obtained after October 30 were not taken into consideration for further discussion and correlation analysis to physical and chemical parameter measured *in situ* and with discrete samples. From October 21 to November 01 the determination of the DFe concentration of the acidified samples was performed in the medium length measurement cell. A detailed illustration of the DFe time series together with the solar irradiation during this period is shown in **Figure 4.6**. Mean values as well as minima and maxima for every acquired parameter between October 21 and October 30 both *in situ* and with discrete samples are reported in **Table 9**.

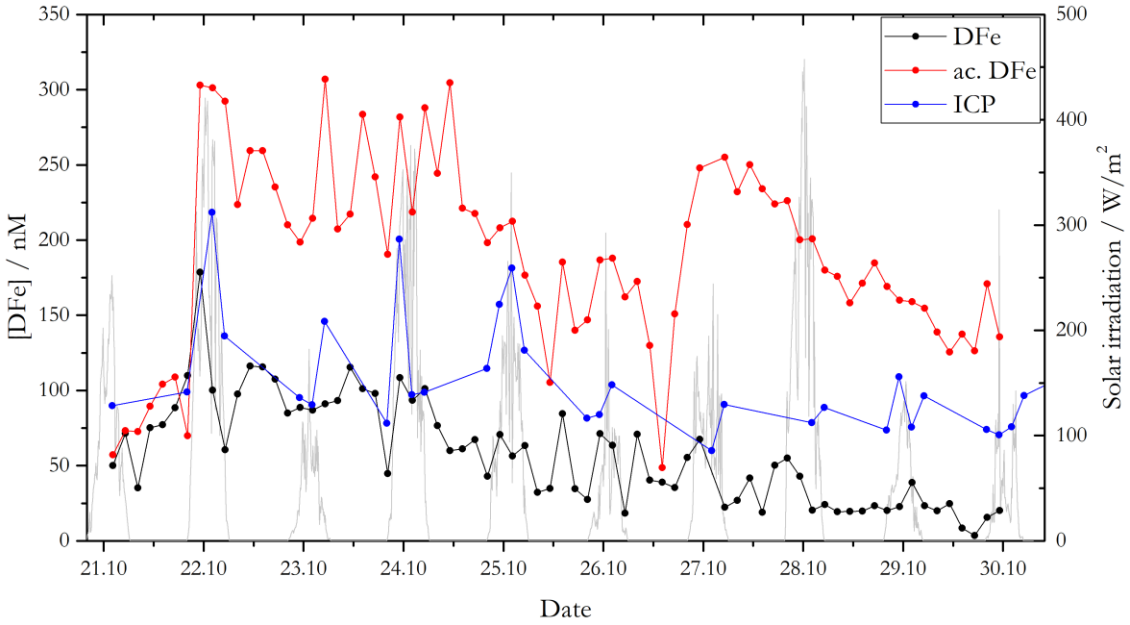

Figure 4.6: DFe time series from October 21 to October 30 determined with the medium channel of the LoC analyzer of unacidified (DFe, black) and acidified samples (ac. DFe, red) together with the time series from the analysis of discrete samples via ICP-MS (blue) and solar irradiation (grey).

Table 9: Mean values including standard deviations as well as minimum and maximum values for acquired parameters measured *in situ* (grey shaded) and from discrete samples for the period October 21 to October 30.

Parameter	Mean ± SD	Min.	Max.
$[Fe(II)]_{in\ situ}$ / nM	18.6 ± 6.2	3.5	39.9
$[DFe]_{in\ situ}$ / nM	58.4 ± 34.8	3.6	179
[ac. DFe]$_{in\ situ}$ / nM	190 ± 62.8	48.7	307
$[DFe]_{ICP\text{-}MS}$ / nM	106 ± 38.4	59.9	218
Temp. / °C	12.8 ± 1.0	11.4	14.1
Salinity	21.2 ± 0.5	19.9	21.8
pH	7.75 ± 0.11	7.60	8.12
$[O_2]$ / mg·L^{-1}	7.67 ± 0.70	5.76	8.88
[Phosphate] / µM	1.39 ± 0.11	1.11	1.55
[Nitrate] / µM	1.85 ± 0.86	0.84	3.81
[DOC] / µM	266 ± 16.2	234	290

A mean *in situ* DFe concentration of 58.4 ± 34.8 nM without the addition of HCl (hence as FZ labile Fe) was determined using the medium channel, with the highest concentration during daytime on October 22 (179 nM) and the lowest during early morning on October 30 (3.6 nM). Data of FZ labile Fe acquired with the long measurement channel of the analyzer (not shown here) were with an average of 59.8 ± 34.4 nM in very good

agreement with those of the medium channel, suggesting a reproducible analyzer performance. The mean value of the discrete samples was 106 ± 38.4 nM and approximately 50 nM higher than the concentrations of FZ labile Fe determined *in situ*, resulting in a mean recovery of ~ 55 %. This value is in the same range as the recovery reported in Geißler et al. (2017), underpinning the need of an on-line acidification step in order to gain full recovery. However, the DFe *in situ* concentration after acidification was on average ~ 130 nM and ~ 85 nM higher than without acidification and of discrete samples, respectively, with maxima around 300 nM (October 22, 23 and 24/25) and the lowest concentration being ~ 50 nM during the night October 26/27. In order to identify statistically significant (anti-)correlations between the DFe time series and hydrographic data a Spearman rank correlation test was conducted using the software 'R' (**Figure 4.7**). Despite the relatively high discrepancy between *in situ* DFe values and discrete samples both time series for unacidified as well as for acidified fjord water show a significant (p value ≤ 0.05) positive correlation to discrete samples with a Spearman correlation coefficient of 0.66 and 0.55, respectively, as illustrated in **Figure 4.7**. There are furthermore indications for a diurnal pattern for all three DFe time series with increasing concentrations during the morning and decreasing concentrations in the evening, especially on October 22, 24 and 25 (**Figure 4.6**). Those variations may be attributed to photochemical processes affecting Fe speciation involving reactive oxygen species induced by sun light as highest solar irradiation values were recorded during these days [Rose and Waite, 2003b; Weber et al., 2005]. A mean DOC concentration of 266 ± 16.2 µM with a low dynamic range of ~65 µM between its minimum and maximum was observed for the presented period of ten days (**Table 9**). Interestingly, the *in situ* DFe time series determined without acidification anti-correlates significantly with the DOC concentration of the discrete samples with a Spearman correlation coefficient of -0.57 (**Figure 4.7**). In contrast, the DFe time series after *in situ* acidification as well as DFe determined from the discrete samples do not show any significant relationship with DOC. Thus it can be assumed, as previously reported [Geißler et al., 2017; Hopwood et al., 2014], that two different Fe species are determined without and with the supply of HCl, weakly bound/kinetically labile Fe (FZ labile Fe) when no protons are provided and strongly complexed Fe when the pH is lowered to pH < 2 prior to analysis. However, the DOC concentrations during the deployment showed relatively small variations (**Table 9**). Critically, one would expect that the DFe concentration correlates positively with the amount of DOC present in the water body as Fe binding ligands prevent Fe from precipitation as Fe(oxyhydr)oxides via the formation of Fe complexes and facilitates therefore Fe solubility and bioavailability

[Gledhill and Buck, 2012]. However, no experiments determining the nature of the natural organic compounds regarding the individual fractions of weak and strong Fe binding ligands have been conducted, and therefore a more detailed examination was not possible. Significant positive correlations with salinity were observed for all determined Fe species, Fe(II), DFe, acidified DFe and discrete DFe values, with Spearman correlation coefficients of 0.41, 0.75, 0.56 and 0.55, respectively. A negative correlation is rather expected due to a non-conservative behavior of Fe at low salinities and its conservative behavior at higher salinities. An increase in ionic strength is supposed to facilitate Fe removal via flocculation of charged dissolved species due to charge neutralization, e.g. during estuary mixing [Boyle et al., 1977]. This non-conservative behavior of Fe is characteristic for estuaries when freshwater is mixed with saltwater, with most of the Fe being rapidly removed at low salinities, e.g. S < 15 [Holliday and Liss, 1976]. At higher salinities, as observed in our study with a relatively high mean value of 21.2 ± 0.5, a more conservative behavior of Fe is expected due to dilution of the freshwater [Holliday and Liss, 1976]. However, it is possible that the significant negative correlations of Fe with oxygen and pH outcompeted the correlation with salinity as a very small dynamic salinity range of < 2 was observed in our study. Fe concentrations and speciation are strongly linked to the oxygen concentration and pH value, according to equation (4.1).

$$-\frac{d[\mathrm{Fe(II)}]}{dt} = k[\mathrm{Fe(II)}][\mathrm{O_2}][\mathrm{OH^-}]^2 \tag{4.1}$$

Here, the rate for the oxidation of Fe(II) to Fe(III) in seawater depends on a rate constant k as well as the Fe(II), oxygen and hydroxide ion concentrations [Millero et al., 1987]. Therefore, the oxidation of Fe(II) is favored under oxic conditions and high pH values, resulting in a negative correlation between Fe(II) and oxygen concentrations, and also pH as observed in Kiel fjord during the ten-day time series with Spearman correlation coefficients of -0.44 and -0.41, respectively (**Figure 4.7**). The formation of Fe in high valence states, e.g. insoluble Fe(oxyhydr)oxides, is promoted which leads to a removal of Fe from the dissolved phase and thus a negative correlation between DFe concentrations and dissolved oxygen concentrations [Zhu et al., 2018]. This oxidative control is more prominent for free or just weakly complexed Fe (from unacidified samples) with a Spearman correlation coefficient of -0.67 than for the whole DFe pool with Spearman correlation coefficients of -0.55 and -0.52 for *in situ* and discrete DFe time series,

respectively. Further, the solubility and hence Fe concentration and speciation in the dissolved phase depends on the pH, with low Fe(III) solubility at high pH values and vice versa [Stumm and Morgan, 1995]. Significant anti-correlation between pH and DFe time series were found in the Kiel fjord with Spearman correlation coefficients between -0.43 and -0.58 (**Figure 4.7**).

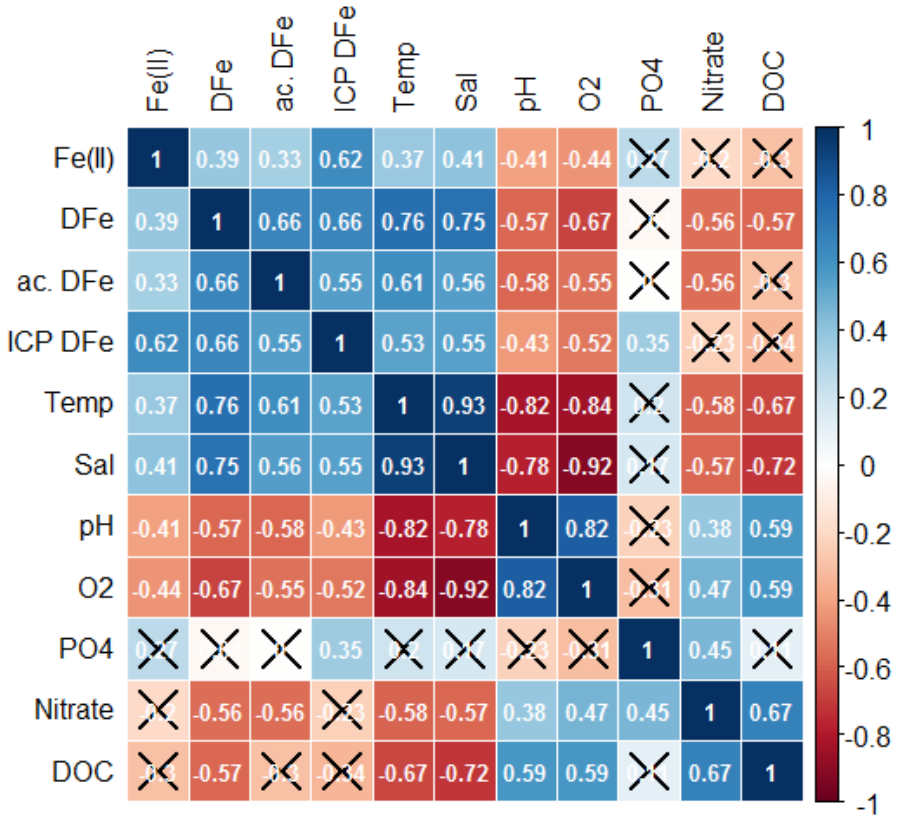

Figure 4.7: Spearman correlation matrix of *in situ* and discretely determined variables calculated with data points from October 21 to 30. Positive correlation coefficients are illustrated in blue boxes, negative ones in red. Not significant correlations (p value ≥ 0.05) are crossed out.

The results of the Spearman rank correlation tests show a positive correlation between the acquired Fe time series, both *in situ* and from discrete samples, as well as relationships to other hydrographic variables. However, as reported in Geißler et al. (2017) *in situ* DFe concentrations without an acidification step are underestimated as just FZ labile Fe is determined, whereas the DFe concentrations determined with an integrated acidification step are overestimated when compared to discrete samples analyzed via ICP-MS. In contrast to the *in situ* analysis without acidification, it can be assumed that spectrophotometric analysis including an *in situ* acidification step and the analysis of the discrete samples via ICP-MS are determining the same DFe pool as both protocols comprised the addition of HCl. This was also shown earlier in section 4.3.1 with spectrophotometric laboratory experiments yielding the same DFe concentrations after

acidification like ICP-MS analysis. Therefore, it has to be assumed that the overestimation observed during the deployment of ~ 85 nM on average is attributed to a of some extent reproducible contamination of the sample caused by the use of HCl, e.g. through Fe leaching from parts of the analyzer which come in contact with the acid, despite the adapted flushing procedure. Nevertheless, leaching tests of those components are required in order to identify the origin of the Fe contamination, so that the affecting parts/materials can be replaced.

4.4 Conclusion

This study demonstrated that acidification of a natural water sample to pH ~ 1 for at least one day prior to the spectrophotometric determination of DFe in marine water from the Kiel fjord using the FZ method, enables a DFe recovery of almost 100 % compared to ICP-MS analysis. An acid treatment for a period of at least two weeks was required when samples were acidified to pH ~ 2. The acidification process liberates Fe from its organic complexes. Therefore, the acidification of a sample to a pH value ≤ 1 is recommended for fast and reliable spectrophotometric DFe analysis using the FZ method.

With these findings a previous design of a microfluidic DFe LoC analyzer was adapted to allow an *in situ* acidification step prior to the analysis. In order to achieve a compromise between effective Fe liberation from its natural occurring organic complexes and the temporal resolution of the *in situ* time series, a period of two hours was chosen for the treatment of the sample with 1.6 M HCl. The adapted FZ method was finally evaluated in the field during a deployment in the Kiel fjord. It was found that *in situ* DFe analysis of unacidified samples underestimated the naturally present DFe concentrations (~ 50 nM on average lower compared to discrete samples), whereas an overestimation (~ 85 nM) was observed for the *in situ* determination including an *in situ* acidification step. The overestimation was attributed to an HCl induced leaching of Fe from the materials used in the analyzer. Here, further investigation is required in order to allow *in situ* DFe determinations yielding concentrations matching those of discrete samples analyzed via ICP-MS. Although the *in situ* concentrations did not match the discrete values, Spearman rank correlation tests showed significant positive correlations among the different acquired DFe time series as well as significant relationships with hydrographic parameter such as dissolved oxygen concentrations, pH value, temperature and salinity. Thus it can be concluded that the presented microfluidic DFe analyzer might be suitable for relative DFe

measurements with the potential for further improvements towards a reliable system matching *in situ* DFe concentrations with those of discrete samples.

5 Lab-on-chip analyzer for the *in situ* determination of dissolved Mn in seawater

Felix Geißler[1], Eric P. Achterberg[1], Alexander D. Beaton[2], Mark J. Hopwood[1], Mario Esposito[1], Matt C. Mowlem[2], Douglas P. Connelly[2], Douglas Wallace[3]

To be submitted

[1]Chemical Oceanography, Marine Biogeochemistry, GEOMAR Helmholtz Centre for Ocean Research Kiel, Kiel, Germany

[2]National Oceanography Centre, Southampton SO14 3ZH, United Kingdom

[3]Department of Oceanography, Dalhousie University, Halifax, Nova Scotia, Canada

Abstract

The spectrophotometric approach for the quantification of dissolved manganese (DMn) with 1-(2-pyridylazo)-2-naphthol (PAN) has been adapted for its *in situ* application in coastal and estuarine waters using a submergible microfluidic lab-on-chip system. Due to its miniaturized design the analyzer is characterized by portability and small power (~ 1.5 W) and reagent consumption (63 µL per sample), being therefore a powerful tool for long-term *in situ* deployments. Laboratory characterization showed an extinction coefficient of 40,838 ± 1,127 $L \cdot mol^{-1} \cdot cm^{-1}$ and a detection limit of 27.2 nM, determined for the 34.6 mm long optical detection cell. Laboratory tests showed that long-term stability of the PAN reagent was assured by the addition of 4 % v/v of the non-ionic surfactant Triton-X100 to the PAN reagent. A 20 % overestimation of Mn(II) concentrations was found when Fe(III) and Mn(II) were present in equimolar concentrations in de-ionized water based standard solutions. However, an underestimation of Mn(II) was found when the Fe(III) masking agents deferoxamine mesylate (DFO-B) or disodium 4,5-dihydroxy-1,3-benzenedisulfonate (Tiron) were added to the PAN reagent in order to suppress any Fe interferences. It was further demonstrated that DFO-B lost its masking strength towards Fe(III) over time due to its limited life time, making it therefore unsuitable for deployments over periods of several days to weeks. The proposed method was tested during a deployment in the Kiel Fjord (Germany), with successful acquisition of 215 *in situ* data points. The *in situ* time series was in good agreement with DMn concentrations determined from discretely collected samples analyzed via inductively coupled plasma mass spectrometry (ICP-MS) as reference technique, exhibiting an accuracy of > 99 % for certain periods and reasonable correlations to other hydrographic parameters. Thus, it was demonstrated that the presented analyzer is a powerful and reliable tool for the *in situ* detection of DMn in seawater with elevated DMn concentrations.

5.1 Introduction

The acquisition of data on concentration, speciation and fluxes of chemical compounds, such as macro- and micronutrients, dissolved gases or organic molecules produced by organisms, is essential for the improvement of our understanding of key biogeochemical processes in marine waters. Conventionally, the determination of those parameters relies on an approach involving collection of discrete water samples during surveys followed by sample analysis either on-site, shipboard or in a home laboratory. However, with this approach the integrity of the sample with respect to changes in physical conditions such as pressure, temperature and light upon removing the sample from the water column, as well as a possible contamination during sample collection, transport and handling cannot be assured [Mills and Fones, 2012]. A sufficient temporal and spatial resolution to investigate environmental phenomena often cannot be provided as this requires substantial logistical efforts with typical time delays of up to several months between sample collection and lab-based chemical analysis. Furthermore, ship-based oceanographic campaigns involve a high carbon-footprint. The deployment of chemical sensors on autonomous platforms can ultimately reduce the environmental footprint of research and simultaneously improve the quality and quantity of data.

In order to overcome the inevitable drawbacks affiliated with sample collection, transport, storage and handling, the parameter of interest has to be determined directly in the water column using *in situ* monitoring technologies [Johnson et al., 1992; Prien, 2007]. This is especially relevant in remote areas, but also in ocean systems exhibiting pronounced variability on short temporal and spatial scales such as the dynamic surface coastal ocean. Of particular interest in the field of sensor development are redox sensitive micronutrients such as the trace metal manganese (Mn), which is an essential micronutrient for marine phytoplankton [Twining and Baines, 2013]. Dissolved (< 0.45 μm) Mn (DMn), the most bioavailable size fraction, may co-limit primary production in some parts of the Southern Ocean [Middag et al., 2011]. Manganese is essential for photosynthesis and the production of active superoxide dismutase, an antioxidant which protects phytoplankton against damage from reactive oxygen species [Peers and Price, 2004].

Manganese in its insoluble oxidized form (+IV) plays an important role in the removal of other trace metals and rare earth elements from the water column due to adsorption processes onto Mn oxide particle surfaces [Tachikawa et al., 1997]. However, oxidized Mn(IV) can be reduced to dissolved Mn(II) via photoreduction induced by sunlight [Sunda

et al., 1983]. As a result of this reductive process, together with atmospheric sources such as dust, relatively high DMn concentrations can be found in the euphotic zone of open ocean waters, e.g. up to 2 nM in the West Atlantic Ocean [van Hulten et al., 2016] and 3.2 nM in the East Atlantic Ocean [Statham et al., 1998]. In surface waters with low atmospheric inputs DMn concentrations up to 1 nM can be found e.g. in the North Pacific Ocean [Bruland et al., 1994]. Concentrations of DMn decrease with depth over the top few hundred meters due to scavenging processes to a mainly homogenous background concentration of ~ 0.15 nM at depth in the world's oceans [Statham et al., 1998; van Hulten et al., 2016], resulting in a scavenged-type depth profile. Deviations from this background concentration can be found near Mn sources such as hydrothermal vents, which generate elevated DMn concentrations of up to several tens to hundreds of nM within the hydrothermal plume [Chin et al., 1994; Sands et al., 2012], with a lateral transport of hydrothermal derived DMn over a distance of up to thousands of kilometers [Resing et al., 2015]. Elevated DMn concentrations are also present in coastal waters and fjordic systems as a result of Mn supply from reducing sediments and continental runoff [Kremling and Hydes, 1988; Statham et al., 2005].

Conventionally, concentrations for Mn, or in general for trace metals, in natural waters are determined from discrete samples in land based laboratories using analytical techniques such as graphite furnace atomic absorption spectroscopy (GFAAS) [Nakashima et al., 1988], inductively coupled plasma mass spectrometry (ICP-MS) [Rapp et al., 2017] or inductively coupled plasma optical emission spectrometry (ICP-OES) [Otero-Romaní et al., 2005]. This requires an on-line or off-line sample preparation procedure prior to analysis to suppress interferences by alleviating matrix effects either by solvent extraction [Statham, 1985], pre-concentration on a chelating resin [McLaren et al., 1993; Rapp et al., 2017] or via sample dilution using diluted ultrapure acids [Leonhard et al., 2002]. However, in order to resolve highly variable DMn concentrations in marine systems, both in space and time, the traditional sample collection and analysis approach needs to be replaced by *in situ* techniques. Utilized on a microfluidic lab-on-chip (LoC) based platform, spectrophotometry is a powerful tool for robust and reliable *in situ* measurements, as previously demonstrated for nutrient and pH analysis [Beaton et al., 2012; Grand et al., 2017; Rérolle et al., 2013].

Lab-on-chip instruments enable all steps of a wet chemical colorimetric analysis from sampling, sample treatment, chemical reaction, detection and data processing on a single unit. The LoC analyzers are characterized by low power (~ 1.5 W) and reagent (in the µL range) consumption per measurement, a small size, portability and ability for long-term

deployments. Colorimetric analyses are based on a chemical reaction between the analyte of interest and an analyte specific reagent forming a colored compound/complex with a wavelength specific absorbance intensity being proportional to the analytes concentration. For Mn the colorimetric method using 1-(2-pyridylazo)-2-naphthol (PAN) as complexing agent has found wide usage as it features a fast reaction and high sensitivity towards Mn(II) with a molar absorptivity of ~ 44,000 $L \cdot mol^{-1} \cdot cm^{-1}$ at 562 nm [Chiswell and O'Halloran, 1991; Goto et al., 1977]. As the PAN reagent itself as well as the purple colored $Mn(PAN)_2$ complex are poorly water soluble the addition of a non-ionic surfactant such as Triton-X100 is required in order to enable micelle formation and solubilize PAN and $Mn(PAN)_2$ in the aqueous phase [Goto et al., 1977]. Additions of the iron (Fe) chelating reagent desferrioxamin B (DFO-B) can be used in order to suppress any interferences generated from the presence of Fe(III), which is thought to be one of the potentially interfering ions in natural waters, together with zinc, nickel, copper and cobalt [Chin et al., 1992].
Here we evaluate the PAN method for the *in situ* detection of DMn using a microfluidic LoC analyzer with respect to the reagent composition (Fe(III) masking agents, surfactants etc.). The method was then adapted for its use in a LoC analyzer, which was deployed in a coastal water system (Kiel fjord, Germany). Discrete samples analyzed via ICP-MS served as a method validation tool.

5.2 Methods and materials

A thorough cleaning procedure was applied to all glass and plastic ware for standard and reagent preparation prior to their use. Soaking in a ~ 2 % v/v acidic detergent bath (Citranox, Sigma-Aldrich) was followed by a 1.2 M HCl bath (reagent grade, Carl-Roth), both at least overnight. Glass and plastic ware was rinsed thoroughly with de-ionized water (MilliQ, 18.2 MΩcm, Merck Millipore) after each treatment.

5.2.1 Preparation of standard and reagent solutions

A working stock solution containing 100 µM Mn(II) was prepared on a weekly basis using 546 µL of a 1000 $mg \cdot L^{-1}$Mn standard (1000 ppm Manganese for ICP, Inorganic Ventures) diluted to 100 mL with de-ionized water. Standard solutions with respective Mn(II) concentrations were obtained by further dilution of the 100 µM Mn(II) working stock with de-ionized water. All Mn(II) solutions were stored at room temperature in opaque low-density polyethylene (LDPE) bottles (Nalgene).

The preparation of the PAN reagent followed, with some adaptations, the method reported by Chin et al. (1992). 0.05 g of 1-(2-Pyridylazo)-2-naphthol (PAN) (general purpose grade, Fisher Scientific) and 5 mL Triton-X100 (laboratory grade, Sigma-Aldrich) were added to approximately 50 mL of de-ionized water and stirred at 80 °C for at least 12 h until the PAN was dissolved completely. The warm orange colored mixture was then poured into 100 mL of a 0.1 M borate buffer (pH ~ 10) and made up to 250 mL with de-ionized water, giving final PAN and Triton-X100 concentrations of 0.8 mM and 2 % v/v (equivalent to 33 mM), respectively. For method evaluation, further PAN reagents were prepared containing 4 % v/v Triton-X100 by the addition of 10 mL Triton-X100 or 2 % w/v of the ionic surfactant sodium dodecyl sulfate (SDS) by the addition of 5 g SDS (ultra pure, Carl Roth). No heat was required for the dispersion made with SDS to solubilize PAN. Borate buffer contained 0.618 g H_3BO_3 (99.99 %, trace metal basis, Acros Organics) and 0.4 g NaOH (98.5 %, Acros Organics) made up to 100 mL with de-ionized water, giving a concentration of 0.1 M for both boric acid and sodium hydroxide. As an interference of Fe(III) ions was reported for the PAN method [Chin et al., 1992], two different Fe specific complexing/masking agents were tested: DFO-B and disodium 4,5-dihydroxy-1,3-benzenedisulfonate (Tiron). A 1.5 mM DFO-B solution was prepared by dissolving 5 mg of deferoxamine mesylate salt (95 %, Acros Organics) in 5 mL de-ionized water. This solution was kept refrigerated when not in use. A 50 mM Tiron stock solution was prepared by dissolving 0.785 g of Tiron (Acros Organics) in 50 mL de-ionized water.

5.2.2 Spectrophotometric benchtop experiments

For benchtop experiments using the PAN method, Mn(II) standard solutions and PAN reagent were mixed using a volumetric ratio of 9:1. For Fe(III) interference studies, the prepared Mn(II) standards were spiked with an acidified 100 µM $FeCl_3$ solution (≥ 98 %, Carl Roth) and a Fe(III) masking agent if required. Absorbance spectra between 400 nm and 800 nm were acquired after 5 minutes with a double beam Shimadzu UV-1800 spectrophotometer using 10 cm quartz cuvettes. Absorbance was processed at the peak maximum of 562 nm, and for the Fe(III) interference experiments also at 768 nm.

5.2.3 Lab-on-chip analyzer

The PAN method was adapted for its application in a microfluidic LoC analyzer. The analyzer was identical to a device characterized for the detection of Fe in coastal waters

using the FZ method [Geißler et al., 2017] because the $Mn(PAN)_2$ complex features the same absorbance maxima at a wavelength of 562 nm as the $Fe(FZ)_3$ complex (**Figure 5.1**).

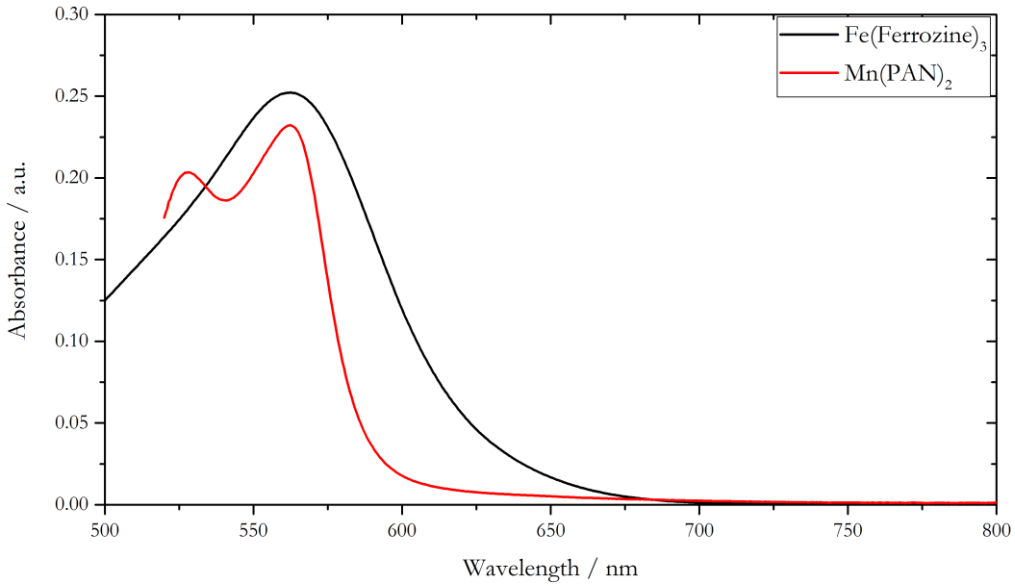

Figure 5.1: Absorbance spectra for the detection of Fe and Mn using the FZ and PAN methods, respectively. Spectra were acquired against the individual reagent blanks using a double beam spectrophotometer.

Briefly, the analyzer comprises a microfluidic chip (119 mm in diameter and 24 mm in thickness) made from tinted Poly(methylmethacrylate) (PMMA) [Floquet et al., 2011], with milled microfluidic channels of the dimensions 160 × 300 µm, forming the end-cap of a watertight polyvinylchloride (PVC) housing. A custom built syringe pumping unit including a stepper motor, two barrels for reagent supply (3.28 mm ID) and one barrel for sample and standard solutions (9.71 mm ID) is mounted onto the microfluidic chip for sample and reagent withdrawal from the reservoirs and injection into the microfluidic channels. Micro-inert solenoid valves (LFNA1250325H, The Lee Company) provide full fluidic control via individual actuation. Sample and standard solutions are mixed on-chip with the PAN reagent in the volumetric ratio of 8.8:1 defined by the volume of the barrels as the plungers of the pumping unit are moving simultaneously at the same speed. After completed chemical reaction and full color development the absorbance can be measured in three individual optical channels of different length (91.6 mm, 34.6 mm and 2.5 mm) using light emitting diodes (LEDs) with a peak wavelength of 575 nm (AlGaInP, P5B-433-20 LED, Roithner LaserTechnik GmbH) as light source at the beginning of each optical cell and photodiodes (PDs) (TSLG257-LF, TAOS) as detection unit of the transmitted light at the end of each optical channel. Monitoring PDs are mounted perpendicular to the LEDs of the optical channel to correct for any temperature induced drift, e.g. due to warming up of

the LED at the beginning of each deployment and due to natural effects. The reagents and standard sample solutions were supplied to the microfluidic channels via PTFE tubing (0.5 mm ID) which connected the fluid reservoirs with fluid inlets on the microfluidic chip. The reservoirs (transparent flexible bags, Flexboy-Bag, Sartorius) were kept in a cylindrical PVC tube (200 mm in diameter, 44 mm in length) mounted on top of the analyzers main housing. A more detailed description of the analyzer design can be found elsewhere [Geißler et al., 2017].

5.2.4 Deployment

The capability of the LoC analyzer for robust and reliable DMn measurements under environmental conditions was tested during a field campaign conducted in October/November 2018 in the inner Kiel fjord (Germany). The analyzer was deployed together with other LoC devices (for *in situ* analysis of Fe(II), DFe, pH) and a SeapHOx unit (SeaFET pH sensor plus SBE 37-SMP-ODO MicroCAT CTD+DO sensor) for continuous acquisition of hydrographic parameters (pH, temperature, salinity and dissolved oxygen concentration). All instruments were mounted on a stainless steel frame which was lowered from a pontoon to a water depth of 2 m.

5.2.4.1 *In situ* measurement routine and data processing

The Mn analyzer was equipped for the deployment with a blank solution, two Mn(II) standard solutions and PAN reagent. Standard solutions were prepared at a salinity of 18 ‰ using South Atlantic seawater with DMn concentrations below the analyzers detection limit in order to account for any matrix effects [Feng et al., 2015]. The analysis of a sample, which was withdrawn through a 0.22 µm membrane filter (Millipore, polyethersulfone (PES)), was undertaken every 90 minutes. Prior to each sample measurement, a calibration procedure was conducted using the blank solution followed by analysis of a 150 nM and a 300 nM Mn(II) standard. The raw output of the PDs for each measurement was converted into absorbance values according to equation (5.1), here as an example for the analysis of a natural water sample.

$$Absorbance = -\log_{10}\left(\frac{V_{Sample}}{V_{Sample}^{R}} \cdot \frac{I_{Sample}^{R}}{I_{Sample}}\right) \tag{5.1}$$

A linear fit between the absorbencies of the blank and the standard solutions was then applied as calibration curve on the absorbance of the sample to calculate the present DMn concentration. For each analysis the system was flushed five times with the respective blank, standard or sample without PAN reagent to minimize carry over effects of the previous solution. At the end of each flushing procedure the output of the PD was used as a mean of five seconds to compensate for any matrix effects, V^R_{Sample} in equation (5.1). After the flushing procedure the blank, standard or sample was injected together with the PAN reagent. A waiting time of 15 minutes was then applied under stopped flow condition in order to allow mixing, chemical reaction and full color development. The five second mean of the raw PD output was then used, as V_{Sample} in equation (5.1), for the calculation of the respective absorbance value. As the illumination intensity of the emitted light from the LEDs varies with temperature a scaling factor I^R_{Sample}/I_{Sample} is integrated in equation (5.1). Here, I^R_{Sample} and I_{Sample} are the raw data of the monitoring PDs after the flushing procedure and after full color development, respectively.

5.2.4.2 Discrete samples

In order to validate the DMn concentrations measured during the field deployment of the *in situ* analyzer, discrete samples for trace metal analysis were taken up to four times per day using a peristaltic pump (Masterflex L/S series, Cole-Palmer) with an acid cleaned 6.4 mm ID C-Flex tubing (Masterflex, Cole-Palmer) attached. Manual sample collection was timed according to the sample aspiration of the analyzer. The inlet of the tubing was attached at the stainless steel frame at the same height as the analyzer's input. At the outlet a 0.2 µm poly(ether sulfone) (PES) filter capsule including a 0.8 µm pre-filter (AcroPak 500, Pall GmbH) was used for filtration of the discrete samples directly at the sampling site. Samples for dissolved trace metal analysis were collected in cleaned 125 mL LDPE Nalgene bottles and acidified in a clean laboratory with 150 µL concentrated HCl (ultra purity acid grade, ROMIL) to pH < 2. After three months of storage dissolved trace metal samples were diluted 1:10 using 1 M distilled HNO_3 (Spa grade, ROMIL, distilled using a sub-boiling PFA distillation system) and analyzed by high resolution ICP-MS (ELEMENT II XR, ThermoFisherScientific). Analysis of NASS-7 and CASS-6 certified reference materials yielded Mn concentrations of 14.36 ± 0.41 nM (certified 13.65 ± 1.09 nM) and 36.5 ± 1.2 nM (certified 40.4 ± 2.2 nM), respectively. Pre-combusted 20 mL glass vials were used for the collection of dissolved organic carbon (DOC) samples. Sample collection was followed by acidification with 25 µL of concentrated HCl (ultra purity acid grade,

ROMIL). Analysis was performed as non-purgeable organic carbon (NPOC) using a high temperature catalytic combustion approach (Shimadzu TOC-L CPH). Samples for macronutrients were collected in 15 mL Falcon centrifuge tubes and kept frozen until analysis using a segmented flow autoanalyzer (QuAAtro, SEAL Analytical).

5.3 Results and discussion

5.3.1 Characterization of PAN method

5.3.1.1 Mn(II) calibration

The PAN method for the spectrophotometric detection of Mn was characterized with regard to its sensitivity and selectivity. Calibration curves were obtained using both the double beam spectrophotometer and LoC device, as shown in **Figure 5.2**.

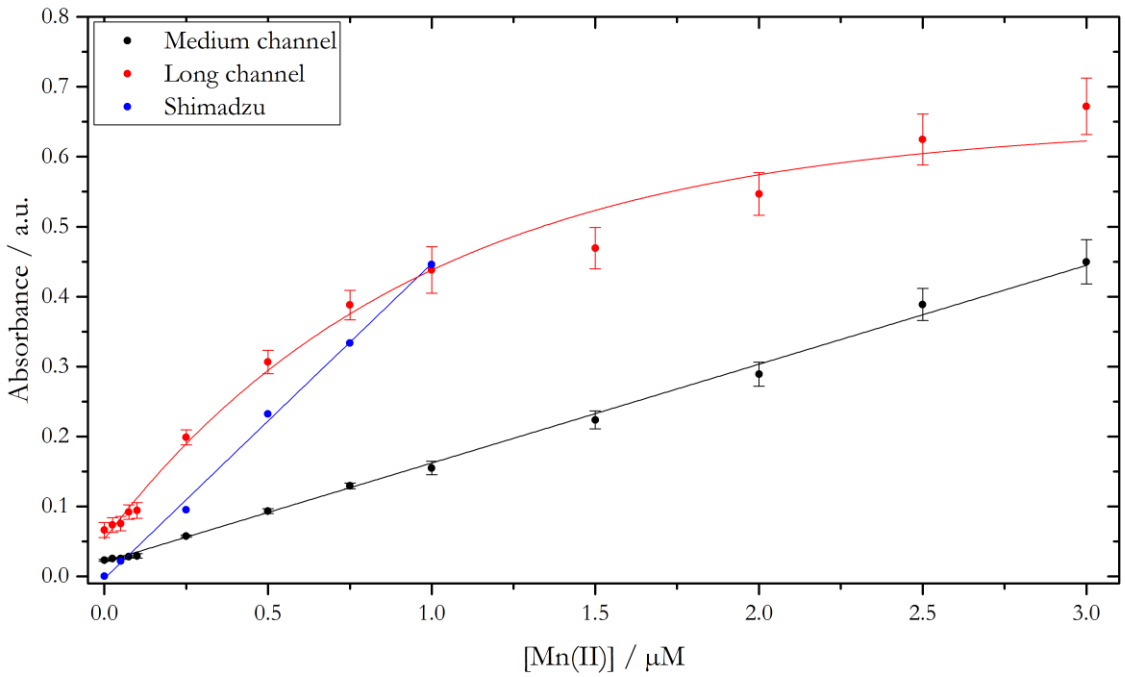

Figure 5.2: Calibration graphs for the detection of Mn using the PAN method (0.8 mM PAN in 4 % v/v Triton-X100) acquired with the LoC analyzer (long (91.6 mm) and medium (34.6 mm) channel) and a Shimadzu benchtop spectrophotometer. Absorbance spectra using the Shimadzu spectrophotometer were measured against a reagent blank and processed at the absorption maximum of 562 nm. Raw data from the LoC analyzer were processed according to equation (5.1).

Absorbance values measured with the double beam spectrophotometer (blue) and the medium channel of the LoC analyzer (black) exhibit a linear relationship over the employed concentration range of 0 µM to 1 µM and 0 µM to 3 µM Mn(II), respectively. In contrast,

absorbance values measured with the long channel of the LoC analyzer (red) became non-linear above 0.5 µM Mn(II) (exponential fit shown in **Figure 5.2**) and also exhibit a lower precision when measurements were repeated (n = 20; error bars shown in **Figure 5.2**). Therefore, the processed absorbencies obtained with the medium measurement channel are preferentially chosen for the spectrophotometric *in situ* quantification of Mn(II). Linear slopes obtained for the Shimadzu double beam spectrophotometer and the medium channel of the LoC analyzer are distinct by a factor of ~ 3, with slopes of $(4.503 \pm 0.102) \cdot 10^{-4}$ L·nmol^{-1} ($R^2 = 0.997$) and $(1.413 \pm 0.039) \cdot 10^{-4}$ L·nmol^{-1} ($R^2 = 0.991$), respectively (**Figure 5.2**). This variation can be ascribed to the different lengths of the used optical paths, with a ~ 3 times longer path for the spectrophotometer (10 cm) than for the LoC analyzer's medium channel (3.46 cm). Normalized with respect to the length of the optical path, an extinction coefficient of 45,030 ± 1,020 L·mol^{-1}·cm^{-1} at 562 nm was obtained for the double beam spectrophotometer, which is in good agreement with reported values of 44,000 L·mol^{-1}·cm^{-1} [Goto et al., 1977] and 46,000 L·mol^{-1}·cm^{-1} [Chiswell and O'Halloran, 1991]. For the medium measurement channel of the LoC analyzer a lower extinction coefficient of 40,838 ± 1,127 L·mol^{-1}·cm^{-1} was obtained, which can be attributed to the peak emission wavelength of 575 nm of the LED not coinciding with the absorption maximum of the $Mn(PAN)_2$ complex at 562 nm. However, the reported value here is still significantly higher than those found for other *in situ* Mn analyzers using the PAN method, such as for the METIS analyzer with 8,000 L·mol^{-1}·cm^{-1} [Meyer et al., 2016] and the SCANNER analyzer with ~ 20,000 L·mol^{-1}·cm^{-1} (estimated from the calibration curve shown in Chin et al. (1992)). As the above mentioned extinction coefficients are not corrected for dilution of the sample with reagent, a comparison of the individual designs in terms of their sensitivity is allowed. The enhanced sensitivity of the LoC analyzer here might be attributed to the high sample to reagent ratio of 8.8:1. The METIS and SCANNER analyzers suffer from a dilution effect of the sample as the sample is mixed with reagent in a 1:1 ratio and a 5:1 ratio, respectively. The detection limit (LOD) for the medium channel of the LoC device was defined as three times the standard deviation for the analysis of a 0 nM Mn(II) blank solution (n = 13). The obtained LOD of 27.2 nM Mn(II) is in the range of the LOD reported for the SCANNER (between 15 nM and 48 nM, depending on the applied matrix) and significantly lower than the LOD reported for the METIS analyzer (77 nM). The LoC analyzer is therefore suitable for the quantification of DMn concentrations in coastal waters and near DMn sources such as hydrothermal vents, where elevated Mn concentrations of up to hundreds of nM can be found [Chin et al., 1994; Statham et al., 2003, 2005].

5.3.1.2 Reagent composition

The PAN reagent prepared with 2 % v/v of non-ionic surfactant Triton-X100 was stable for four weeks. Precipitation of orange colored PAN crystals was observed when stored over longer time periods. As any kind of particle formation needs to be avoided when using microfluidic technology, due to a high vulnerability to clogging, an adaptation of the reagent composition with regards to the concentration or the nature of the used surfactant was necessary. Therefore, two different batches of PAN reagent were prepared; (a) with 2 % w/v of the ionic surfactant SDS instead of Triton-X100 and (b) with an increased concentration of 4 % v/v of Triton-X100. Both reagents showed good stability as no particle formation was observable even after several months of storage, which is a requirement for remote long-term deployments. The response of the LoC analyzer using reagents containing 2 % v/v and 4 % v/v Triton-X100 as well as 2 % w/v SDS was tested.

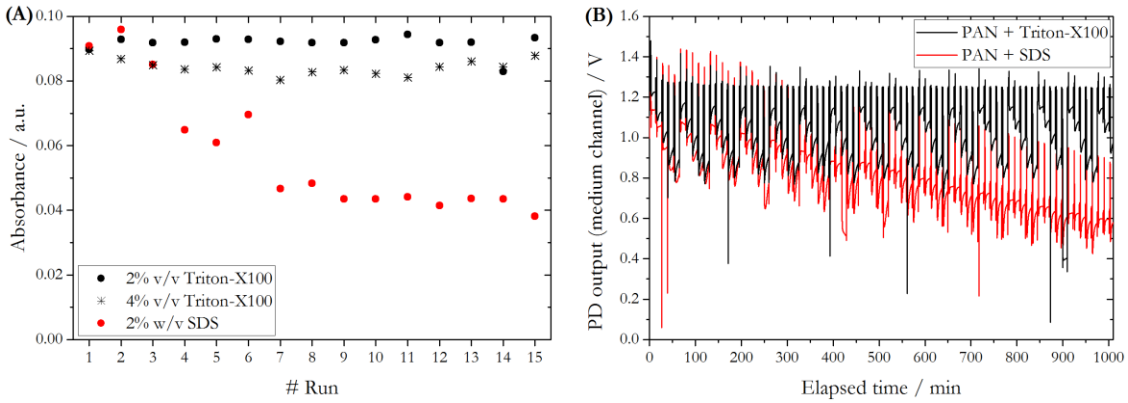

Figure 5.3: (A) Processed absorbance values of the analyzers medium channel of a 500 nM Mn standard solution analyzed using three differently prepared 0.8 mM PAN reagents. **(B)** PD raw output from medium channel of LoC analyzer for 15 consecutive runs of a calibration using four different Mn(II) standard solution and 0.8 mM PAN reagent prepared with 2 % v/v Triton-X100 and 2 % w/v SDS.

Processed absorbance values obtained from the medium measurement channel of 15 consecutive analysis of a 500 nM Mn(II) standard solution with each reagent are shown in **Figure 5.3(A)**. For both reagents prepared with Triton-X100 absorbance values show little variation (R.S.D. = ± 2.9 %) indicating stable sensitivity over time. In contrast, when using SDS as surfactant the absorbance decreased over time, resulting in a loss of sensitivity. **Figure 5.3(B)** indicates that the reduced sensitivity over time, when applying the PAN reagent prepared with SDS, is linked to a decrease of the overall PD output, whereas a stable signal was obtained using PAN reagent prepared with Triton-X100. This might be explained by the formation of a light absorbing coating mediated by SDS on the optical windows which separate the flow path from LEDs and PDs. Consistent with this

explanation, rigorous flushing with moderately concentrated sodium hydroxide solution brought the PD output back to the initial value. Additionally, SDS forms a precipitation at temperatures < 15 °C, inhibiting its use in field-deployable systems for temperate and polar waters. Clinton-Bailey et al. (2017) suggested therefore the use of the dispersant polyvinylpyrrolidone (PVP) in microfluidic devices. However, PAN is not soluble in aqueous solutions containing PVP, even after stirring for one day at 80 °C. Therefore, the use of a PAN reagent containing 4 % v/v Triton-X100 was chosen as optimum reagent solution, ensuing stable sensitivity and no observable precipitation of PAN crystals over a period of several months.

5.3.1.3 Iron interference

It has been reported that the metals iron, zinc, nickel, copper and cobalt show significant interferences with the PAN method at a wavelength of 562 nm when prevalent in a free ionic form and in equimolar concentrations with Mn [Chin et al., 1992]. Therefore, a masking agent with high affinity to those cations may be necessary in order to suppress potential interferences when analyzing natural samples. The siderophore type chelating agent DFO-B and the catechol type ligand Tiron can bind these cations, with a highest affinity to Fe(III) [Evers et al., 1989; Hernlem et al., 1996]. DFO-B was used in several studies, as strongest interferences were expected from Fe especially in natural waters with elevated Fe concentrations such as near hydrothermal vents or in coastal systems [Chin et al., 1992; Meyer et al., 2016; Statham et al., 2005].

The spectrum obtained for the Mn(II) plus Fe(III) standard solution (solid red, **Figure 5.4**) features a broad absorption band at wavelengths > 650 nm as well as an increased absorbance at 562 nm compared to the 1 μM Mn(II) standard solution (black, **Figure 5.4**). The absorbance at 562 nm of the mixed standard (1 μM Mn(II) + 1 μM Fe(III)) is equivalent to a processed Mn(II) concentration of 1.2 μM and thus an Mn overestimation of 20 %, which is in agreement with the value reported by Chin et al. (1992). With the use of DFO-B as Fe masking agent, the absorption spectrum of the mixed standard containing both Mn(II) and Fe(III) (dashed line, **Figure 5.4**) features no absorption band at wavelength > 650 nm indicating efficient Fe(III) masking capability. However, the absorbance at 562 nm also decreased compared to a 1 μM Mn(II) standard resulting in an Mn(II) underestimation of ~ 15 %. It can be assumed that the DFO-B is removing some Mn(II) from the PAN accessible pool via DFO-B promoted oxidation to Mn(III) and

subsequent stabilization of the higher oxidation state [Duckworth and Sposito, 2005]. An underestimation of *in situ* determined DMn concentrations using the PAN method with DFO-B compared to ICP-MS measurements of discrete samples was also found with the METIS analyzer [Meyer et al., 2016]. Whilst this was ascribed to internal hardware issues rather than to DFO-B related issues, it might be a combination of both based on our findings.

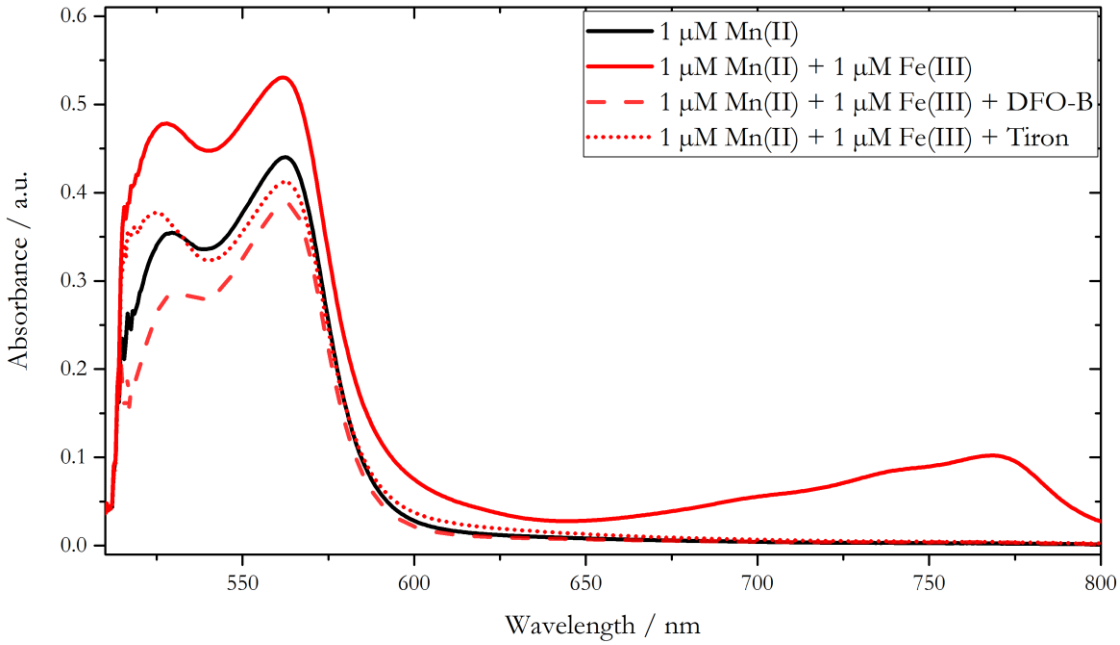

Figure 5.4: Absorbance spectra of a 1 µM Mn(II) standard solution and 1 µM Mn(II) solutions containing 1 µM Fe(II) with DFO-B and Tiron, added as Fe masking agents. All spectra were measured using 0.8 mM PAN reagent prepared with 2 % v/v Triton-X100.

It was further found that the Fe masking strength of DFO-B decreased over time, when storing the mixed PAN/DFO-B reagent at room temperature (**Figure 5.5**). Three days after the preparation of the mixed PAN/DFO-B reagent, any Fe(III) interference was effectively suppressed. This was also the case when Fe(III) was present in large excess in a 500 nM Mn(II) standard solution, for reagents stored at room temperature (black) and at 7 °C (red). The measured absorbance values here are on the same level as for a standard solution without Fe(III) addition. Increased absorbance values were observed for the analysis of standards containing 5 µM and 10 µM Fe(III) after a storage time of eight days at room temperature. Within 15 days storage at room temperature, degradation of DFO-B led to observable Fe interferences even at equimolar concentrations of Mn(II) and Fe(III) (500 nM of each). Whereas, storage at lower temperatures impeded the degradation of DFO-B and up to 5 µM Fe(III) were effectively masked even 15 days after reagent preparation.

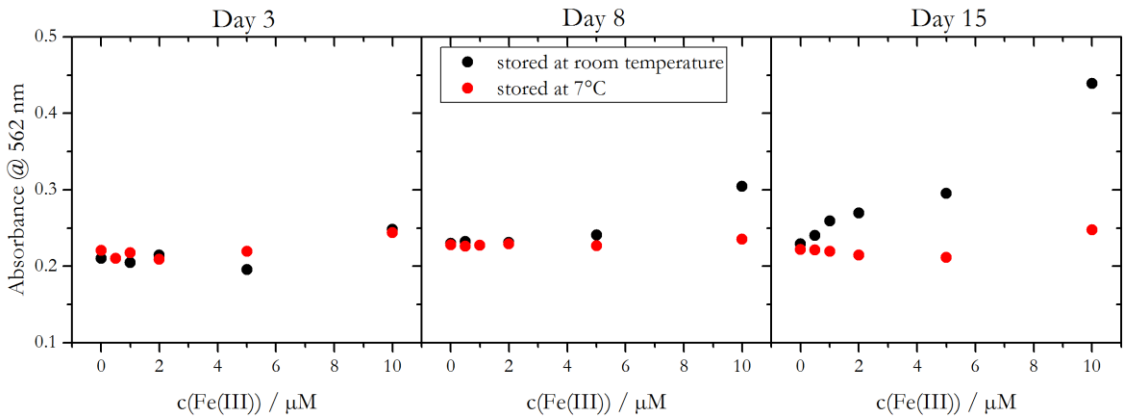

Figure 5.5: Absorbance at 562 nm of a 500 nM Mn(II) standard solution spiked with different amounts of Fe(III). Values were obtained after mixing standard solutions with two differently stored PAN/DFO-B reagents (at room temperature – black, at 7 °C – red) three, eight and fifteen days after preparation. The two mixed PAN reagents contained 0.8 mM PAN and 400 µM DFO-B.

Like DFO-B, the catechol type Fe complexing agent Tiron showed effective Fe masking capability. No absorption band was observable at wavelength > 650 nm (**Figure 5.4**, dotted line). However, a lower absorbance at 562 nm was found for the 1 µM Mn(II) + 1 µM Fe(III) standard solution when applying Tiron compared to the 1 µM Mn(II) standard analyzed without Tiron. This suggests that also Tiron complexes Mn(II) resulting in an underestimation of Mn(II).

These findings suggest that neither DFO-B nor Tiron are suitable as masking agent for the *in situ* determination of Mn(II) using the PAN method; because of (1) a potential underestimation of Mn(II) and (2) the limited life time of DFO-B. Degradation might be especially a problem for remote *in situ* deployments over extended durations of weeks to months. However, in natural waters, such as the Kiel fjord, the metals which are interfering with the PAN method occur at low concentrations compared to Mn(II) (see section 5.3.2.2) and are naturally prevalent in open ocean as well as in coastal waters as strongly bound organic complexes [Gledhill and Buck, 2012; Rose and Waite, 2003a], which limits its availability to form a complex with PAN reagent over short equilibration time periods [Chin et al., 1992; Feng et al., 2015]. Therefore, we hypothesized that the addition of a masking agent to the PAN reagent was not required, when deploying the LoC analyzer in an estuary, such as the Kiel fjord.

5.3.2 *In situ* time series

5.3.2.1 Hydrographic setting

The performance of the DMn *in situ* analyzer was evaluated during a deployment in the inner Kiel Fjord from October 22 to November 17, 2018. The Kiel Fjord, which represents the southernmost part of the Kiel Bay, is characterized by considerable anthropogenic impact due to its extensive use for shipping, dockyards and a population of ca. 250,000 in the surrounding areas. The main sources of freshwater input includes rainwater run-off from the city of Kiel, the Schwentine River which is located at the eastern shore of the inner Kiel Fjord, and the Kiel-Canal which represents one of the busiest artificial waterways worldwide, located at the western shore of the fjord. The Kiel Fjord has a mean depth of ~13 m, with water level changes of up to ±1 m caused by winds and pressure gradients over the Baltic Sea. During the period of the deployment, a storm flood approached Kiel Bay in two phases with a water level rise of up to 0.7 m on October 27 and up to 1.0 m on October 29 due to strong northerly winds. This hydrological extreme event caused a reduction in salinity and water temperature of 1.5 and 1.5 °C, respectively, within less than 12 hours (**Figure 5.6(A)**). Before and after the storm flood, salinity and temperature were almost constant with mean salinities and temperatures of 21.5 ± 0.1 and 13.5 ± 0.3 °C (October 22 to 27) as well as 20.4 ± 0.1 and 10.7 ± 0.1 °C (November 07 to 16), respectively. Almost no response of pH and oxygen concentration was observable upon the storm flood. During the period of the deployment, mean pH values of 7.74 ± 0.10 and oxygen concentrations of 7.9 ± 0.9 $mg \cdot L^{-1}$ were measured. Analysis of discrete samples for the macronutrients nitrate and phosphate as well as for DOC showed mean concentrations of 2.1 ± 0.7 μM, 1.3 ± 0.1 μM and 257 ± 15 μM, respectively, over the time period October 22 to November 17, 2018.

5.3.2.2 Evaluation of the analyzers performance

During the period October 29 to November 07 the system did not produce reliable data for both the calibration and measurement of the natural water samples, with a relative change of up to 70 % between adjacent time points and negative calibration slopes. This period was therefore excluded from the time series shown in **Figure 5.6**. Replacement of the filter attached to the sample inlet and a careful cleaning procedure of the microfluidic manifold with detergent and de-ionized water resolved the issues and therefore we assume

that the fault was caused by clogged filter membrane and microfluidic channels as a consequence of the storm flood event.

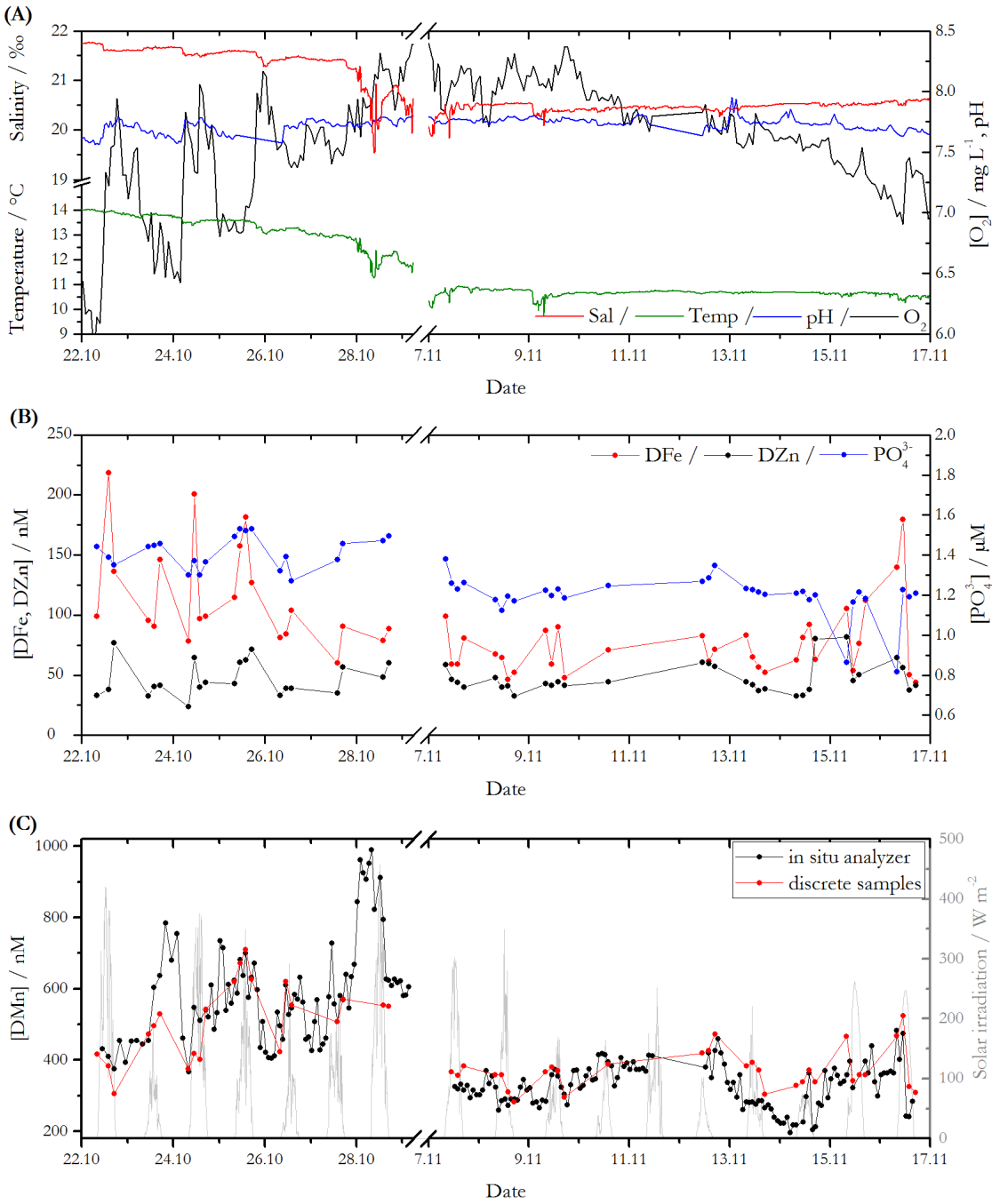

Figure 5.6: Time series for the periods October 22 to 29, 2018, and November 07 to 17, 2018, of **(A)** *in situ* determined hydrographic data and **(B)** discrete samples for phosphate, DFe and the nutrient type trace metal Zn. **(C)** DMn time series determined with *in situ* LoC analyzer (black) and from discrete samples analyzed via ICP-MS (red).

Reliable absorbance values for natural water samples mixed with the PAN reagent, with a relative change of less than 35 % between adjacent time points, were obtained by the analyzer for the periods October 22 to 29 and November 07 to 17, exhibiting a strong statistical correlation (Spearman correlation coefficient of 0.873) with DMn concentrations determined using ICP-MS in discretely collected samples (**Figure 5.7**). However, the

analysis of onboard blank and standards for the purpose of calibration produced highly variable calibration parameters, probably due to problems with their supply towards the microfluidic manifold and related carry-over effects. Slopes ranging from $-1.307 \cdot 10^{-4}$ L·nmol^{-1} to $4.607 \cdot 10^{-4}$ L·nmol^{-1} (mean: $(1.955 \pm 0.751) \cdot 10^{-4}$ L·nmol^{-1}) and intercepts in the range from 0.011 to 0.123 (mean: 0.038 ± 0.020) were obtained when applying a linear fit. Therefore, the absorbance values of the natural water sample, which were unaffected by these issues, were processed with calibration parameters generated from laboratory characterization of the analyzer with standards prepared at a salinity of 18 (i.e. calibration curve slope = $1.104 \cdot 10^{-4}$ L·nmol^{-1} / intercept = 0.046). **Figure 5.6(C)** shows the corresponding processed DMn concentrations of both 215 *in situ* measurements and 47 discrete samples analyzed via ICP-MS as validation method. Both time series show a strong significant correlation with a Spearman correlation coefficient of 0.873 ($p < 0.01$, $n = 47$; see **Figure 5.7** and **Figure 5.8**). Especially during the period October 24 to 27 DMn concentrations determined with the two individual methods were in close agreement with a high accuracy of > 99 %. Between November 08 and 13, a mean offset of < 6% of the *in situ* determined concentrations compared to discrete samples was observed.

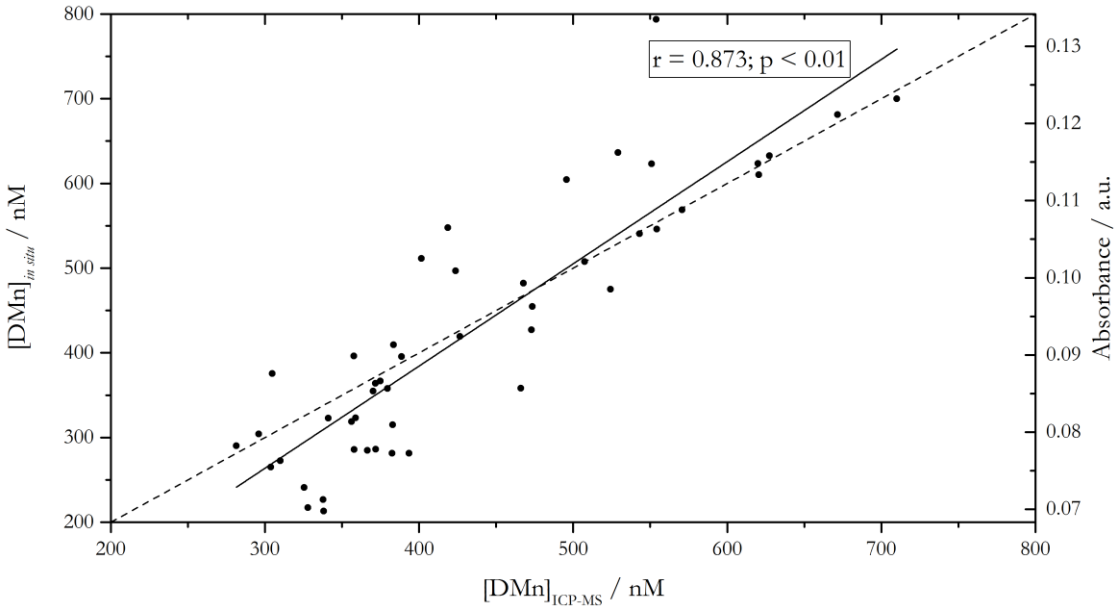

Figure 5.7: Scatter plot of *in situ* absorbance/DMn concentration vs. ICP-MS analysis (Spearman correlation parameters: $r = 0.873$, $p = 1.3 \cdot 10^{-15}$, $n = 47$); $y = x$ (dashed line) is displayed for clarity.

Considering all data points (**Figure 5.6(C)**), DMn concentrations determined in the discrete samples were in the range 282 nM and 710 nM, with a mean DMn concentration of 430 ± 104 nM (n = 52). Using the *in situ* LoC analyzer, a minimum of 196 nM and a maximum of 990 nM was found, with a mean DMn concentration of 435 ± 163 nM

(n = 215), being in good agreement with the value obtained from discrete samples. However, as shown in **Figure 5.6(C)**, there are certain periods where *in situ* determined DMn concentrations are either under- or overestimated compared to discrete samples, also indicated by the divergent extreme values of both time series. For example, distinct overestimation of 18 ± 12 % on average was observed at the beginning of the deployment from October 22 to 24, whereas the period November 12 to 16 was characterized by 17 ± 14 % on average lower *in situ* DMn concentrations compared to those of discretely collected samples. The discrepancies between the two time series might be attributed to three facts: (1) analysis of slightly different waters due to the used deployment/sampling setup, (2) presence of Mn(III) species in the dissolved phase which is detectable with ICP-MS but not spectrophotometrically with the PAN method and (3) a lower temporal resolution of collected samples which may have missed a concentration peak observed by the analyzer.

As to (1), the sample inlet of the LoC analyzer was orientated horizontally at a water depth of ca. 2 m. Prior to each *in situ* analysis, 2.8 mL of the fjord water were aspirated in order to flush the system with the natural *in situ* water sample. In contrast, the inlet of the hose used for collecting discrete samples was orientated vertically towards the seabed at the same depth as the analyzers inlet, but 1.5 m laterally apart. Approximately 10 L of fjord water were pumped with a flow rate of ca. 1.5 $L \cdot min^{-1}$ through the system prior to sample collection to ensure a careful flushing of the hose and the attached filter cartridge. Due to the different orientation of the water inlet as well as a 3,000 times higher water throughput for flushing purposes, it is possible that water from greater depths with slightly lower DMn concentrations was aspirated with the setup for the discrete sample collection. Those differences in DMn concentrations depending on the depth might be a result of stratification of the water body, a decrease of light driven redox processes with depth as well as external DMn input to the upper layers e.g. through wet deposition. In particular, a prominent overestimation of up to ~100 nM DMn was observed at the beginning of the time series from October 22 to 24, as shown in **Figure 5.6(C)**. On October 22, almost no cloud cover was observable with a peak solar irradiation of 420 $W \cdot m^{-2}$. It can be therefore assumed that the DMn overestimation of the *in situ* analyzer compared to discrete samples was generated due to photo-enhanced reduction of high-valent Mn to the dissolved Mn(II) fraction, as the discrete samples were presumably collected from greater depths with less efficient irradiation. In contrast, the overestimation as well as increasing DMn concentrations during October 23 might be attributed to an external input of DMn from

extensive wet deposition (7.8 $L \cdot m^{-2}$ within 12 hours) combined with slower mixing of the rainwater with increasing depths. For example, Deutsch et al. (1997) found that atmospheric precipitation can be an important DMn source, with DMn concentrations of up to ~200 nM in rainwater samples collected in Darmstadt, Germany.

As to (2), in contrast to the speciation of Fe in seawater, where the presence of organic ligands plays an important role, there is only limited evidence for organic complexation of Mn in seawater [Roitz and Bruland, 1997]. However, a recent study suggested the presence of organically complexed and therefore stabilized Mn(III) species by humic ligands in the DMn pool [Oldham et al., 2017]. Speciation studies showed that 17.6 % of the DMn pool occurred as complexed Mn(III) species at 3 m depth, with increasing relative concentrations with depth in the St. Lawrence Estuary. Critically, those species are within the ICP-MS detectable DMn pool, whereas the spectrophotometrically detectable DMn pool, using the PAN method, accounts for only soluble Mn(II). Thus, the presence of dissolved Mn(III) species might cause lower spectrophotometrically determined *in situ* DMn concentrations than those from discrete samples, e.g. from November 13 onwards (**Figure 5.6(C)**).

As to (3), the variability in DMn concentrations over the time series from October 27 to 29 highlights the need for temporally well resolved data, achievable only with *in situ* measurements. The observed dynamic nature of DMn concentration, with an increase of about 400 nM DMn during the night October 27 to 28, might be attributed to extreme weather conditions as a storm flood approached the Kiel Bay which was linked to an inflow of fresh water (drop of salinity of 1.5), a water level rise of up to 1 m a.s.l. and wind speeds of up to 13 $m \cdot s^{-1}$. This dynamic could not be resolved with discrete samples as especially under those extreme weather conditions sample collection is inconvenient and hazardous.

Overestimation due to the cross-sensitivity of the PAN reagent to other ions can be neglected as all interfering ions occurred at low concentrations compared to DMn, with mean values of 90.8 nM, 47.1 nM, 15.0 nM, 6.1 nM and 0.7 nM for dissolved Fe, Zn, Cu, Ni and Co species, respectively. Additionally, no statistically significant evidence of a correlation between the time series of these elements and the overestimated DMn fraction was found.

According to a Spearman rank correlation test, DMn concentrations showed reasonable relationships to other hydrographic parameters (**Figure 5.8**; for time series see **Figure 5.6(A)** and **(B)**).

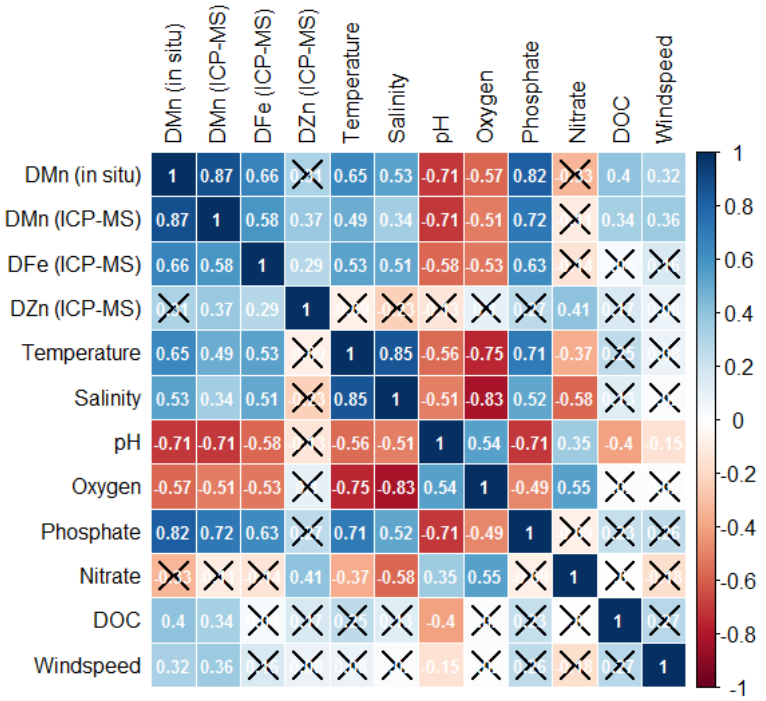

Figure 5.8: Spearman correlation matrix of *in situ* and discretely determined variables calculated with data points from October 22 to November 17, 2018; *in situ* DMn data for the period October 29 to November 07 were excluded for statistical analysis. Positive correlation coefficients are illustrated in blue boxes, negative ones in red. Insignificant correlations (p value ≥ 0.01) are crossed out.

For example, *in situ* DMn concentrations anti-correlate significantly with oxygen concentrations and pH, with correlation coefficients of -0.57 and -0.71. The transformation between Mn(IV)oxides and dissolved Mn(II) species can be described as follows:

$$Mn^{2+} + \frac{1}{2}O_2 + H_2O \rightleftarrows MnO_2 + 2H^+ \tag{5.2}$$

where the reaction towards the right is referred to oxidation and towards the left to reduction. According to equation (5.2), the oxidation reaction, and therefore a decrease of dissolved Mn(II) species, is favored if high oxygen concentrations and high pH values are prevalent. In contrast, reduction of Mn(VI)oxides towards Mn(II) takes place under low oxygen concentrations and low pH values. The reduction pathway is sun light mediated, which is responsible for high DMn concentrations in the euphotic zone [Sunda et al., 1983; van Hulten et al., 2016]. Furthermore, organic matter can mediate the (photo)-chemical

reduction of Mn oxides to soluble Mn(II) [Sunda et al., 1983], which would explain the correlation between observed *in situ* determined DMn and DOC concentrations (r = 0.40). A positive correlation with a Spearman correlation coefficient of 0.53 between DMn concentrations and salinity was found. This value might be biased due to the experienced storm flood, as we would rather expect an increase of DMn with decreasing salinity because freshwater, e.g. through riverine input or rainwater, represents a major source of DMn species. When considering the two time phases individually, before and after the flood event, anti-correlations between DMn and salinity were found with correlation coefficients of -0.27 and -0.30, respectively. A strong statistical correlation was found between DMn and phosphate concentration (r = 0.82), suggesting that the marine biogeochemical pathways of both species are, together with oxygen, intimately connected. Under elevated oxygen concentrations, DMn species are oxidized towards Mn(IV)oxides (according to equation (5.2)). In natural waters, those Mn(IV) oxides act as important adsorbents of phosphate, which leads to a removal of phosphate from the dissolved phase [Yao and Millero, 1996].

5.4 Conclusion

In this study, the PAN method for the spectrophotometric determination of DMn in seawaters was successfully adapted for the purpose of *in situ* measurements using LoC technology. It was found that long-term stability of the mixed PAN reagent, which is key for *in situ* long-term deployments, was enhanced from weeks to at least several months when prepared with 4 % v/v of the non-ionic surfactant Triton-X100, instead of previously reported concentration of 2 % v/v. Whilst inorganic Fe(III) interferes with the PAN method when present in Mn equimolar concentrations (and higher), its interference can be neglected in aquatic environments which exhibit an excess of Mn(II) compared to Fe(III) and where Fe(III) is bound by natural organic ligands. It was further found that the use of the Fe(III) masking agent DFO-B leads to an underestimation of DMn, as this organic ligand also removes PAN accessible Mn(II) species from the dissolved phase. Additionally, the use of a mixed PAN reagent containing DFO-B is not suitable for long-term deployments due to its fast degradation at elevated temperatures.

We demonstrated the LoC analyzer's capability of measuring DMn over a linear range between 27.9 nM (LOD) and at least 3 μM using the analyzer's medium cell with a length of 34.6 mm. Thus, *in situ* deployments over a wide range of marine environments can be

facilitated, e.g. in coastal waters and estuaries, in benthic boundary waters and within the vicinity of hydrothermal vents. The performance of the analyzer using the adapted PAN method was evaluated during a deployment over several weeks in an estuarine environment. A reliable DMn time series was recorded *in situ*, with concentrations being in good agreement with those quantified from discrete samples via ICP-MS as validation method (accuracy of > 99 % for certain periods and Spearman coefficient of $r = 0.873$ with $p = 1.3 \cdot 10^{-15}$). Furthermore, reasonable correlations between analyzer derived DMn concentrations and other hydrographic parameters were obtained, emphasizing the reliability of the here presented system. Furthermore, the time series highlights the ability of LoC analyzers to produce temporally well resolved measurements of trace metals, achievable only with *in situ* systems. Thus, the here presented analyzer is an ideal tool for unraveling biogeochemical questions, for example in remote areas, environments with highly variable DMn concentrations over short time scales or during hydrological extreme events.

6 Conclusion and future directions

The overall aim of the here presented PhD project was (1) the adaptation of wet chemical spectrophotometric approaches from macro to micro scale for the determination of dissolved Fe and Mn species in order to undertake *in situ* measurements of these trace metals in natural waters, and (2) the evaluation and validation of the performance of the developed *in situ* LoC analyzers deployed in marine environments. As the essential micronutrients Fe and Mn play a key role in biogeochemical and biological processes, temporally and spatially well resolved time series of these redox sensitive trace metals are needed to better understand and quantify oceanic processes, and predict their future development and interactions with the overall earth system. Trace metal concentrations in the low nM regime up to several μM can be found in natural waters. Thus, *in situ* analyzers must be capable of measurements covering a large concentration range. Additionally, a low reagent and power consumption, *in situ* calibration, minimum user intervention and adequate measurement frequency are needed for long-term deployments. All these requirements can be satisfied using LoC technology, as already demonstrated for the determination of macro nutrients and pH, and this approach was therefore preferentially chosen in this study.

6.1 Determination of dissolved iron

In chapters 3 and 4, the utilization of the spectrophotometric FZ approach was presented for the *in situ* quantification of dissolved Fe species with a LoC analyzer. With the LoC technology, all analysis steps, from sample collection and treatment, chemical reaction, photometric analysis to data processing, are integrated into a stand-alone field-deployable and robust system. The developed LoC analyzer comprised a syringe pumping unit for the transport of reagent, on-board standards and sample through the microfluidic manifold and a photometric detection unit for the measurement of the absorbance of the colored $Fe(FZ)_3$ complex. The sulfonic acid derivate FZ binds selectively Fe(II). For the analysis of the total DFe pool (Fe(II) + Fe(III)), ascorbic acid was applied as reducing agent in order to reduce Fe(III) to FZ accessible Fe(II) prior to analysis. An extinction coefficient of 27,900 $L \cdot mol^{-1} \cdot cm^{-1}$ at the absorption maximum of 562 nm was reported for this method [Stookey, 1970]. A slightly reduced sensitivity with an extinction coefficient of 22,100 ± 240 $L \cdot mol^{-1} \cdot cm^{-1}$ was obtained with the LoC analyzer due to the use of LEDs

with a slightly higher peak wavelength of 575 nm. However, a significantly lower LOD of 1.9 nM was found compared to reported LODs of other Fe *in situ* analyzers based on the FZ method, e.g. the SCANNER (LOD = 25 nM)[Chin et al., 1994; Coale et al., 1991], CHEMINI (LOD = 300 nM) [Vuillemin et al., 2009], ALCHIMIST (LOD = 70 nM) [Sarradin et al., 2005] and the IonConExplorer (LOD = 27.25 nM) [Jin et al., 2013]. Due to the combined use of three different detection cell lengths, DFe concentrations ranging from LOD to [DFe] > 20 μM are detectable with our LoC system. This broad range enables flexibility with respect to the deployment site, ranging from coastal and surface waters, where concentrations down to the low nM range can be found, to regions with high and variable DFe concentrations such as benthic boundary waters or hydrothermal vent plumes. The low reagent consumption (63 μL per sample) and a measurement frequency of up to eight samples per hour, as defined by the time required for complete diffusive mixing of sample and reagent, is adequate for long-term *in situ* monitoring.

The *in situ* capability of a first prototype of the LoC analyzer was tested in Kiel fjord during a nine day test deployment in September 2016. It was found that *in situ* determined DFe concentrations, ranging from 27 nM to 57 nM, were considerably lower than those obtained through ICP-MS analysis of discretely collected samples as validation tool (between 61 nM and 235 nM DFe). This resulted in a highly variable underestimation between 16 % and 75 %. It was hypothesized that both methods determine different DFe pools due to different sample treatments. Samples for ICP-MS measurements were stored acidified (pH < 1.9, according to GEOTRACES protocol) in order to liberate Fe from its natural organic complexes. Laboratory experiments, undertaken with a natural water sample from Kiel fjord on a double beam spectrophotometer, revealed that 100 % recovery of the FZ method can be achieved when implementing an acidification step of the sample prior to mixing of the sample with FZ/AA reagent. Thus, the original layout of the LoC analyzer was re-designed in order to enable an on-line acidification step. The improved design comprised an additional syringe barrel for the supply of HCl and a microfluidic holding loop to allow efficient reaction of sample and acid. However, for full recovery an acid treatment for the duration of one day at pH ~ 1 was necessary. As this duration would lead to an insufficient temporal resolution for *in situ* monitoring, a period of two hours was chosen for the treatment of the sample with HCl, as a compromise between efficient Fe liberation and sampling frequency. Within two hours a recovery of almost 90 % was obtained by extrapolation of laboratory based acidification experiments. *In situ* evaluation of the new design revealed an underestimation of DFe for unacidified

samples (~ 50 nM on average lower compared to discrete samples), as previously reported, whereas a mean overestimation of ~ 85 nM was observed when the on-line acidification was applied. Those high DFe concentrations were attributed to Fe contaminations, generated from acid induced leaching of Fe from the materials used in the analyzer. Thus, investigation of other materials used for the fabrication of the microfluidic chip, e.g. Teflon instead of PMMA or titanium barrels instead of glass barrels, is required in the future in order to allow reliable *in situ* DFe determinations yielding concentrations comparable to those of ICP-MS analysis of discretely collected samples. However, the presented analyzer might be suitable for tracking relative changes in DFe concentrations as the *in situ* DFe time series after acidification showed significant correlation with DFe concentrations determined of discrete samples analyzed via ICP-MS, despite the observed overestimation. Furthermore, time series showed reasonable relationships to other hydrographic parameters such as dissolved oxygen, pH, temperature and salinity.

6.2 Determination of dissolved manganese

The capability of a microfluidic analyzer to reliably determine DMn concentrations *in situ* was successfully demonstrated in chapter 5. The *in situ* acquisition of temporally as well as spatially well resolved time series for DMn is especially important as Mn is an essential micronutrient for phytoplankton, co-limits primary production and is involved in photosynthetic processes. Thus, information about distributions and fluxes of DMn can help to better understand those processes, project their connections on a global scale and predict consequences of future changes.

The Mn sensitive spectrophotometric PAN method was chosen for the here presented study, as the $Mn(PAN)_2$ complex exhibits the same wavelength of its absorption maximum as the $Fe(FZ)_3$ complex, at 562 nm. This allows the use of the same microfluidic hardware setup as for DFe analysis introduced in chapter 3. However, the PAN method as proposed by Chin et al. (1992) required adaptation for the special needs of autonomous *in situ* long-term measurements in seawater using LoC analyzers. We found that the lifetime of the PAN reagent, which is key for long-term *in situ* measurements, was limited when preparation followed the recipe from Chin et al. (1992). Here, the PAN reagent comprised 2 % v/v of the non-ionic surfactant Triton-X100 in order to create a micellar medium with the ability to solubilize the water insoluble PAN molecules and the $Mn(PAN)_2$ chelates. However, this composition seemed unsuitable for its use in microfluidic devices, as PAN

crystals were observed after a period of four weeks. Any kind of particles could cause malfunction of such devices due to its high vulnerability to clogging. With the use of 4 % v/v Triton-X100 stability was improved without any loss of sensitivity. It was further proposed that the use of the Fe masking agent DFO-B prevents an overestimation of DMn due to the cross sensitivity of the PAN reagent to other metals, such as Fe, when prevalent at high concentrations compared to Mn. However, our critical evaluation of the masking strategy revealed that also Mn(II) was removed from the PAN accessible pool when applying Fe masking agents, such as DFO-B and Tiron, resulting in an Mn underestimation. We further demonstrated a limited lifetime of DFO-B ranging from days to weeks, depending on the temperature, making it unsuitable for autonomous long-term deployments where constant Fe masking strength is required. Therefore and because of the assumption that interfering ions are either prevalent as natural organic complexes, which limits the accessibility to PAN, and/or in low quantity compared to DMn, we decided not to use any masking agent. With this adapted PAN method an extinction coefficient of 40,838 ± 1,127 $L \cdot mol^{-1} \cdot cm^{-1}$ and a LOD of 27.2 nM were obtained on the 34.6 mm long measurement channel of the LoC analyzer. The here presented analyzer exhibits therefore an enhanced sensitivity compared to previously reported *in situ* Mn systems, such as the SCANNER and the METIS devices. The achieved LOD enables the acquisition of DMn time series in regions where elevated DMn concentrations are expected, such as coastal and estuarine systems or in regions characterized by hydrothermal activity. Other methods such as an on-line pre-concentration step prior to optical detection or more sensitive approaches such as fluorescence and chemiluminescence could be possibly used for the detection of concentrations found in open ocean region (down to the pM range). However, extensive research has to be undertaken to utilize such methods for autonomous *in situ* measurements.

The analyzers performance was evaluated under environmental conditions during a test campaign undertaken in October/November 2018 in the Kiel fjord. Here, analyzer derived DMn concentrations were in good agreement with those determined via ICP-MS from discretely collected samples as validation tool. For certain periods accuracies of > 99 % were achieved. According to statistical analysis (Spearman rank correlation test) the relative changes of DMn concentrations (anti-)correlated reasonably with the time series found for other hydrographic parameters such as temperature, salinity, oxygen or phosphate concentrations. It was therefore successfully demonstrated that systems based on LoC technology and the utilized spectrophotometric PAN method represent a powerful tool for

the acquisition of temporally well resolved reliable DMn time series, which would not be achievable with collecting discrete samples followed by laboratory based analysis. Thus, future deployments should focus on the investigation of biogeochemical questions which are linked to elevated DMn concentrations, such as DMn fluxes in hydrothermal vicinities, dissolution characteristics of dust or the effect of anthropogenic Mn inputs on coastal and estuarine ecosystems.

6.3 Requirements for trace metal analyzers and future developments

The here presented findings are an important contribution towards the development of integrated autonomous observing systems for dissolved trace metals in marine waters, where a deployment duration of month to year and an hourly to biweekly temporal resolution are desired [Grand et al., 2019]. However, the achieved LODs are still too high and require further improvement to allow open ocean observations. At present there is no system available which is capable of resolving such low micronutrient concentrations as required for open ocean monitoring. The desired detection limits are 0.1 nM for both DFe and DMn in order to monitor seasonal changes of those trace metals in the euphotic zone [Grand et al., 2019]. Regarding microfluidic LoC technology, hyphenation techniques including adequate pre-concentration systems need to be developed to achieve such sensitivities. As the current LoC systems rely on spectrophotometric determination, more sensitive optical detection principles could be integrated, e.g. fluorescence or chemiluminescence. The 'Ocean Technology and Engineering Group' at NOC Southampton for example, is currently adapting the chemiluminescent luminol approach for the detection of Fe, usually used in flow injection systems, for its use in LoC based manifolds. Furthermore, a remodeling of the conceptual design, especially a replacement of the used solenoid valves and syringe pump, could help to improve robustness of the systems and mitigate the need for maintenance. The solenoid valves and the syringe pump turned out to be the most vulnerable hardware components of the LoC manifold. Thus, future developments could focus on the manufacturing of miniaturized valve-free systems using e.g. osmotic pumps or piezoelectric micro pumps as an alternative to syringe pumping units. With this approach reagent consumption could be reduced further, whilst achieving higher measurement frequencies. This could also be achieved by changing the design towards droplet-based microfluidic systems [Nightingale et al., 2015; Song et al., 2006]. Here, sub-microliter scale droplets containing sample and reagent are generated at rates of several Hz, separated by an immiscible fluid or gas. This approach is characterized

by a high sample throughput and rapid mixing of reagent with sample due to the small size of the compartmentalized droplets. Each droplet represents a distinct sample and can be analyzed individually, e.g. through fluorescence based techniques due to the small optical path length defined by the droplets size.
However, an ultimate goal should be the shift from wet chemical *in situ* analyzers towards the development of optical sensors which operate without the supply of reagent solutions such as optodes, not only for the determination of trace metals but also for e.g. macro-nutrients, toxic decomposition products of plastics or ammunitions to name a few. Those sensors are already widely used for the autonomous *in situ* determination of parameters such as pH as well as O_2 and CO_2 concentrations. The approach relies on the diffusion of the respective analyte into a polymer membrane containing an embedded analyte sensitive fluorescent compound. As the fluorescence intensity/life time of the immobilized reagent is linked to the analytes concentration and assuming a reversible chemical reaction, temporally well resolved time series can be acquired. Future work could focus on the immobilization of fluorescent compounds specifically sensitive to micronutrients (either via quenching or increasing of fluorescence) and the development of such optode based sensors, which would be revolutionary in the field of *in situ* trace metal analysis.

As micronutrients are essential for marine organisms, profound knowledge has to be acquired about their supply, concentrations and cycling in the marine environment. This knowledge can be an important contributor in order to assess the status quo of our oceans. However, the conventional ship-board discrete sampling approach followed by home-based analysis provides just a one-time snapshot of the actual condition and is thus inadequate to resolve highly variable trace metal distributions, associated fluxes and the biological and climatological response. There is hence an urgent need for setting up a global scale network of observation systems, preferentially based on reliable and accurate user friendly 'Plug & Play' devices. However, in order to provide accurate and precise time series, the integrity, reliability and comparability of monitoring systems, deployed on a global scale, need to be assured. Therefore, best practices and standardization methods need to be developed on different levels. Processes for sensor calibration, data acquisition and quality assessment have to be standardized and inter-comparability across networks has to be assured. Standardization parameters of interest are for example consistent filter pore size, standardized validation method, preservation of calibration solutions, regular analysis of certified reference materials to name just a few. Furthermore, standards regarding the platform interfaces are required to allow interoperability across marine observation

networks and assure efficient data flow from the sensor directly to data repositories and end-users, preferentially in real time e.g. through satellite based transmission protocols.

Finally, rapid progress in developing reliable, cost-effective and robust sensor systems as well as establishing global sensor networks is of great interest for industry, governments as well as non-governmental organizations. The present undersampling of the oceans may lead to inaccurate conclusions about the distribution and fate of the respective analyte. Thus, the acquisition of high quality data (validated and on well resolved temporal and spatial scale) will allow a better understanding of the biogeochemical cycles of trace metals and will contribute to the assessment of the status quo of the world's oceans. The time series will be used as model inputs to predict future developments and climate-driven changes on sensitive ecosystems and will thus ultimately contribute to decision-making processes of international organizations and governments towards a sustainable management and conservation of important marine ecosystems.

7 References

Abe, S., Saito, T., and Suda, M. (1986). Simultaneous determination of iron(II) and iron(III) in aqueous solution by kinetic spectrophotometry with tiron. *Anal. Chim. Acta* 181, 203–209. doi:10.1016/S0003-2670(00)85235-6.

Achterberg, E. P., Holland, T. W., Bowie, A. R., Mantoura, R. F. C., and Worsfold, P. J. (2001). Determination of iron in seawater. *Anal. Chim. Acta* 442, 1–14. doi:10.1016/S0003-2670(01)01091-1.

Ahmed, M. J., and Roy, U. K. (2009). A simple spectrophotometric method for the determination of iron(II) aqueous solutions. *Turkish J. Chem.* 33, 709–726. doi:10.3906/kim-0802-9.

Al-Halhouli, A., Alshare, A., Mohsen, M., Matar, M., Dietzel, A., and Büttgenbach, S. (2015). Passive Micromixers with Interlocking Semi-Circle and Omega-Shaped Modules: Experiments and Simulations. *Micromachines* 6, 953–968. doi:10.3390/mi6070953.

Aly, K. M., and Esmail, E. (1993). Refractive index of salt water: effect of temperature. *Opt. Mater. (Amst).* 2, 195–199. doi:10.1080/713676580.

Baker, A. R., Jickells, T. D., Witt, M., and Linge, K. L. (2006). Trends in the solubility of iron, aluminium, manganese and phosphorus in aerosol collected over the Atlantic Ocean. *Mar. Chem.* 98, 43–58. doi:10.1016/j.marchem.2005.06.004.

Barber, J. (2012). Photosystem II: The Water-Splitting Enzyme of Photosynthesis. *Cold Spring Harb. Symp. Quant. Biol.* 77, 295–307. doi:10.1101/sqb.2012.77.014472.

Basu, S., and Mackey, K. R. M. (2018). Phytoplankton as Key Mediators of the Biological Carbon Pump: Their Responses to a Changing Climate. *Sustainability* 10, 869. doi:10.3390/su10030869.

Beaton, A. D., Cardwell, C. L., Thomas, R. S., Sieben, V. J., Legiret, F.-E., Waugh, E. M., et al. (2012). Lab-on-chip measurement of nitrate and nitrite for in situ analysis of natural waters. *Environ. Sci. Technol.* 46, 9548–56. doi:10.1021/es300419u.

Beaton, A. D., Sieben, V. J., Floquet, C. F. A., Waugh, E. M., Abi Kaed Bey, S., Ogilvie, I. R. G., et al. (2011). An automated microfluidic colourimetric sensor applied in situ to determine nitrite concentration. *Sensors Actuators, B Chem.* 156, 1009–1014. doi:10.1016/j.snb.2011.02.042.

Bennett, S. A., Achterberg, E. P., Connelly, D. P., Statham, P. J., Fones, G. R., and German, C. R. (2008). The distribution and stabilisation of dissolved Fe in deep-sea hydrothermal plumes. *Earth Planet. Sci. Lett.* 270, 157–167. doi:10.1016/j.epsl.2008.01.048.

Boiteau, R. M., Mende, D. R., Hawco, N. J., McIlvin, M. R., Fitzsimmons, J. N., Saito, M. A., et al. (2016). Siderophore-based microbial adaptations to iron scarcity across the eastern Pacific Ocean. *Proc. Natl. Acad. Sci.* 113, 14237–14242. doi:10.1073/pnas.1608594113.

Bowie, A. R., Achterberg, E. P., Mantoura, R. F. C., and Worsfold, P. J. (1998). Determination of sub-nanomolar levels of iron in seawater using flow injection with chemiluminescence detection. *Anal. Chim. Acta* 361, 189–200. doi:10.1016/S0003-2670(98)00015-4.

Box, J. (1984). Observations on the use of iron (II) complexing agents to fractionate the total filterable iron in natural water samples. *Water Res.* 18. doi:10.1016/0043-1354(84)90146-5.

Boyd, P. W., and Ellwood, M. J. (2010). The biogeochemical cycle of iron in the ocean. *Nat. Geosci.* 3, 675–682. doi:10.1038/ngeo964.

Boyd, P. W., Jickells, T., Law, C. S., Blain, S., Boyle, E. A., Buesseler, K. O., et al. (2007). Mesoscale Iron Enrichment Experiments 1993-2005: Synthesis and Future Directions. *Science (80-.).* 315, 612–617. doi:10.1126/science.1131669.

Boyd, P. W., Law, C. S., Wong, C. S., Nojiri, Y., Tsuda, A., Levasseur, M., et al. (2004). The decline and fate of an iron-induced subarctic phytoplankton bloom. *Nature* 428, 549–553. doi:10.1038/nature02437.

Boyle, E. A., Edmond, J. M., and Sholkovitz, E. R. (1977). The mechanism of iron removal in estuaries. *Geochim. Cosmochim. Acta* 41, 1313–1324. doi:10.1016/0016-7037(77)90075-8.

Brand, L. E., Sunda, W. G., and Guillard, R. R. L. (1983). Limitation of marine phytoplankton reproductive rates by zinc, manganese, and iron. *Limnol. Oceanogr.* 28, 1182–1198. doi:10.4319/lo.1983.28.6.1182.

Braungardt, C. B., Achterberg, E. P., Axelsson, B., Buffle, J., Graziottin, F., Howell, K. A., et al. (2009). Analysis of dissolved metal fractions in coastal waters: An inter-comparison of five voltammetric in situ profiling (VIP) systems. *Mar. Chem.* 114, 47–55. doi:10.1016/j.marchem.2009.03.006.

Braungardt, C. B., Howell, K. A., Tappin, A. D., and Achterberg, E. P. (2011). Temporal variability in dynamic and colloidal metal fractions determined by high resolution in situ measurements in a UK estuary. *Chemosphere* 84, 423–431. doi:10.1016/j.chemosphere.2011.03.050.

Breitbarth, E., Achterberg, E. P., Ardelan, M. V., Baker, a. R., Bucciarelli, E., Chever, F., et al. (2010). Iron biogeochemistry across marine systems - progress from the past decade. *Biogeosciences* 7, 1075–1097. doi:10.5194/bg-7-1075-2010.

Breitbarth, E., Gelting, J., Walve, J., Hoffmann, L. J., Turner, D. R., Hassellöv, M., et al. (2009). Dissolved iron (II) in the Baltic Sea surface water and implications for

cyanobacterial bloom development. *Biogeosciences Discuss.* 6, 2397–2420. doi:10.5194/bgd-6-3803-2009.

Bruland, K. W., Franks, R. P., Knauer, G. A., and Martin, J. H. (1979). Sampling and analytical methods for the determination of copper, cadmium, zinc, and nickel at the nanogram per liter level in sea water. *Anal. Chim. Acta* 105, 233–245. doi:10.1016/S0003-2670(01)83754-5.

Bruland, K. W., Orians, K. J., and Cowen, J. P. (1994). Reactive trace metals in the stratified central North Pacific. *Geochim. Cosmochim. Acta* 58, 3171–3182. doi:10.1016/0016-7037(94)90044-2.

Bruland, K. W., and Rue, E. L. (2001). "Analytical methods for determination of concentrations and speciation of iron," in *The Biogeochemistry of Iron in Seawater*, eds. D. R. Turner and K. A. Hunter (John Wiley & Sons Ltd.), 255–289.

Buck, K. N., Lohan, M. C., Berger, C. J. M., and Bruland, K. W. (2007). Dissolved iron speciation in two distinct river plumes and an estuary: Implications for riverine iron supply. *Limnol. Oceanogr.* 52, 843–855. doi:10.4319/lo.2007.52.2.0843.

Buesseler, K. O., Andrews, J. E., Pike, S. M., and Charette, M. A. (2004). The Effects of Iron Fertilization on Carbon Sequestration in the Southern Ocean. *Science (80-.).* 304, 414 LP – 417. doi:10.1126/science.1086895.

Burdige, D. J. (1993). The biogeochemistry of manganese and iron reduction in marine sediments. *Earth-Science Rev.* 35, 249–284. doi:10.1016/0012-8252(93)90040-E.

Byrne, R. H., and Kester, D. R. (1976). Solubility of hydrous ferric oxide and iron speciation in seawater. *Mar. Chem.* 4, 255–274. doi:10.1016/0304-4203(76)90012-8.

Campos, C. D. M., and da Silva, J. a. F. (2013). Applications of autonomous microfluidic systems in environmental monitoring. *RSC Adv.* 3, 18216. doi:10.1039/c3ra41561a.

Carpenter, J. H. (1965). The Chesapeake Bay institute technique for the Winkler dissolved oxygen method. *Limnol. Oceanogr.* 10, 141–143. doi:10.4319/lo.1965.10.1.0141.

Chapin, T., Jannasch, H., Chapin, T. P., Jannasch, H. W., and Johnson, K. S. (2002). In situ osmotic analyzer for the year-long continuous determination of Fe in hydrothermal systems In situ osmotic analyzer for the year-long continuous determination of Fe in hydrothermal systems. doi:10.1016/S0003-2670(02)00423-3.

Chever, F., Sarthou, G., Bucciarelli, E., Blain, S., and Bowie, A. R. (2010). An iron budget during the natural iron fertilisation experiment KEOPS (Kerguelen Islands, Southern Ocean). *Biogeosciences* 7, 455–468. doi:10.5194/bg-7-455-2010.

Chin, C. S., Coale, K. H., Elrod, V. A., Johnson, K. S., Massoth, G. J., and Baker, E. T. (1994). In situ observations of dissolved iron and manganese in hydrothermal vent plumes, Juan de Fuca Ridge. *J. Geophys. Res.* 99, 4969–4984. doi:10.1029/93JB02036.

Chin, C. S., Johnson, K. S., and Coale, K. H. (1992). Spectrophotometric determination of dissolved manganese in natural waters with 1-(2-pyridylazo)-2-naphthol: application to analysis in situ in hydrothermal plumes. *Mar. Chem.* 37, 65–82. doi:10.1016/0304-4203(92)90057-H.

Chiswell, B., and O'Halloran, K. R. (1991). Comparison of three colorimetric methods for the determination of manganese in freshwaters. *Talanta* 38, 641–647. doi:10.1016/0039-9140(91)80149-T.

Clinton-Bailey, G. S., Grand, M. M., Beaton, A. D., Nightingale, A. M., Owsianka, D. R., Slavik, G. J., et al. (2017). A Lab-on-Chip Analyzer for in Situ Measurement of Soluble Reactive Phosphate: Improved Phosphate Blue Assay and Application to Fluvial Monitoring. *Environ. Sci. Technol.* 51, 9989–9995. doi:10.1021/acs.est.7b01581.

Coale, K. H., Chin, C. S., Massoth, G. J., Johnson, K. S., and Baker, E. T. (1991). Insitu Chemical Mapping of Dissolved Iron and Manganese in Hydrothermal Plumes. *Nature* 352, 325–328. doi:10.1038/352325a0.

Coale, K. H., Johnson, K. S., Fitzwater, S. E., Gordon, R. M., Tanner, S., Chavez, F. P., et al. (1996). A massive phytoplankton bloom induced by an ecosystem-scale iron fertilization experiment in the equatorial Pacific Ocean. *Nature* 383, 495–501. doi:10.1038/383495a0.

Coo, L. D., Cardwell, T. J., Cattrall, R. W., and Kolev, S. D. (1998). Spectrophotometric study of the solubility and the protolytic properties of 1-(2-pyridylazo)-2-naphthol in different ethanol-water solutions. *Anal. Chim. Acta* 360, 153–159. doi:10.1016/S0003-2670(97)00712-5.

Cooper, L. H. N. (1935). Iron in the Sea and in Marine Plankton. *Proc. R. Soc. B Biol. Sci.* 118, 419–438. doi:10.1098/rspb.1935.0064.

Crusius, J., Schroth, A. W., Gassó, S., Moy, C. M., Levy, R. C., and Gatica, M. (2011). Glacial flour dust storms in the Gulf of Alaska: Hydrologic and meteorological controls and their importance as a source of bioavailable iron. *Geophys. Res. Lett.* 38, 1–5. doi:10.1029/2010GL046573.

Dale, A. W., Nickelsen, L., Scholz, F., Hensen, C., Oschlies, A., and Wallmann, K. (2015). A revised global estimate of dissolved iron fluxes. *Global Biogeochem. Cycles* 29, 691–707. doi:10.1002/2014GB005017.Received.

Davison, W., and Seed, G. (1983). The kinetics of the oxidation of ferrous iron in synthetic and natural waters. *Geochim. Cosmochim. Acta* 47, 67–79. doi:10.1016/0016-7037(83)90091-1.

de Baar, H. J. W., Boyd, P. W., Coale, K. H., Landry, M. R., Tsuda, A., Assmy, P., et al. (2005). Synthesis of iron fertilization experiments: From the iron age in the age of enlightenment. *J. Geophys. Res. C Ocean.* 110, 1–24. doi:10.1029/2004JC002601.

de Baar, H. J. W., and de Jong, J. T. M. (2001). "Distributions, sources and sinks of iron in

seawater," in *The Biogeochemistry of Iron in Seawater*, eds. D. R. Turner and K. A. Hunter (John Wiley & Sons Ltd.), 123–253.

Dean, J. (2009). Iron Fertilization : A Scientific Review with International Policy Recommendations. *Environs Environ. Law Policy J.* 32, 321–344.

Deutsch, F., Hoffmann, P., and Ortner, H. M. (1997). Analytical characterization of manganese in rainwater and snow samples. *Fresenius. J. Anal. Chem.* 357, 105–111. doi:10.1007/s002160050121.

Dias, A. C. B., Borges, E. P., Zagatto, E. A. G., and Worsfold, P. J. (2006). A critical examination of the components of the Schlieren effect in flow analysis. *Talanta* 68, 1076–1082. doi:10.1016/j.talanta.2005.06.071.

Dickson, A. G. (1990a). Standard potential of the reaction: AgCl(s) + 1/2H2(g) = Ag(s) + HCl(aq), and the standard acidity constant of the ion HSO4- in synthetic sea water from 273.15 to 318.15 K. *J. Chem. Thermodyn.* 22, 113–127. doi:10.1016/0021-9614(90)90074-Z.

Dickson, A. G. (1990b). Thermodynamics of the dissociation of boric acid in synthetic seawater from 273.15 to 318.15 K. *Deep Sea Res. Part A, Oceanogr. Res. Pap.* 37, 755–766. doi:10.1016/0198-0149(90)90004-F.

Dickson, A. G., and Millero, F. J. (1987). A comparison of the equilibrium constants for the dissociation of carbonic acid in seawater media. *Deep Sea Res. Part A, Oceanogr. Res. Pap.* 34, 1733–1743. doi:10.1016/0198-0149(87)90021-5.

Douville, E., Charlou, J. ., Oelkers, E. ., Bienvenu, P., Jove Colon, C. ., Donval, J. ., et al. (2002). The rainbow vent fluids (36°14'N, MAR): the influence of ultramafic rocks and phase separation on trace metal content in Mid-Atlantic Ridge hydrothermal fluids. *Chem. Geol.* 184, 37–48. doi:10.1016/S0009-2541(01)00351-5.

Duckworth, O. W., and Sposito, G. (2005). Siderophore-manganese (III) interactions. I. Air-oxidation of manganese(II) promoted by desferrioxamine B. *Environ. Sci. Technol.* 39, 6037–6044. doi:10.1021/es050275k.

Elmagirbi, A., Sulistyarti, H., and Atikah (2012). Study of Ascorbic Acid as Iron(III) Reducing Agent for Spectrophotometric Iron Speciation. *J. Pure Appl. Chem. Res.* 1, 11–17.

Emerson, S., Kalhorn, S., Jacobs, L., Tebo, B. M., Nealson, K. H., and Rosson, R. A. (1982). Environmental oxidation rate of manganese(II): bacterial catalysis. *Geochim. Cosmochim. Acta* 46, 1073–1079. doi:10.1016/0016-7037(82)90060-6.

Evers, A., Hancock, R. D., Martell, A. E., and Motekaitis, R. J. (1989). Metal ion recognition in ligands with negatively charged oxygen donor groups. Complexation of iron(III), gallium(III), indium(III), aluminum(III), and other highly charged metal ions. *Inorg. Chem.* 28, 2189–2195. doi:10.1021/ic00310a035.

Fan, S. M. (2008). Photochemical and biochemical controls on reactive oxygen and iron speciation in the pelagic surface ocean. *Mar. Chem.* 109, 152–164. doi:10.1016/j.marchem.2008.01.005.

Farid, H. T., Schulz, K. G., and Rose, A. L. (2018). Measuring total dissolved Fe concentrations in phytoplankton cultures in the presence of synthetic and organic ligands using a modified ferrozine method. *Mar. Chem.*, #pagerange#. doi:10.1016/j.marchem.2018.04.003.

Feng, S., Huang, Y., Yuan, D., Zhu, Y., and Zhou, T. (2015). Development and application of a shipboard method for spectrophotometric determination of trace dissolved manganese in estuarine and coastal waters. *Cont. Shelf Res.* 92, 37–43. doi:10.1016/j.csr.2014.11.004.

Floquet, C. F. A., Sieben, V. J., Milani, A., Joly, E. P., Ogilvie, I. R. G., Morgan, H., et al. (2011). Nanomolar detection with high sensitivity microfluidic absorption cells manufactured in tinted PMMA for chemical analysis. *Talanta* 84, 235–239. doi:10.1016/j.talanta.2010.12.026.

Gallant, R. M., and Von Damm, K. L. (2006). Geochemical controls on hydrothermal fluids from the Kairei and Edmond Vent Fields, 23°-25°S, Central Indian Ridge. *Geochemistry, Geophys. Geosystems* 7, n/a-n/a. doi:10.1029/2005GC001067.

Geißler, F., Achterberg, E. P., Beaton, A. D., Hopwood, M. J., Clarke, J. S., Mutzberg, A., et al. (2017). Evaluation of a Ferrozine Based Autonomous in Situ Lab-on-Chip Analyzer for Dissolved Iron Species in Coastal Waters. *Front. Mar. Sci.* 4. doi:10.3389/fmars.2017.00322.

Gerringa, L. J. A., Rijkenberg, M. J. A., Wolterbeek, H. T., Verburg, T. G., Boye, M., and de Baar, H. J. W. (2007). Kinetic study reveals weak Fe-binding ligand, which affects the solubility of Fe in the Scheldt estuary. *Mar. Chem.* 103, 30–45. doi:10.1016/j.marchem.2006.06.002.

Giannitsis, A. T., and Min, M. (2010). Usage of microfluidic lab-on-chips in biomedicine. in *2010 12th Biennial Baltic Electronics Conference* (IEEE), 249–252. doi:10.1109/BEC.2010.5630239.

Gibbs, C. R. (1976). Characterization and Application of FerroZine Iron Reagent as a Ferrous Iron Indicator. 48, 1197–1201. doi:10.1021/ac50002a034.

Gledhill, M., and Buck, K. N. (2012). The organic complexation of iron in the marine environment: A review. *Front. Microbiol.* 3, 1–17. doi:10.3389/fmicb.2012.00069.

Gledhill, M., and van den Berg, C. M. G. (1995). Measurement of the redox speciation of iron in seawater by catalytic cathodic stripping voltammetry. *Mar. Chem.* 50, 51–61. doi:10.1016/0304-4203(95)00026-N.

Goto, K., Taguchi, S., Fukue, Y., Ohta, K., and Watanabe, H. (1977). Spectrophotometric determination of manganese with 1-(2-pyridylazo)-2-naphthol and a non-ionic

surfactant. *Talanta* 24, 752–753. doi:10.1016/0039-9140(77)80206-3.

Grand, M. M., Clinton-Bailey, G. S., Beaton, A. D., Schaap, A. M., Johengen, T. H., Tamburri, M. N., et al. (2017). A Lab-On-Chip Phosphate Analyzer for Long-term In Situ Monitoring at Fixed Observatories: Optimization and Performance Evaluation in Estuarine and Oligotrophic Coastal Waters. *Front. Mar. Sci.* 4, 1–16. doi:10.3389/fmars.2017.00255.

Grand, M. M., Laes-Huon, A., Fietz, S., Resing, J. A., Obata, H., Luther, G. W., et al. (2019). Developing Autonomous Observing Systems for Micronutrient Trace Metals. *Front. Mar. Sci.* 6. doi:10.3389/fmars.2019.00035.

Hawkes, J. A., Connelly, D. P., Gledhill, M., and Achterberg, E. P. (2013). The stabilisation and transportation of dissolved iron from high temperature hydrothermal vent systems. *Earth Planet. Sci. Lett.* 375, 280–290. doi:10.1016/j.epsl.2013.05.047.

Hennessy, D. J., Reid, G. R., Smith, F. E., and Thompson, S. L. (1984). Ferene — a new spectrophotometric reagent for iron. *Can. J. Chem.* 62, 721–724. doi:10.1139/v84-121.

Hernlem, B. J., Vane, L. M., and Sayles, G. D. (1996). Stability constants for complexes of the siderophore desferrioxamine B with selected heavy metal cations. *Inorganica Chim. Acta* 244, 179–184. doi:10.1016/0020-1693(95)04780-8.

Hirayama, K., and Unohara, N. (1988). Spectrophotometric Catalytic Determination of an Ultratrace Amount of Iron(II1) in Water Based on the Oxidation of N ,N-Dimethyl-p -phenylenediamine by Hydrogen Peroxide. *Anal. Chem.* 60, 2573–2577.

Holliday, L. M., and Liss, P. S. (1976). The behaviour of dissolved iron, manganese and zinc in the Beaulieu Estuary, S. England. *Estuar. Coast. Mar. Sci.* 4, 349–353. doi:10.1016/0302-3524(76)90066-9.

Hopwood, M. J., Statham, P. J., and Milani, A. (2014). Dissolved Fe(II) in a river-estuary system rich in dissolved organic matter. *Estuar. Coast. Shelf Sci.* 151, 1–9. doi:10.1016/j.ecss.2014.09.015.

Hopwood, M. J., Statham, P. J., Skrabal, S. A., and Willey, J. D. (2015). Dissolved iron (II) ligands in river and estuarine water. *Mar. Chem.* 173, 173–182. doi:10.1016/j.marchem.2014.11.004.

Howell, Jr, P. B., Mott, D. R., Golden, J. P., and Ligler, F. S. (2004). Design and evaluation of a Dean vortex-based micromixer. *Lab Chip* 4, 663. doi:10.1039/b407170k.

Huang, Y., Yuan, D., Ma, J., Zhang, M., and Chen, G. (2009). Rapid speciation of trace iron in rainwater by reverse flow injection analysis coupled to a long path length liquid waveguide capillary cell and spectrophotometric detection. *Microchim. Acta* 166, 221–228. doi:10.1007/s00604-009-0193-8.

Huang, Y., Yuan, D., Zhu, Y., and Feng, S. (2015). Real-time redox speciation of iron in

estuarine and coastal surface waters. *Environ. Sci. Technol.* 49, 3619–3627. doi:10.1021/es505138f.

ISO/IEC 17025 (2005). General requirements for the competence of testing and calibration laboratories (ISO/IEC 17025:2005).

Jacq, V., Ridame, C., L'Helguen, S., Kaczmar, F., and Saliot, A. (2014). Response of the unicellular diazotrophic cyanobacterium Crocosphaera watsonii to iron limitation. *PLoS One* 9. doi:10.1371/journal.pone.0086749.

Javidpour, J., Molinero, J. C., Peschutter, J., and Sommer, U. (2009). Seasonal changes and population dynamics of the ctenophore Mnemiopsis leidyi after its first year of invasion in the Kiel Fjord, Western Baltic Sea. *Biol. Invasions* 11, 873–882. doi:10.1007/s10530-008-9300-8.

Jickells, T. D., An, Z. S., Andersen, K. K., Baker, A. R., Bergametti, G., Brooks, N., et al. (2005). Global Iron Connections Between Desert Dust, Ocean Biogeochemistry, and Climate. *Science (80-.).* 308, 67–71. doi:10.1126/science.1105959.

Jickells, T. D., and Spokes, L. J. (2001). "Atmospheric iron inputs to the oceans," in *The Biogeochemistry of Iron in Seawater*, eds. D. R. Turner and K. A. Hunter (John Wiley & Sons Ltd.), 85–121.

Jin, B., Chen, Z. W., and Zhu, S. Q. (2013). Development of an In Situ Analyzer for Iron in Deep Sea Environment. *Adv. Mater. Res.* 694–697, 1187–1191. doi:10.4028/www.scientific.net/AMR.694-697.1187.

Johnson, K. M., Wills, K. D., Butler, D. B., Johnson, W. K., and Wong, C. S. (1993). Coulometric total carbon dioxide analysis for marine studies: maximizing the performance of an automated gas extraction system and coulometric detector. *Mar. Chem.* 44, 167–187. doi:10.1016/0304-4203(93)90201-X.

Johnson, K. S., Beehler, C. L., and Sakamoto-Arnold, C. M. (1986). A submersible flow analysis system. *Anal. Chim. Acta* 179, 245–257. doi:10.1016/S0003-2670(00)84469-4.

Johnson, K. S., Coale, K. H., and Jannasch, H. W. (1992). Analytical chemistry in oceanography. *Anal. Chem.* 64, 1065A-1075A. doi:10.1021/ac00046a001.

Johnson, K. S., Michael Gordon, R., and Coale, K. H. (1997). What controls dissolved iron concentrations in the world ocean? *Mar. Chem.* 57, 137–161. doi:10.1016/S0304-4203(97)00043-1.

Kolber, Z. S., Barber, R. T., Coale, K. H., Fitzwater, S. E., Greene, R. M., Johnson, K. S., et al. (1994). Iron Limitation of Phytoplankton Photosynthesis in the Equatorial Pacific-Ocean. *Nature* 371, 145–149. doi:10.1038/371145a0.

Krauskopf, K. B. (1957). Separation of manganese from iron in sedimentary processes. *Geochim. Cosmochim. Acta* 12, 61–84. doi:10.1016/0016-7037(57)90018-2.

Kremling, K., Andreae, M. O., Brügmann, L., van den Berg, C. M. G., Prange, A., Schirmacher, M., et al. (2007). Determination of trace elements. *Methods Seawater Anal.* doi:10.1002/9783527613984.ch12.

Kremling, K., and Hydes, D. (1988). Summer distribution of dissolved Al, Cd, Co, Cu, Mn and Ni in surface waters around the British Isles. *Cont. Shelf Res.* 8, 89–105. doi:10.1016/0278-4343(88)90026-X.

Kuma, K., Nishioka, J., and Matsunaga, K. (1996). Controls on iron(III) hydroxide solubility in seawater: The influence of pH and natural organic chelators. *Limnol. Oceanogr.* 41, 396–407. doi:10.4319/lo.1996.41.3.0396.

Laes-Huon, A., Cathalot, C., Legrand, J., Tanguy, V., and Sarradin, P. M. (2016). Long-Term in situ survey of reactive iron concentrations at the Emso-Azores observatory. *IEEE J. Ocean. Eng.* 41, 744–752. doi:10.1109/JOE.2016.2552779.

Laes-Huon, A., Legrand, J., Tanguy, V., Cathalot, C., Blandin, J., and Rolin, J. (2014). Long term in situ monitoring of total dissolved iron concentrations on the MoMAR observatory. *2014 IEEE Sens. Syst. a Chang. Ocean* 17, 5270. doi:10.1109/SSCO.2014.7000366.

Lampitt, R. S., Achterberg, E. P., Anderson, T. R., Hughes, J. A., Iglesias-Rodriguez, M. D., Kelly-Gerreyn, B. A., et al. (2008). Ocean fertilization: A potential means of geoengineering? *Philos. Trans. R. Soc. A Math. Phys. Eng. Sci.* 366, 3919–3945. doi:10.1098/rsta.2008.0139.

Le Bris, N., Sarradin, P.-M., Birot, D., and Alayse-Danet, A.-M. (2000). A new chemical analyzer for in situ measurement of nitrate and total sulfide over hydrothermal vent biological communities. *Mar. Chem.* 72, 1–15. doi:10.1016/S0304-4203(00)00057-8.

Lee, K., Kim, T. W., Byrne, R. H., Millero, F. J., Feely, R. A., and Liu, Y. M. (2010). The universal ratio of boron to chlorinity for the North Pacific and North Atlantic oceans. *Geochim. Cosmochim. Acta* 74, 1801–1811. doi:10.1016/j.gca.2009.12.027.

Legiret, F. E., Sieben, V. J., Woodward, E. M. S., Abi Kaed Bey, S. K., Mowlem, M. C., Connelly, D. P., et al. (2013). A high performance microfluidic analyser for phosphate measurements in marine waters using the vanadomolybdate method. *Talanta* 116, 382–387. doi:10.1016/j.talanta.2013.05.004.

Leonhard, P., Pepelnik, R., Prange, A., Yamada, N., and Yamada, T. (2002). Analysis of diluted sea-water at the ng L-1 level using an ICP-MS with an octopole reaction cell. *J. Anal. At. Spectrom.* 17, 189–196. doi:10.1039/b110180n.

Liang, Y., Yuan, D., Li, Q., and Lin, Q. (2007). Flow injection analysis of nanomolar level orthophosphate in seawater with solid phase enrichment and colorimetric detection. *Mar. Chem.* 103, 122–130. doi:10.1016/j.marchem.2006.06.013.

Lin, J., and Kester, D. R. (1992). The kinetics of Fe(II) complexation by Ferrozine in seawater. *Mar. Chem.* 38, 283–301. doi:10.1016/0304-4203(92)90038-C.

Lippiatt, S. M., Lohan, M. C., and Bruland, K. W. (2010). The distribution of reactive iron in northern Gulf of Alaska coastal waters. *Mar. Chem.* 121, 187–199. doi:10.1016/j.marchem.2010.04.007.

Lunvongsa, S., Oshima, M., and Motomizu, S. (2006). Determination of total and dissolved amount of iron in water samples using catalytic spectrophotometric flow injection analysis. *Talanta* 68, 969–973. doi:10.1016/j.talanta.2005.06.067.

Luther, G. W., Reimers, C. E., Nuzzio, D. B., and Lovalvo, D. (1999). In Situ Deployment of Voltammetric, Potentiometric, and Amperometric Microelectrodes from a ROV To Determine Dissolved O 2 , Mn, Fe, S(−2), and pH in Porewaters. *Environ. Sci. Technol.* 33, 4352–4356. doi:10.1021/es9904991.

Luther, G. W., Shellenbarger, P. A., and Brendel, P. J. (1996). Dissolved organic Fe(III) and Fe(II) complexes in salt marsh porewaters. *Geochim. Cosmochim. Acta* 60, 951–960. doi:10.1016/0016-7037(95)00444-0.

Luther, G. W., Sundby, B., Lewis, B. L., Brendel, P. J., and Silverberg, N. (1997). Interactions of manganese with the nitrogen cycle: Alternative pathways to dinitrogen. *Geochim. Cosmochim. Acta* 61, 4043–4052. doi:10.1016/S0016-7037(97)00239-1.

Madison, A. S., Tebo, B. M., and Luther, G. W. (2011). Simultaneous determination of soluble manganese(III), manganese(II) and total manganese in natural (pore)waters. *Talanta* 84, 374–381. doi:10.1016/j.talanta.2011.01.025.

Mäntele, W., and Deniz, E. (2017). UV–VIS absorption spectroscopy: Lambert-Beer reloaded. *Spectrochim. Acta Part A Mol. Biomol. Spectrosc.* 173, 965–968. doi:10.1016/j.saa.2016.09.037.

Mao, Y., Zhang, M., and Xu, J. (2015). Limitation of ferrozine method for Fe(II) detection: reduction kinetics of micromolar concentration of Fe(III) by ferrozine in the dark. *Int. J. Environ. Anal. Chem.* 95, 1424–1434. doi:10.1080/03067319.2015.1114107.

Marczenko, Z., and Balcerzak, M. (2000). "Chapter 4 - Spectrophotometric reagents," in *Separation, Preconcentration and Spectrophotometry in Inorganic Analysis*, eds. Z. Marczenko and M. Balcerzak (Elsevier), 53–73. doi:10.1016/S0926-4345(00)80068-1.

Martin, J. H. (1990). Glacial-interglacial CO2 change: The Iron Hypothesis. *Paleoceanography* 5, 1–13. doi:10.1029/PA005i001p00001.

Martin, J. H., Gordon, M., and Fitzwater, S. E. (1991). The case for iron. *Limnol. Oceanogr.* 36, 1793–1802. doi:10.4319/lo.1991.36.8.1793.

Martinez, S., Pearlman, J., Achterberg, E. P., Walsh, I., and Delory, E. (2018). "Evolving standards and best practices for sensors and systems – sensors," in *Challenges and Innovations in Ocean In Situ Sensors*, eds. E. Delory and J. Pearlman (Elsevier).

Massoth, G. J., Baker, E. T., Feely, R. A., Butterfield, D. A., Embley, R. E., Lupton, J. E.,

et al. (1995). Observations of manganese and iron at the CoAxial Seafloor Eruption Site, Juan de Fuca Ridge. *Geophys. Res. Lett.* 22, 151–154. doi:10.1029/94GL02662.

Massoth, G. J., Baker, E. T., Feely, R. A., Lupton, J. E., Collier, R. W., Gendron, J. F., et al. (1998). Manganese and iron in hydrothermal plumes resulting from the 1996 Gorda Ridge event. *Deep. Res. Part II Top. Stud. Oceanogr.* 45, 2683–2712. doi:10.1016/S0967-0645(98)00089-7.

McClelland, J. W., Holmes, R. M., Dunton, K. H., and Macdonald, R. W. (2012). The Arctic Ocean Estuary. *Estuaries and Coasts* 35, 353–368. doi:10.1007/s12237-010-9357-3.

McLaren, J. W., Lam, J. W. H., Berman, S. S., Akatsuka, K., and Azeredo, M. A. (1993). On-line method for the analysis of sea-water for trace elements by inductively coupled plasma mass spectrometry. Plenary lecture. *J. Anal. At. Spectrom.* 8, 279–286. doi:10.1039/ja9930800279.

McMahon, J. W. (1969). The annual and diurnal variation in the vertical distribution of acid-soluble ferrous and total iron in a small dimictic lake. *Limnol. Oceanogr.* 14, 357–367. Available at: https://aslopubs.onlinelibrary.wiley.com/doi/abs/10.4319/lo.1969.14.3.0357.

Mehrbach, C., Culberson, C. H., Hawley, J. E., and Pytkowicx, R. M. (1973). Measurement of the Apparent Dissociation Constants of Carbonic Acid in Seawater at Atmospheric Pressure. *Limnol. Oceanogr.* 18, 897–907. doi:10.4319/lo.1973.18.6.0897.

Meybeck, M., and Ragu, A. (1997). Presenting the GEMS-GLORI, a compendium of world river discharge to the oceans. *Freshw. Contam. (Proceedings Rabat Symp. S4, April. IAHS Publ.* 243, 3–14. doi:10.1029/JC088iC14p09671.

Meyer, D., Prien, R. D., Dellwig, O., Connelly, D. P., and Schulz-Bull, D. E. (2012). In situ determination of iron(II) in the anoxic zone of the central Baltic Sea using ferene as spectrophotometric reagent. *Mar. Chem.* 130–131, 21–27. doi:10.1016/j.marchem.2011.12.002.

Meyer, D., Prien, R. D., Dellwig, O., Waniek, J. J., Schuffenhauer, I., Donath, J., et al. (2016). A multi-pumping flow system for in situ measurements of dissolved manganese in aquatic systems. *Sensors (Switzerland)* 16. doi:10.3390/s16122027.

Middag, R., de Baar, H. J. W., Laan, P., Cai, P. H., and van Ooijen, J. C. (2011). Dissolved manganese in the Atlantic sector of the Southern Ocean. *Deep. Res. Part II Top. Stud. Oceanogr.* 58, 2661–2677. doi:10.1016/j.dsr2.2010.10.043.

Milani, A., Statham, P. J., Mowlem, M. C., and Connelly, D. P. (2015). Development and application of a microfluidic in-situ analyzer for dissolved Fe and Mn in natural waters. *Talanta* 136, 15–22. doi:10.1016/j.talanta.2014.12.045.

Millero, F. J., Sotolongo, S., and Izaguirre, M. (1987). The oxidation kinetics of Fe(II) in seawater. *Geochim. Cosmochim. Acta* 51, 793–801. doi:10.1016/0016-7037(87)90093-7.

Millero, F. J., Yao, W., and Aicher, J. (1995). The speciation of Fe(II) and Fe(III) in natural waters. *Mar. Chem.* 50, 21–39. doi:10.1016/0304-4203(95)00024-L.

Mills, G., and Fones, G. (2012). A review of *in situ* methods and sensors for monitoring the marine environment. *Sens. Rev.* 32, 17–28. doi:10.1108/02602281211197116.

Mintrop, L., Perez, F. F., Gonzales-Davila, M., Santana-Casiano, J. M., and Körtzinger, A. (2000). Alkalinity determination by potentiometric titration: intercalibration using three different methods. *Ciencias Mar.* 26(1), 23–37. doi:10.7773/cm.v26i1.573.

Moffett, J. W. (2001). "Transformations Among DIfferent Forms of Iron in the Ocean," in *The Biogeochemistry of Iron in Seawater*, eds. D. R. Turner and K. A. Hunter (John Wiley & Sons Ltd.), 343–372.

Moore, C. M., Mills, M. M., Arrigo, K. R., Berman-Frank, I., Bopp, L., Boyd, P. W., et al. (2013). Processes and patterns of oceanic nutrient limitation. *Nat. Geosci* 6, 701–710. doi:10.1038/ngeo1765.

Morel, F. M. M., and Price, N. M. (2007). The Biogeochemical Cycles of Trace Metals. *Science (80-.).* 944, 944–948. doi:10.1126/science.1083545.

Murray, J. W., Codispoti, L. A., and Friederich, G. E. (1995). "Oxidation-Reduction Environments," in *Aquatic Chemistry*, eds. C. P. Huang, C. R. O'Melia, and J. J. Morgan (American Chemical Society), 157–176. doi:10.1021/ba-1995-0244.ch007.

Nakashima, S., Sturgeon, R. E., Willie, S. N., and Berman, S. S. (1988). Determination of trace metals in seawater by graphite furnace atomic absorption spectrometry with preconcentration on silica-immobilized 8-hydroxyquinoline in a flow-system. *Fresenius' Zeitschrift für Anal. Chemie* 330, 592–595. doi:10.1007/BF00473773.

Nightingale, A. M., Beaton, A. D., and Mowlem, M. C. (2015). Trends in microfluidic systems for in situ chemical analysis of natural waters. *Sensors Actuators B Chem.* 221, 1398–1405. doi:10.1016/j.snb.2015.07.091.

Ogilvie, I. R. G., Sieben, V. J., Floquet, C. F. A., Zmijan, R., Mowlem, M. C., and Morgan, H. (2010). Reduction of surface roughness for optical quality microfluidic devices in PMMA and COC. *J. Micromechanics Microengineering* 20, 65016. doi:10.1088/0960-1317/20/6/065016.

Ogilvie, I. R. G., Sieben, V. J., Mowlem, M. C., and Morgan, H. (2011). Temporal optimization of microfluidic colorimetric sensors by use of multiplexed stop-flow architecture. *Anal. Chem.* 83, 4814–4821. doi:10.1021/ac200463y.

Oldham, V. E., Mucci, A., Tebo, B. M., and Luther, G. W. (2017). Soluble Mn(III)–L complexes are abundant in oxygenated waters and stabilized by humic ligands. *Geochim. Cosmochim. Acta* 199, 238–246. doi:10.1016/j.gca.2016.11.043.

Otero-Romaní, J., Moreda-Piñeiro, A., Bermejo-Barrera, A., and Bermejo-Barrera, P.

(2005). Evaluation of commercial C18 cartridges for trace elements solid phase extraction from seawater followed by inductively coupled plasma-optical emission spectrometry determination. *Anal. Chim. Acta* 536, 213–218. doi:10.1016/j.aca.2004.12.046.

Öztürk, M., Steinnes, E., and Sakshaug, E. (2002). Iron speciation in the Trondheim fjord from the perspective of iron limitation for phytoplankton. *Estuar. Coast. Shelf Sci.* 55, 197–212. doi:10.1006/ecss.2001.0897.

Pascoa, R., Toth, I., and Rangel, A. (2009). OCEANOGRAPHY : METHODS Sequential injection trace determination of iron in natural waters using a long-pathlength liquid core waveguide and different spectrophotometric chemistries. *Limnol. Oceanogr. Methods* 7, 795–802.

Pascualreguera, M., Ortegacarmona, I., and Molinadiaz, A. (1997). Spectrophotometric determination of iron with ferrozine by flow-injection analysis. *Talanta* 44, 1793–1801. doi:10.1016/S0039-9140(97)00050-7.

Peers, G., and Price, N. M. (2004). A role for manganese in superoxide dismutases and growth of iron-deficient diatoms. *Limnol. Oceanogr.* 49, 1774–1783. doi:10.4319/lo.2004.49.5.1774.

Pollard, R. T., Salter, I., Sanders, R. J., Lucas, M. I., Moore, C. M., Mills, R. A., et al. (2009). Southern Ocean deep-water carbon export enhanced by natural iron fertilization. *Nature* 457, 577–580. doi:10.1038/nature07716.

Pollock, E. N., and Miguel, A. N. (1967). Determination of iron(II) in the presence of thousand-to-one ratio of iron(III) using bathophenanthroline. *Anal. Chem.* 39, 272–272. doi:10.1021/ac60246a019.

Postma, D. (1985). Concentration of Mn and separation from Fe in sediments—I. Kinetics and stoichiometry of the reaction between birnessite and dissolved Fe(II) at 10°C. *Geochim. Cosmochim. Acta* 49, 1023–1033. doi:10.1016/0016-7037(85)90316-3.

Prien, R. D. (2007). The future of chemical in situ sensors. *Mar. Chem.* 107, 422–432. doi:10.1016/j.marchem.2007.01.014.

Pullin, M. J., and Cabaniss, S. E. (2001). Colorimetric flow-injection analysis of dissolved iron in high DOC waters. *Water Res.* 35, 363–372. doi:10.1016/S0043-1354(00)00259-1.

Qu, R.-J., Wang, X.-H., Feng, M.-B., Li, Y., Liu, H.-X., Wang, L.-S., et al. (2013). The toxicity of cadmium to three aquatic organisms (Photobacterium phosphoreum, Daphnia magna and Carassius auratus) under different pH levels. *Ecotoxicol. Environ. Saf.* 95, 83–90. doi:10.1016/j.ecoenv.2013.05.020.

Raiswell, R., Benning, L. G., Tranter, M., and Tulaczyk, S. (2008). Bioavailable iron in the Southern Ocean: the significance of the iceberg conveyor belt. *Geochem. Trans.* 9, 7. doi:10.1186/1467-4866-9-7.

Raiswell, R., and Canfield, D. E. (2012). The Iron Biogeochemical Cycle Past and Present. *Geochemical Perspect.* 1, 1–220. doi:10.7185/geochempersp.1.1.

Raiswell, R., Hawkings, J., Elsenousy, A., Death, R., Tranter, M., and Wadham, J. (2018). Iron in Glacial Systems: Speciation, Reactivity, Freezing Behavior, and Alteration During Transport. *Front. Earth Sci.* 6. doi:10.3389/feart.2018.00222.

Rapp, I., Schlosser, C., Rusiecka, D., Gledhill, M., and Achterberg, E. P. (2017). Automated preconcentration of Fe, Zn, Cu, Ni, Cd, Pb, Co, and Mn in seawater with analysis using high-resolution sector field inductively-coupled plasma mass spectrometry. *Anal. Chim. Acta* 976, 1–13. doi:10.1016/j.aca.2017.05.008.

Rérolle, V. M. C., Floquet, C. F. A., Harris, A. J. K., Mowlem, M. C., Bellerby, R. R. G. J., and Achterberg, E. P. (2013). Development of a colorimetric microfluidic pH sensor for autonomous seawater measurements. *Anal. Chim. Acta* 786, 124–131. doi:10.1016/j.aca.2013.05.008.

Resing, J. A., and Mottl, M. J. (1992). Determination of Manganese in Seawater Using Flow Injection Analysis with On-Line Preconcentration and Spectrophotometric Detection. *Anal. Chem.* 64, 2682–2687. doi:10.1021/ac00046a006.

Resing, J. A., Sedwick, P. N., German, C. R., Jenkins, W. J., Moffett, J. W., Sohst, B. M., et al. (2015). Basin-scale transport of hydrothermal dissolved metals across the South Pacific Ocean. *Nature* 523, 200–203. doi:10.1038/nature14577.

Roitz, J. S., and Bruland, K. W. (1997). Determination of dissolved manganese(II) in coastal and estuarine waters by differential pulse cathodic stripping voltammetry. *Anal. Chim. Acta* 344, 175–180. doi:10.1016/S0003-2670(97)00041-X.

Rose, A. L., and Waite, T. D. (2003a). Kinetics of iron complexation by dissolved natural organic matter in coastal waters. *Mar. Chem.* 84, 85–103. doi:10.1016/S0304-4203(03)00113-0.

Rose, A. L., and Waite, T. D. (2003b). Predicting iron speciation in coastal waters from the kinetics of sunlight-mediated iron redox cycling. *Aquat. Sci.* 65, 375–383. doi:10.1007/s00027-003-0676-3.

Rue, E. L., and Bruland, K. W. (1995). Complexation of iron(III) by natural organic ligands in the Central North Pacific as determined by a new competitive ligand equilibration/adsorptive cathodic stripping voltammetric method. *Mar. Chem.* 50, 117–138. doi:10.1016/0304-4203(95)00031-L.

Ruttenberg, K. C., and Sulak, D. J. (2011). Sorption and desorption of dissolved organic phosphorus onto iron (oxyhydr)oxides in seawater. *Geochim. Cosmochim. Acta* 75, 4095–4112. doi:10.1016/j.gca.2010.10.033.

Safari, Z., Gholivand, M. B., and Hosseinzadeh, L. (2011). Spectrophotometric study of complex formations between 1-(2-pyridylazo)-2- naphthol (PAN) and some metal ions in organic solvents and the determination of thermodynamic parameters.

Spectrochim. Acta - Part A Mol. Biomol. Spectrosc. 78, 1606–1610. doi:10.1016/j.saa.2011.02.014.

Sands, C. M., Connelly, D. P., Statham, P. J., and German, C. R. (2012). Size fractionation of trace metals in the Edmond hydrothermal plume, Central Indian Ocean. *Earth Planet. Sci. Lett.* 319–320, 15–22. doi:10.1016/j.epsl.2011.12.031.

Santana-Casiano, J. M., González-Dávila, M., and Millero, F. J. (2006). The role of Fe(II) species on the oxidation of Fe(II) in natural waters in the presence of O2 and H2O2. *Mar. Chem.* 99, 70–82. doi:10.1016/j.marchem.2005.03.010.

Sarradin, P. M., Le Bris, N., Le Gall, C., and Rodier, P. (2005). Fe analysis by the ferrozine method: Adaptation to FIA towards in situ analysis in hydrothermal environment. *Talanta* 66, 1131–1138. doi:10.1016/j.talanta.2005.01.012.

Sarthou, G., Bucciarelli, E., Chever, F., Hansard, S. P., González-Dávila, M., Santana-Casiano, J. M., et al. (2011). Labile Fe(II) concentrations in the Atlantic sector of the Southern Ocean along a transect from the subtropical domain to the Weddell Sea Gyre. *Biogeosciences* 8, 2461–2479. doi:10.5194/bg-8-2461-2011.

Sholkovitz, E. R. (1978). The flocculation of dissolved Fe, Mn, Al, Cu, Ni, Co and Cd during estuarine mixing. *Earth Planet. Sci. Lett.* 41, 77–86. doi:10.1016/0012-821X(78)90043-2.

Sholkovitz, E. R., Boyle, E. A., and Price, N. B. (1978). The removal of dissolved humic acids and iron during estuarine mixing. *Earth Planet. Sci. Lett.* 40, 130–136. doi:10.1016/0012-821X(78)90082-1.

Song, H., Chen, D. L., and Ismagilov, R. F. (2006). Reactions in droplets in microfluidic channels. *Angew. Chemie - Int. Ed.* 45, 7336–7356. doi:10.1002/anie.200601554.

Spyres, G., Nimmo, M., Worsfold, P. J., Achterberg, E. P., and Miller, A. E. J. (2000). Determination of dissolved organic carbon in seawater using high temperature catalytic oxidation techniques. *TrAC Trends Anal. Chem.* 19, 498–506. doi:10.1016/S0165-9936(00)00022-4.

Stallard, R. F., and Edmond, J. M. (1983). Geochemistry of the Amazon: 2. The influence of geology and weathering environment on the dissolved load. *J. Geophys. Res. Ocean.* 88, 9671–9688. doi:10.1029/JC088iC14p09671.

Statham, P. J. (1985). The determination of dissolved manganese and cadmium in sea water at low nmol 1-1 concentrations by chelation and extraction followed by electrothermal atomic absorption spectrometry. *Anal. Chim. Acta* 169, 149–159. doi:10.1016/S0003-2670(00)86217-0.

Statham, P. J., Connelly, D. P., German, C. R., Brand, T., Overnell, J. O., Bulukin, E., et al. (2005). Spatially Complex Distribution of Dissolved Manganese in a Fjord as Revealed by High-Resolution in Situ Sensing Using the Autonomous Underwater Vehicle Autosub. *Environ. Sci. Technol.* 39, 9440–9445. doi:10.1021/es050980t.

Statham, P. J., Connelly, D. P., German, C. R., Bulukin, E., Millard, N., McPhail, S., et al. (2003). Mapping the 3D spatial distribution of dissolved manganese in coastal waters using an in situ analyser and the autonomous underwater vehicle Autosub. *Underw. Technol.* 25, 129–134. doi:10.3723/175605403783379679.

Statham, P. J., Yeats, P. A., and Landing, W. M. (1998). Manganese in the eastern Atlantic Ocean: Processes influencing deep and surface water distributions. *Mar. Chem.* 61, 55–68. doi:10.1016/S0304-4203(98)00007-3.

Stookey, L. L. (1970). Ferrozine---a new spectrophotometric reagent for iron. *Anal. Chem.* 42, 779–781. doi:10.1021/ac60289a016.

Stumm, W., and Morgan, J. J. (1995). *Aquatic chemistry: chemical equilibria and rates in natural waters*. 3rd Editio. Wiley, New York.

Subramanian, K. S., Chakrabarti, C. L., Sueiras, J. E., and Maines, I. S. (1978). Preservation of Some Trace Metals in Samples of Natural Waters. 50, 444–448. doi:10.1021/ac50025a022.

Sultanova, N., Kasarova, S., and Nikolov, I. (2009). Dispersion Properties of Optical Polymers. *Acta Phys. Pol. A* 116, 585–587. doi:10.12693/APhysPolA.116.585.

Sunda, W. G. (2001). "Bioavailability and Bioaccumulation of Iron in the Sea," in *The Biogeochemistry of Iron in Seawater*, eds. D. R. Turner and K. A. Hunter (John Wiley & Sons Ltd.), 41–84.

Sunda, W. G., and Huntsman, S. A. (1987). Microbial oxidation of manganese in a North Carolina estuary. *Limnol. Oceanogr.* 32, 552–564. doi:10.4319/lo.1987.32.3.0552.

Sunda, W. G., Huntsman, S. A., and Harvey, G. R. (1983). Photoreduction of manganese oxides in seawater and its geochemical and biological implications. *Nature* 301, 234–236. doi:10.1038/301234a0.

Tachikawa, K., Handel, C., and Dupré, B. (1997). Distribution of rare earth elements and neodymium isotopes in settling particulate material of the tropical Atlantic Ocean (EUMELI site). *Deep Sea Res. Part I Oceanogr. Res. Pap.* 44, 1769–1792. doi:10.1016/S0967-0637(97)00057-5.

Tagliabue, A., Bowie, A. R., Philip, W., Buck, K. N., Johnson, K. S., and Saito, M. A. (2017). The integral role of iron in ocean biogeochemistry. *Nature* 543, 51–59. doi:10.1038/nature21058.

Tagliabue, A., and Resing, J. (2016). Impact of hydrothermalism on the ocean iron cycle. *Philos. Trans. R. Soc. A Math. Phys. Eng. Sci.* 374, 20150291. doi:10.1098/rsta.2015.0291.

Taylor, S. R. (1964). Abundance of chemical elements in the continental crust: a new table. *Geochim. Cosmochim. Acta* 28, 1273–1285. doi:10.1016/0016-7037(64)90129-2.

Tercier-Waeber, M.-L., Buffle, J., Confalonieri, F., Riccardi, G., Sina, A., Graziottin, F., et al. (1999). Submersible voltammetric probes for in situ real-time trace element measurements in surface water, groundwater and sediment-water interface. *Meas. Sci. Technol.* 10, 1202–1213. doi:10.1088/0957-0233/10/12/312.

Tercier, M.-L., Buffle, J., and Graziottin, F. (1998). A Novel Voltammetric In-Situ Profiling System for ContinuousReal-Time Monitoring of Trace Elements in Natural Waters. *Electroanalysis* 10, 355–363. doi:10.1002/(SICI)1521-4109(199805)10:6<355::AID-ELAN355>3.0.CO;2-F.

Tiller, G. E., Mueller, T. J., Dockter, M. E., and Struve, W. G. (1984). Hydrogenation of Triton X-100 eliminates its fluorescence and ultraviolet light absorption while preserving its detergent properties. *Anal. Biochem.* 141, 262–266. doi:10.1016/0003-2697(84)90455-X.

Twining, B. S., and Baines, S. B. (2013). The Trace Metal Composition of Marine Phytoplankton. *Ann. Rev. Mar. Sci.* 5, 191–215. doi:10.1146/annurev-marine-121211-172322.

Ussher, S. J., Achterberg, E. P., and Worsfold, P. J. (2004). Marine Biogeochemistry of Iron. *Environ. Int.* 1, 67–80. doi:10.1071/EN04053.

Ussher, S. J., Milne, A., Landing, W. M., Attiq-ur-Rehman, K., Séguret, M. J. M., Holland, T., et al. (2009). Investigation of iron(III) reduction and trace metal interferences in the determination of dissolved iron in seawater using flow injection with luminol chemiluminescence detection. *Anal. Chim. Acta* 652, 259–265. doi:10.1016/j.aca.2009.06.011.

van Heuven, S., Pierrot, D., Rae, J. W. B., Lewis, E., and Wallace, D. W. R. (2011). MATLAB Program Developed for CO2 System Calculations. ORNL/CDIAC-105b. Carbon Dioxide Information Analysis Center, Oak Ridge National Laboratory, U.S. Department of Energy, Oak Ridge, Tennessee. doi:10.3334/CDIAC/otg.CO2SYS_MATLAB_v1.1.

van Hulten, M., Dutay, J.-C., Middag, R., de Baar, H., Roy-Barman, M., Gehlen, M., et al. (2016). Manganese in the world ocean: a first global model. *Biogeosciences Discuss.*, 1–38. doi:10.5194/bg-2016-282.

Varney, M. S. (2000). *Chemical Sensors in Oceanography*. Amsterdam: Gordon and Breach Science Publishers.

Verschoor, M. J., and Molot, L. A. (2013). A comparison of three colorimetric methods of ferrous and total reactive iron measurement in freshwaters. *Limnol. Oceanogr. Methods* 11, 113–125. doi:10.4319/lom.2013.11.113.

Vieira, L. H., Achterberg, E. P., Scholten, J., Beck, A. J., Liebetrau, V., Mills, M. M., et al. (2018). Benthic fluxes of trace metals in the Chukchi Sea and their transport into the Arctic Ocean. *Mar. Chem.* 208, 43–55. doi:10.1016/j.marchem.2018.11.001.

Viollier, E., Inglett, P. W., Hunter, K., Roychoudhury, A. N., and Van Cappellen, P. (2000). The ferrozine method revisited: Fe(II)/Fe(III) determination in natural waters. *Appl. Geochemistry* 15, 785–790. doi:10.1016/S0883-2927(99)00097-9.

Vuillemin, R., Le Roux, D., Dorval, P., Bucas, K., Sudreau, J. P., Hamon, M., et al. (2009). CHEMINI: A new in situ CHEmical MINIaturized analyzer. *Deep. Res. Part I Oceanogr. Res. Pap.* 56, 1391–1399. doi:10.1016/j.dsr.2009.02.002.

Wahl, M., Buchholz, B., Winde, V., Golomb, D., Guy-Haim, T., Müller, J., et al. (2015). A mesocosm concept for the simulation of near-natural shallow underwater climates: The Kiel Outdoor Benthocosms (KOB). *Limnol. Oceanogr. Methods* 13, 651–663. doi:10.1002/lom3.10055.

Waite, T. D. (2001). "Thermodynamics of the Iron System in Seawater," in *The Biogeochemistry of Iron in Seawater*, eds. D. R. Turner and K. Hunter (John Wiley & Sons Ltd.), 291–342.

Waite, T. D., and Szymczak, R. (1993). Manganese dynamics in surface waters of the eastern Caribbean. *J. Geophys. Res. Ocean.* 98, 2361–2369. doi:10.1029/92JC02770.

Weber, L., Völker, C., Schartau, M., and Wolf-Gladrow, D. A. (2005). Modeling the speciation and biogeochemistry of iron at the Bermuda Atlantic Time-series Study site. *Global Biogeochem. Cycles* 19, 1–23. doi:10.1029/2004GB002340.

Wedepohl, K. H. (1995). The composition of the continental crust. *Geochim. Cosmochim. Acta* 59, 1217–1232. doi:10.1016/B978-0-08-095975-7.00301-6.

Whittaker, S., Bidle, K. D., Kustka, A. B., and Falkowski, P. G. (2011). Quantification of nitrogenase in Trichodesmium IMS 101: Implications for iron limitation of nitrogen fixation intheocean. *Environ. Microbiol. Rep.* 3, 54–58. doi:10.1111/j.1758-2229.2010.00187.x.

Windom, H. L., Moore, W. S., Niencheski, L. F. H., and Jahnke, R. A. (2006). Submarine groundwater discharge: A large, previously unrecognized source of dissolved iron to the South Atlantic Ocean. *Mar. Chem.* 102, 252–266. doi:10.1016/j.marchem.2006.06.016.

Wolfe-Simon, F., Starovoytov, V., Reinfelder, J. R., Schofield, O., and Falkowski, P. G. (2006). Localization and Role of Manganese Superoxide Dismutase in a Marine Diatom. *Plant Physiol.* 142, 1701–1709. doi:10.1104/pp.106.088963.

Worsfold, P. J., Lohan, M. C., Ussher, S. J., and Bowie, A. R. (2014). Determination of dissolved iron in seawater: A historical review. *Mar. Chem.* 166, 25–35. doi:10.1016/j.marchem.2014.08.009.

Wu, J., Dong, M., Rigatto, C., Liu, Y., and Lin, F. (2018). Lab-on-chip technology for chronic disease diagnosis. *npj Digit. Med.* 1, 7. doi:10.1038/s41746-017-0014-0.

www.refractiveindex.info Available at: https://refractiveindex.info/?shelf=3d&book=plastics&page=pmma [Accessed December 5, 2018].

Yao, W., and Millero, F. J. (1996). Adsorption of Phosphate on Manganese Dioxide in Seawater. *Environ. Sci. Technol.* 30, 536–541. doi:10.1021/es950290x.

Yuecel, M., Beaton, A. D., Dengler, M., Mowlem, M. C., Sohl, F., and Sommer, S. (2015). Nitrate and nitrite variability at the seafloor of an oxygen minimum zone revealed by a novel microfluidic in-situ chemical sensor. *PLoS One* 10, 1–16. doi:10.1371/journal.pone.0132785.

Zagatto, E. A. G., Arruda, M. A. Z., Jacintho, A. O., and Mattos, I. L. (1990). Compensation of the Schlieren effect in flow-injection analysis by using dual-wavelength spectrophotometry. *Anal. Chim. Acta* 234, 153–160. doi:10.1016/S0003-2670(00)83550-3.

Zhu, Y., Hu, X., Pan, D., Han, H., Lin, M., Lu, Y., et al. (2018). Speciation determination of iron and its spatial and seasonal distribution in coastal river. *Sci. Rep.* 8, 2576. doi:10.1038/s41598-018-20991-0.

Declaration

I, Felix Geißler, hereby declare that I have written this PhD thesis independently, under compliance of the rules for good scientific practice of the German Research Foundation. I declare that I have used only the sources, the data and the support that I have clearly mentioned. Moreover, I assure that this PhD thesis has not been submitted for the conferral of a degree elsewhere, and that none of my academic degrees has ever been withdrawn. Published manuscripts are identified at the relevant places.

Kiel, August 2019

_____

Felix Geißler